uOttawa

L'Université canadienne
Canada's university

FACULTÉ DES ÉTUDES SUPÉRIEURES ET POSTOCTORALES

u Ottawa

L'Université canadienne
Canada's university

FACULTY OF GRADUATE AND POSDOCTORAL STUDIES

Carolyne Cléroux
AUTEUR DE LA THÈSE / AUTHOR OF THESIS

M.Sc. (Cellular and Molecular Medicine)
GRADE / DEGREE

Department of Cellular and Molecular Medicine
FACULTÉ, ÉCOLE, DÉPARTEMENT / FACULTY, SCHOOL, DEPARTMENT

Biodegradable Nanoparticles for Sustained Occular Drug Delivery
TITRE DE LA THÈSE / TITLE OF THESIS

Catherine Tsilfidis
DIRECTEUR (DIRECTRICE) DE LA THÈSE / THESIS SUPERVISOR

CO-DIRECTEUR (CO-DIRECTRICE) DE LA THÈSE / THESIS CO-SUPERVISOR

Ruth Slack

Robert Korneluk

Gary W. Slater
Le Doyen de la Faculté des études supérieures et postdoctorales / Dean of the Faculty of Graduate and Postdoctoral Studies

BIODEGRADABLE NANOPARTICLES FOR SUSTAINED OCCULAR DRUG DELIVERY

by Carolyne Cléroux

This thesis is submitted as a partial fulfillment of the M.Sc. program in Cellular and Molecular Medicine

Submitted September 22, 2009

Department of Cellular and Molecular Medicine
Faculty of Medicine
University of Ottawa

Your file Votre référence
ISBN: 978-0-494-65507-8
Our file Notre référence
ISBN: 978-0-494-65507-8

ABSTRACT

Apoptosis (programmed cell-death) is a common final pathway through which cells die in retinal degenerative diseases. The purpose of this project was to develop biodegradable nanoparticles that quickly deliver XIAP, an inhibitor of apoptosis, to retinal cells following acute insults. *In vitro* protein release profiles from different formulations were established, and two cell types were incubated with nanoparticles to assess cellular uptake. Subretinal injections were carried out in rats to assess *in vivo* localization and possible toxicity. *In vitro* studies showed an initial burst of protein followed by sustained release, with overall low levels of protein release. Cell culture experiments suggest that particles are mostly membrane-bound, and some may be internalized. *In vivo* experiments revealed no signs of toxicity, and protein localized within the photoreceptor layer. In conclusion, nanoparticles may provide a good delivery system for XIAP; however higher levels of protein release are needed for neuroprotection, warranting further investigation.

TABLE OF CONTENTS

LIST OF TABLES

LIST OF FIGURES

LIST OF ABBREVIATIONS

AAV	Adeno-associated virus
AMD	Age-related macular degeneration
ANOVA	Analysis of variance
BIR	Baculoviral IAP repeat
BSA	Bovine serum albumin
CBA	Chicken β-actin
cGMP	3',5'-cyclic guanosine monophosphate
CPP	Cell penetrating peptide
CTP	Cytoplasmic transduction peptide
CS	Chitosan
DAPI	4',6'-Diamindino-2-phenylindole dihydrochloride
EGFP	Enhanced green fluorescent protein
ELISA	Enzyme-linked immunosorbent assay
ERG	Electroretinography
GCL	Ganglion cell layer
GDNF	Glial-derived neurotrophic factor
IAP	Inhibitor of apoptosis
INL	Inner nuclear layer
IPL	Inner plexiform layer
MPTP	1-Methyl-4-phenyl-1,2,3,6-tetrahydropyridine
OCT	Ornithine carbamoyltransferase
ONL	Outer nuclear layer
OP	Oscillatory potential

OPL	Outer plexiform layer
PBS	Phosphate buffered saline
PDE	Phosphodiesterase
PEG	Poly(ethylene glycol)
PFA	Paraformaldehyde
PGA	Polyglycolic acid
PLA	Polylactic acid
PLGA	Poly(lactic-co-glycolic) acid
pNPP	*p*-Nitrophenyl phosphate
PTD	Protein transduction domain
PVA	Polyvinyl alcohol
RING	Really interesting new gene
RP	Retinitis pigmentosa
RPE	Retinal pigment epithelium
RZF	RING zinc finger
SEM	Scanning electron microscopy
TBS	Tris-buffered saline
XIAP	X-linked inhibitor of apoptosis

ACKNOWLEDGEMENTS

I owe many thanks to my supervisor, Dr. Catherine Tsilfidis, for taking me on as a student in her lab, and for her patience and guidance over the course of this project. These past two years have been a valuable learning experience, which she has made possible.

Special thanks to Dr. Mehrdad Rafat, who has been involved with the project since the early stages, in the design and synthesis of nanoparticles, as well as in providing expertise on all things chemistry.

I also wish to thank Adam Baker, for his training on many techniques and help with experiments, and Dr. Wai Gin Fong, for contributing protein stocks, and for sharing his wealth of scientific knowledge. Thanks to Dr. Brian Leonard and Dr. Michael O'Connor, for taking time out of their busy schedules to assist with *in vivo* experiments. I'd like to thank my advisory committee, Dr. May Griffith and Dr. Robert Korneluk, for their advice throughout my project.

To the members of the Tsilfidis lab, thank you for making the lab a pleasant work environment, lending an occasional hand, for sharing in the frustration when experiments go awry (and in the rejoicing when they succeed).

I am extremely grateful to my friends and family, for supporting me in all my endeavours, academic and otherwise, and for being a source of moral support when needed. Thanks to my mom, whose continued encouragement has allowed me to get to where I am today.

1. Introduction

Retinal degenerative diseases affect millions of individuals all over the world, and often result in irreversible loss of vision. The underlying causes, in many cases, are either unknown or poorly understood. Retinitis pigmentosa alone is associated with mutations in over 40 genes (Daiger, 2009). Developing a treatment based on underlying causes would constitute a task of vast proportions, and require the exact gene and mutation to be known for each patient, to select the best approach on an individual basis.

In many retinal degenerative diseases, cell-death occurs by apoptosis, a process of programmed cell-death (Travis, 1998). This common denominator presents a potentially useful tool for the prevention of retinal degenerations. Previous work in this laboratory has shown that XIAP, an inhibitor of apoptosis, can protect photoreceptors in animal models of retinal degeneration (Renwick et al., 2006; Petrin et al., 2003; Leonard et al., 2007; Zadro-Lamoureux et al., 2008). Studies to date have used an AAV vector for the long-term delivery of XIAP. Viral delivery may be effective for the treatment of progressive degenerative diseases, however in the case of acute retinal insults such as retinal detachment and retinal ischemia, photoreceptor cell death peaks within days, and a more rapid delivery is needed. Delivering XIAP in protein form, fused with a protein transduction peptide, may represent an effective alternative. However the problem of ocular delivery remains. A direct protein delivery may confer protection for a few days, but longer-term protection is preferable.

This thesis investigates the use of biodegradable nanoparticles for controlled, sustained delivery of Tat-XIAP to the retina. Protein release was evaluated both *in vitro* and *in vivo*, focusing on release profiles, cellular uptake, toxicity and *in vivo* localization.

1.1 The Retina

The retina, located at the back of the eye, is responsible for the detection of light, for transforming the sensory input into action potentials, and for relaying this information to the central nervous system. The mammalian retina is comprised of six distinct layers, containing the neurons and their dentritic and axonal projections. These are the layer of photoreceptor outer segments, the outer nuclear layer (ONL), the outer plexiform layer (OPL), the inner nuclear layer (INL), the inner plexiform layer (IPL) and the ganglion cell layer (GCL). The retina also contains one epithelial cell layer, called the retinal pigment epithelium (RPE). (Bear et al., 2007; Purves et al., 2008). Figure 1 illustrates the different layers of the retina, and the main cell types found in each layer.

Light entering the eye passes through all the neural layers, to be detected by photosensitive pigments in the photoreceptor outer segments. The ONL consists of the inner segments of the photoreceptor cells, or the cell bodies. Photoreceptors synapse with bipolar cells, which are found in the INL. Bipolar cells then synapse with ganglion cells, located in the GCL. The axons of ganglion cells extend to the central nervous system, and form the optic nerve. The INL also contains two other cell types, horizontal cells and amacrine cells, which are involved in lateral interactions. Synaptic contacts between photoreceptors and bipolar cells or horizontal cells are found in the OPL, while bipolar cells and amacrine cells synapse with ganglion cells in the IPL (Bear et al., 2007). The RPE is not involved in the detection and propagation of the visual input, but plays a role in the maintenance of the neural layers, regeneration of photopigments, and reduces light scatter at the back of the retina (Greenstein and Greenstein, 2000). The outer layers of the retina receive blood supply

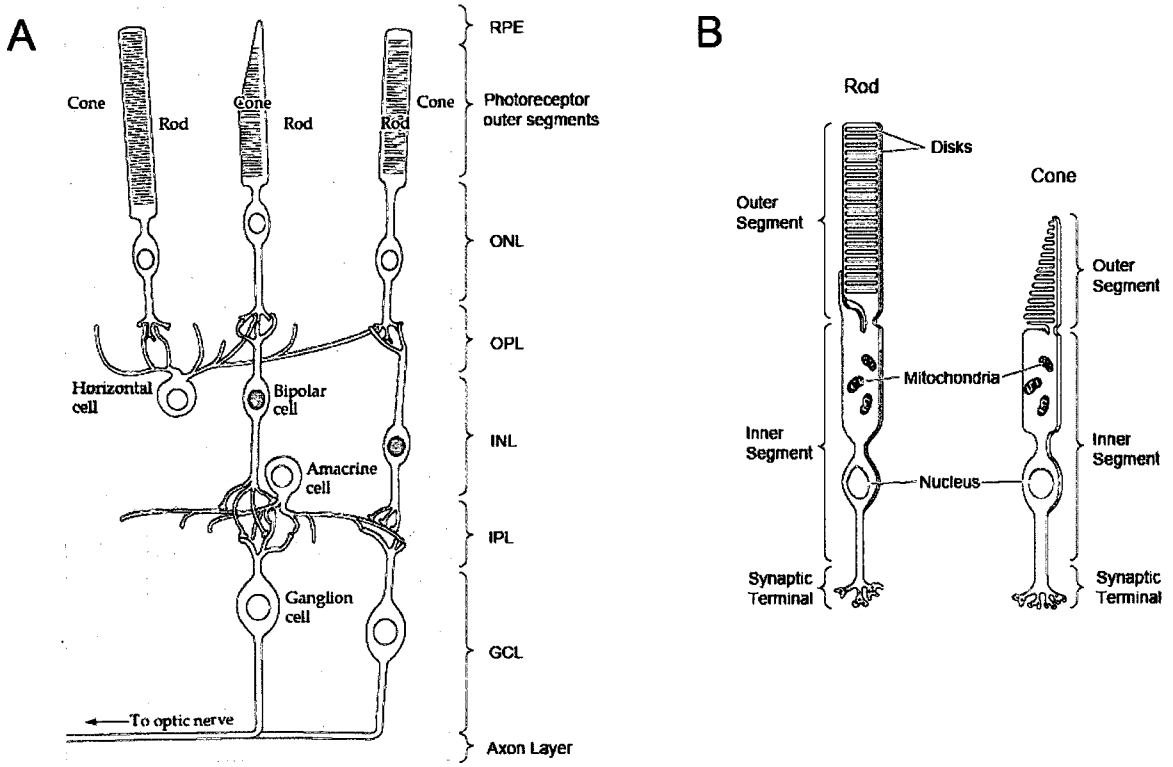

Figure 1. Layered structure and cell types of the mammalian retina. (A) Depicts the different layers of the retina: the retinal pigment epithelium (RPE), photoreceptor outer segments, outer nuclear layer (ONL), outer plexiform layer (OPL), inner nuclear layer (INL), inner plexiform layer (IPL), ganglion cell layer (GLC) and ganglion cell axons. (B) Depicts photoreceptor cell anatomy. *Modified from Purves et al., 2008.*

from the choroidal blood vessels, while the inner layers receive blood supply from the central retinal artery (Kolb et al., 2009).

1.1.1 Photoreceptors and Light Transduction

Photoreceptor cells are composed of an outer segment, filled with membrane stacks, or discs, which contain light-detecting photopigments, an inner segment, containing the cell body, mitochondria and ribosomes, and a synaptic terminal (Bear et al., 2007; Kolb et al., 2009). There are two types of photoreceptors, rods and cones, which differ in function. Rods are involved in peripheral vision, and vision under low light conditions, while cones are involved in daylight vision, colour vision and visual acuity. There are three types of cones, differing in the photopigment they contain, which each absorb a different light wavelength, and allow colour discrimination (Bear et al., 2007).

Light transduction occurs in the outer segments of photoreceptors. The photosensitive pigments consist of a protein, an opsin, and a chromophore, called retinal. Unlike most neurons, the resting potential of photoreceptors in the absence of a light stimulus is -40mV, accompanied by a constant release of neurotransmitter at the synaptic terminal (Kolb et al., 2009). When retinal absorbs a photon, it rapidly changes conformation from 11-*cis* to all-*trans*, which induces conformational changes in the opsin (Kolb et al., 2009; Nicholls, 2001). These changes lead to the activation of a G protein, Transducin, which in turns activates a cGMP phosphodiesterase. Depletion of intracellular cGMP causes cGMP-gated cation channels to close, thus ceasing normal sodium influx into the cell, and causing the membrane to hyperpolarize. A major advantage of this biochemical process is that it allows for amplification of the signal at different stages in the cascade. A conscious response to light

stimulus can be obtained from individual quanta of light (Hecht et al., 1942). Once released from the opsin, all-*trans* retinal undergoes chemical changes and is recycled by the retinal pigment epithelium. It is first reduced to all-*trans* retinol, then converted to 11-*cis* retinol by esterification, and oxidized to restore 11-*cis* retinal. It is then transported back to the photoreceptor outer segments where it is bound to a new opsin (Kolb et al., 2009).

Calcium plays an important role in photoreceptor adaptation to light. When cation channels are closed, intracellular calcium levels decrease, which leads to adaptive changes to moderate photoreceptor response to light. These include increased affinity of cGMP for cation channels, increased cGMP levels, and lowered activation of transducin (Nicholls, 2001).

1.2 Electroretinography

Retinal function can be assessed by electroretinography (ERG), which consists of recording the electrical response following light stimulation of the retina. In a clinical setting, this is typically recorded by electrodes placed on the cornea. In a full-field ERG, the response of the whole retina is recorded, and results represent an average of all the cells. The detection of potentials at the cornea is possible because of the propagation of electrical currents in the extracellular matrix. Electrical potential is recorded over time, and an ERG trace is generated (Kolb et al., 2009).

The two major waves of the ERG trace, the a-wave and the b-wave, were first reported by Gotch at the dawn of the 20th century (Gotch, 1903). A typical ERG trace is shown in figure 2. The a-wave, generated by photoreceptor cells, is the first to appear. It has a negative potential, and reflects the hyperpolarization of photoreceptors (Penn and Hagins, 1969; Brown, 1968). It can reflect either a combination of cones and rods, or cones alone, depending on adaptation conditions (Hébert and Lachapelle, 2003). The b-wave, which follows the a-wave, is positive, and believed to originate from retinal cells that are post-synaptic to photoreceptors. There is some debate regarding the specific source of the b-wave. In the 1960s, it was believed that it originated from Müller cells, retinal glial cells which span the retina, and caused by increases in extracellular potassium following neuron depolarization (Kolb et al., 2009; Miller, 1973). In the 1990s, evidence suggested that the b-wave origin lies in bipolar cells (Karwoski and Xu, 1999; Green and Kapousta-Bruneau, 1999; Masu et al., 1995). More recent studies suggest a contribution of third order neurons (amacrine and ganglion cells) to the generation of b-waves (Dong and Hare, 2000). Likely,

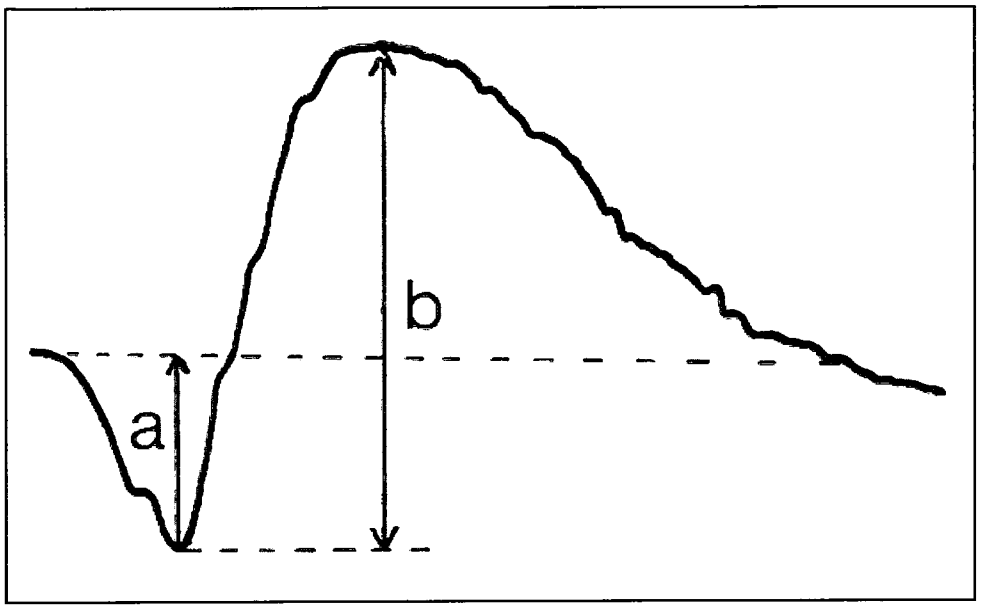

Figure 2. Typical ERG trace, depicting the negative a-wave and positive b-wave. *Modified from Kolb et al., 2009.*

the b-wave results from more than one cell type, the contributions of which have yet to be identified (Kolb et al., 2009). With longer duration light stimuli, the ERG trace can also display a c-wave and a d-wave. These do not appear in human ERGs, where rapid flashes of light are used. The c-wave originates in the RPE, and the d-wave from bi-polar cells and possible involvement of 3rd order neurons (Kolb et al., 2009). Often discernable on the ascending segment of the b-wave are oscillatory potentials (OPs), high frequency waves, which have clinical relevance because they can reflect the equilibrium between the metabolic requirements of the retina and the vascular blood supply (Kolb et al., 2009).

ERG traces can be influenced by several factors such as light adaptation, the wavelength of light stimulus, light intensity, as well as factors specific to the subject (such as age or pupil dilation). It is therefore important to perform ERGs under the same conditions when assessing changes in retinal function. ERGs are a useful tool for assessing retinal function by comparing a-wave and b-wave amplitudes, for example before and after a treatment or experimental manipulation, or to follow the progression of eye diseases. Often, b-wave to a-wave ratios are calculated, as these are less susceptible to environmental factors than amplitudes (Kolb et al., 2009).

1.3 Apoptosis

Apoptosis is a process of programmed cell-death, essential to multicellular organisms. In animals, it plays an important role in development and tissue homeostasis (Li and Yuan, 1999). It is involved in the regulation of the number of cells in adult tissues, and in the elimination of cells exhibiting abnormal behaviour (e.g. following overexpression of oncogenes) (Alberts et al., 2002). Apoptosis is characterized by a decrease in cell size, condensation of the chromatin, blebs on the membrane and the formation of apoptotic bodies, which are then eliminated by phagocytes (Kerr et al., 1972). At a cellular level, apoptosis is marked by DNA fragmentation (Nagata, 2000), and transfer of phosphatidylserine to the outer cell membrane, (which plays a role in signaling for phagocytic cells) (Schlegel and Williamson, 2001). At a molecular level the activation of apoptosis is dependant on proteases, which cleave key cellular targets. Caspases, a family of cysteine proteases, have over 100 known targets, which are cleaved near aspartate residues (Earnshaw et al., 1999; Kaufmann and Hengartner, 2001). Caspases -2, -3, -6, -7, -8, -9 and -10 are involved in the apoptotic pathways (Kaufmann and Hengartner, 2001; Strasser et al., 2000). Caspases are synthesized as precursor proteins named procaspases. These precursors are composed of an N-terminal prodomain, a large subunit containing the active site, and a small C-terminal subunit (Chahory and Torriglia, 2006; Hunter et al., 2007).

1.3.1 Apoptotic Pathways

Apoptosis can be triggered by extracellular factors through the extrinsic pathway, or intracellular factors, through the intrinsic pathway (Hunter et al., 2007). The initiation of apoptosis requires the recruitment of initiator procaspases into groups or aggregates. In the

extrinsic pathway, extracellular apoptotic factors interact with death receptors on the cell surface, such as Fas/CD95 or TNFα. These in turn recruit adaptors, which activate procaspase-8, an initiator caspase, by proteolytic cleavage between the prodomain and the large subunit. Activated caspase-8 then triggers the caspase cascade, leading to the activation of effector caspases, such as caspases-3 and -7. Effector caspases cleave target cell-death proteins, such as DNAse inhibitors or lamins. Alternately, caspase-8 can cleave Bid, a member of the Bcl-2 family (Budihardjo et al., 1999), leading to the release of Cytochrome C from mitochondria, thus recruiting the intrinsic pathway (Kaufmann and Hengartner, 2001). The intrinsic pathway can be initiated by proteolytic cleavage of Bid (Heibein et al., 2000; Stoka et al., 2001) or DNA damage (Kaufmann and Hengartner, 2001). Cytochrome C, once released from mitochondria, forms a complex with Apaf-1 and initiator procaspase-9, the apoptosome (Li et al., 1997). Recruitment of procaspase-9 to the apoptosome results in its activation, and downstream activation of effector caspases -3 and -7 (Bratton et al., 2001; Zou et al., 1999; Adrain and Martin, 2001). Downstream activation of caspases -3 and -7 is common to both the extrinsic and intrinsic pathways (MacFarlane and Williams, 2004).

1.3.2 Apoptosis in the Eye

Apoptosis is involved in the development of ocular structures, both in the anterior and posterior segments of the eye (Chahory and Torriglia, 2006). It also plays a role in the maintenance of certain ocular tissues, such as the corneal epithelium (Ren and Wilson, 1996), and is involved in corneal wound healing (Wilson et al., 2007). Many diseases of the anterior segment of the eye have been associated with apoptotic cell death, such as dry eye disease, graft rejection or cataract formation (Chahory and Torriglia, 2006). In the retina, developmental apoptosis occurs in two phases, the early phase (where cell death is mediated

by neurotrophic factors, interactions with glial cells and electrical activity) and the late phase (where cell death is mostly associated with the absence of trophic factors) (Vecino et al., 2004). Apoptosis has also been shown to be a common cell-death mechanism in retinal degenerations (Travis, 1998; Xu et al., 1996; Nickells and Zack, 1996). (Doonan and Cotter, 2004)

Photoreceptor cells are thought to have predisposing characteristics which make them susceptible to apoptotic death. Factors such as the use of cGMP-PDE as an effector molecule in the light transduction pathway, which requires elevated metabolic activity to maintain resting "dark" current might contribute to the vulnerability of photoreceptors to apoptosis (Travis, 1998). This elevated metabolism is reflected in the high numbers of mitochondria in photoreceptors, and high oxygen requirements (Steinberg, 1987). Oxidative stress can induce apoptosis through the activation of caspases as well as calpains, another family of cystein proteases (Sanvicens et al., 2004).

It has been shown that continuous light stimulation and activation of the transduction cascade can result in energy depletion, enzyme activation or inhibition, or affect signaling molecules, and thus induce apoptosis in photoreceptors. Even in the absence of light stimulation, perpetual activation of the transduction cascade can result from vitamin A deprivation (as vitamin A is a precursor of 11-*cis*-retinal) or mutations in components of the transduction cascade or in proteins responsible for recycling photopigments (Fain, 2006).

Increases in intracellular levels of calcium play a role in apoptosis induction in retinal cells, through the activation of secondary messengers, impaired electron transport (and increased levels of reactive oxygen species), DNA damage or calpain activation (Cregan et

al., 2004; Marigo, 2007). Calpains I and II are expressed in the retina (Chiu et al., 2005). Activated calpains can result in activation of caspase-12 (which can directly activate caspase-9, (Morishima et al., 2002)) or in the release of the apoptosis inducing factor (AIF) from mitochondria, thus recruiting caspase-independent apoptotic pathways (Sanges et al., 2006). Calpain involvement has been shown in models of retinal ischemia, light-induced degeneration and retinal detachment (Doonan and Cotter, 2004). Similar calpain activation can occur as a result of protein misfolding (Sanges et al., 2006).

The main excitatory neurotransmitter of the mammalian retina is glutamate (Massey, 1990). This may also contribute to photoreceptor susceptibility to apoptosis, as glutamate is often associated with excitotoxicity, where elevated neurotransmitter release or impaired reuptake from synapses result in overactivation of glutamate receptors and increased calcium influx (Cregan et al., 2004).

1.4 Inhibitors of Apoptosis

Caspase-dependent apoptosis is a very multifaceted and highly regulated pathway, involving many regulator proteins. Two families of proteins that are known to regulate apoptosis are the Bcl-2 family and the inhibitor of apoptosis (IAP) proteins. Members of the Bcl-2 family regulate the intrinsic pathway of apoptosis by mediating mitochondrial outer membrane permeabilization (MOMP) and subsequent release of intermembrane space (IMS) molecules such as cytochrome C, IAP inhibitors (eg Smac/DIABLO) or other pro-apoptotic factors (eg Endonuclease G, AIF) (Kuwana and Newmeyer, 2003). Proteins of the Bcl-2 family are characterized by the presence of Bcl-2 homology domains (BH1-4). Effectors proteins such as Bax and Bak permeabilize mitochondrial membranes by forming proteolipid pores in response to pro-apoptotic signals (Leber et al., 2007). Anti-apoptotic members Bcl-2 and Bcl-X_L prevent pore formation and block release of IMS molecules by interaction with Bax and Bak, or with their activators (Dewson and Kluck, 2009). Members of the Bcl-2 family containing only the BH3 domain regulate apoptosis by interaction with other members. Bid, for example, interacts with and activates pro-apoptotic Bax and Bak, while Bad is an inhibitor of anti-apoptotic Bcl-2 and Bcl-X_L (Letai et al., 2002). Bid, which can be proteolytically cleaved and activated by caspase-8, allows recruitment of the intrinsic apoptotic pathway by the extrinsic pathway (Li et al., 1998). Bcl-2 proteins can also indirectly regulate mitochondrial membrane permeabilization by mediating release of calcium from the endoplasmic reticulum (Scorrano et al., 2003).

IAPs are characterized by the presence of at least one baculoviral IAP repeat (BIR) domain, which is cysteine-histidine rich and of a globular structure (reviewed by Liston et al., 2003). BIR domains are not unique to IAPs, which are further characterized by their

ability to inhibit apoptosis. One member of the IAP family, the X-linked inhibitor of apoptosis (XIAP), possesses three BIR domains, a Really Interesting New Gene (RING) Zinc Finger (RZF), and an internal ribosome entry site (IRES). A functional map of XIAP is shown in figure 3. XIAP's ability to inhibit caspase activity has been attributed to the BIR domains. The BIR2 and BIR3 domains of XIAP inhibit caspases-3 and -7, and -9, respectively. Inhibition of caspase-3 and -7 by BIR2 is largely dependent on the BIR1-2 linker region (Sun et al., 1999). XIAP inhibits these two caspases by preventing the normal caspase substrates from entering the catalytic sites. Caspase-3 is inhibited by a competitive mechanism requiring only the BIR2 linker region (Huang et al., 2001), while Caspase-7 is inhibited by a competitive and a noncompetitive mechanism involving the linker region and the BIR2 domain itself (Suzuki et al., 2001a). Caspase-9 inhibition by XIAP is possible following self-cleavage of caspase-9, which enables the binding of XIAP's BIR3 domain. This induces a conformation change, which prevents homodimerization of caspase-9 and stabilizes it in an inactive state (Shiozaki et al., 2003). Through its RZF domain, XIAP can trigger ubiquitination of caspases-3 and -7 and target them for degradation by the proteasome (Suzuki et al., 2001b). XIAP can also self-ubiquinate, leading to degradation (Yang et al., 2000). The third XIAP BIR domain, BIR1, is believed to be involved in reducing XIAP self-ubiquitination, playing a role in its stabilization (Dan et al., 2004). XIAP itself is regulated by many factors, such as XAF1, Smac or Omi, which interfere with caspase inhibition (reviewed by Hunter et al., 2007).

1.4.1 XIAP gene therapy

Because of its ability to inhibit caspases-3, -7 and -9, and thus intervene in both the intrinsic and extrinsic apoptotic pathways, XIAP shows great potential for therapeutic use in

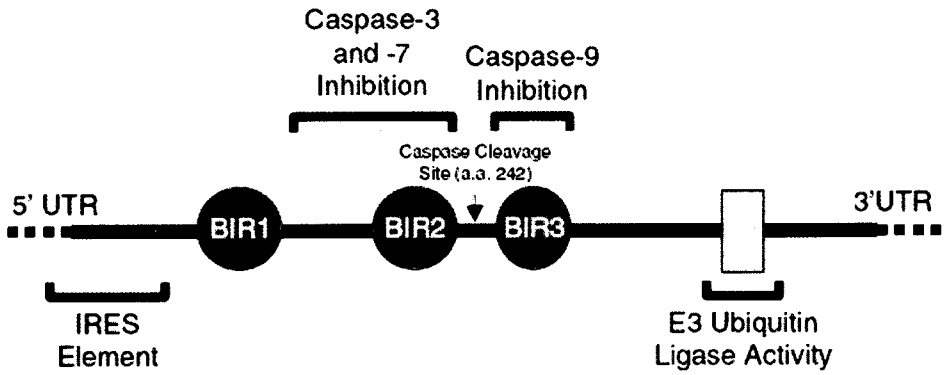

Figure 3. Functional map of XIAP activities and interactions. The 5' and 3' UTR regions are not shown to scale. BIR: baculoviral IAP repeat, IRES: internal ribosome entry site, UTR: untranslated region. *Modified from Liston et al., 2003.*

various diseases where unwanted cell-death occurs. Gene therapy opportunities using XIAP have been a popular topic of investigation in the past decade. In the brain, XIAP has been shown to protect neurons in a four-vessel occlusion global ischemia model (Xu et al., 1999), where CA1 neurons were preserved on a histological basis, and showed functional rescue. XIAP neuroprotection has also been seen in a Parkinson's disease model, in response to MPTP toxicity (Eberhardt et al., 2000; Crocker et al., 2003). In retinal disease models, XIAP protection has been shown in a hypertensive glaucoma model in the rat (McKinnon et al., 2002) and in an optic nerve axotomy model (Kugler et al., 2000).

Studies from our lab have investigated a neuroprotective role for XIAP in retinal degeneration models. In a chemically induced model of retinal degeneration using *N*-methyl-*N*-nitrosourea (MNU), injection of a recombinant adeno associated virus (rAAV)-XIAP vector resulted in fewer apoptotic (TUNEL-positive) cells in the ONL than control uninjected eyes, and even showed functional protection (Petrin et al., 2003). Similar protection in cell numbers and function was also observed in rat models of retinitis pigmentosa (Leonard et al., 2007), a genetic disease marked by progressive photoreceptor death. In a retinal ischemia model where an adeno-associated viral vector expressing XIAP was injected prior to induction of ischemia, preservation of cells in the INL of the retina and in the ganglion cell layer (GCL) was seen as well as functional protection (Renwick et al., 2006). In a model of retinal detachment, preemptive delivery of XIAP protected photoreceptors from apoptosis (Zadro-Lamoureux et al., 2009).

1.5 Cell Penetrating Peptides (CPPs)

Cell penetrating peptides, also called protein transduction domains (PTDs), are peptides that have the ability to cross cell membranes. Their ability to do so presents a potentially useful tool for the delivery of amphiphilic or large molecules or compounds to intracellular targets. Many CPPs have been identified, originating from various proteins. Some of the major families include the Tat family (Tat and its derivatives), penetratins (e.g. pAntp), chimeric CPPs (e.g. transportan) and human calcitonin (hCT)-derived peptides (reviewed by Foerg and Merkle, 2008). CPPs are typically cationic in nature, often rich in arginine residues (the number of Arg residues is believed to correlate with efficiency of transduction) (Foerg and Merkle, 2008; Wadia and Dowdy, 2002). They have been used to carry a variety of cargos, including proteins (Harada et al., 2002; Fawell et al., 1994), siRNA (Simeoni et al., 2005), DNA (Rudolph et al., 2003; Ignatovich et al., 2003) and nanoparticles (Koch et al., 2003; Lewin et al., 2000).

The Tat peptide used in this project, Tat(47-57), consists of eleven residues of the HIV-1 Tat (trans-activator of transcription) protein, YGRKKRRQRRR (Wadia and Dowdy, 2002). For the purpose of this thesis, Tat(45-57) will simply be referred to as "Tat", although several other Tat-derived CPPs exist. While early reports believed Tat transduction to be a passive process, independent of endocytosis (Vives et al., 1997; Derossi et al., 1994), these conclusions were later attributed to experimental artefacts. There is no consensus as to the mechanism by which Tat traverses cell membranes. There is evidence to support transduction by macropinocytosis (Wadia et al., 2004; Kaplan et al., 2005; Sugita et al., 2008), while other groups believe in a different, lipid-raft independent endocytic pathway (Richard et al., 2003;

Richard et al., 2005). Tat has been shown to internalize cargos as large as 100 kDa, and can be transduced into most tissues and cell types, *in vitro* (Fawell et al., 1994) and *in vivo* (Schwarze et al., 1999), with a few exceptions (e.g. cells which form tight junctions) (Violini et al., 2002). It has also been reported that Tat is more resistant to metabolic degradation than other CPPs (hCT(9-32) and penetratin) (Trehin et al., 2004). Despite many advantages, Tat does present one disadvantage for protein transduction into the cytoplasm: reports show that it eventually translocates from the cytoplasm to the nucleus along with the attached proteins (Vives et al., 1997).

To address the issue of nuclear localization, a cytoplasmic transduction peptide (CTP) was designed by Kim et al. (2006). Amino acids in the Tat sequence were substituted to eliminate the nuclear localization sequence (NLS). In culture, CTP displayed a higher transduction potential than Tat and a fully cytoplasmic localization. It was able to deliver cargo into various cell types, and internalized protein remained functional. The internalization mechanism was suggested to be independent of lipid-raft based macropinocytosis. CTP could be a promising alternative to the Tat transduction peptide for cytoplasmic targets.

1.6 Retinal Degeneration

1.6.1 Progressive Diseases

Retinal diseases such as retinitis pigmentosa (RP), glaucoma or age-related macular degeneration (AMD) are leading causes of vision loss. Retinitis pigmentosa is estimated to affect 1.5 million individuals worldwide (Foundation Fighting Blindness, 2009). It is characterized by a loss of rod photoreceptor cells, and in late stages, of cone photoreceptors. Patients initially experience a loss of night vision, gradually worsening to tunnel vision (Purves et al., 2008). RP is associated with over 40 genetic loci, and can be inherited in autosomal dominant, recessive, or X-linked fashions (Daiger, 2009; Foundation Fighting Blindness, 2009). While there are no currently available therapies to cure or slow the progress of RP, many treatment approaches are under scientific investigation. These include nutritional supplementation, growth factors, retinal transplantation, stem cell therapy, electrical stimulation and gene therapy (Rivas and Vecino, 2009). Many gene therapy approaches focus on individual genetic mutations, and would be unpractical in a clinical setting, where genetic screening would be required for each patient presenting with RP.

AMD, affecting over 800 000 Canadians, is marked by photoreceptor cell degeneration in the macula, a small area of the retina responsible for central vision and visual acuity (Foundation Fighting Blindness, 2009). While current treatments aim to reduce damaging effects of fluid and blood accumulation in the space below the macula, other approaches are under investigation, including siRNA, steroids and neurotrophic factors (Foundation Fighting Blindness, 2009; Emerson and Lauer, 2008).

Glaucoma, while not classified as a retinal degenerative disease, involves the death of retinal ganglion cells (RGCs) and vision loss (Quigley and Green, 1979). Cell death has been shown to occur via apoptosis in animal animals of glaucoma as well as in humans (Garcia-Valenzuela et al., 1995; Kerrigan et al., 1997).

1.6.2 Acute Retinal Insults

While some retinal degenerative diseases involve progressive vision loss, other retinal insults such as retinal ischemia and retinal detachment can occur unexpectedly and lead to rapid cell-death. Retinal ischemia results from reduced blood supply from the central retinal artery to the retina, which may be caused by vasoconstriction or thrombosis (Rosenbaum et al., 1997b; Rosenbaum et al., 1997a). Deprived of sufficient oxygen levels to support their high metabolic activity, cells in the ganglion cell layer (GCL), followed by the INL and the ONL, are subject to physiological changes which lead to apoptosis (Rosenbaum et al., 1997a). Cell death may be initiated within hours of the ischemic event (Kuroiwa et al., 1998). Studies into the causes of this cell death have revealed the involvement of caspase activation (Katai and Yoshimura, 1999; Singh et al., 2001). Current approaches to treat retinal ischemia are directed towards restoring normal circulation and preventing excessive damage to the retina (Renwick et al., 2006). They include laser therapy, ocular massage, anticoagulants, vasodilators and neuroprotective compounds. However existing treatments are often associated with risks, and only address certain aspects of ischemia without conferring long-term protection (Rosenbaum et al., 1997a; Rumelt et al., 1999; Seigel et al., 2000; Fontaine et al., 2002; Lafuente et al., 2002; Vallee et al., 2002). Previous work in our laboratory has shown both structural and functional protection of the retina following viral delivery of XIAP (Renwick et al., 2006).

Retinal detachment is the separation of the neural retina from the underlying retinal pigment epithelium, which results in a loss of metabolic support for the photoreceptors (Cook et al., 1995; Zacks et al., 2003). Retinal detachments can occur following trauma or ocular surgery, and are often associated with other eye diseases (Kang and Luff, 2008). They can be caused by a retinal break which allows fluid from the vitreous to infiltrate the subretinal space (rhegmatogenous detachment), fluid accumulation from behind the retina into the subretinal space (exudative detachment) or mechanical separation of the retina from the RPE (tractional detachment) (Kang and Luff, 2008; Ho et al., 2003). While timely surgical intervention and reattachment of the retina can allow partial recovery (Lewis et al., 2002), cell death by apoptosis prior to reattachment can cause irreversible vision loss, with a peak in photoreceptor apoptosis around 1-3 days following detachment (Cook et al., 1995; Arroyo et al., 2005). Assays of caspase activation following retinal detachment have shown that caspases-3, -7 and -9 are activated (Zacks et al., 2003). Viral delivery of XIAP prior to retinal detachment has demonstrated its ability to preserve photoreceptor cells in the ONL of the rat retina up to two months after detachment (Zadro-Lamoureux et al., 2008).

1.7 Ocular Drug Delivery

1.7.1 Routes of Administration

Drugs can be administered to the eye through the topical, systemic and intraocular routes. Topical administration is a common choice for drug administration to the anterior segment of the eye, as it is non-invasive and inexpensive. Administered drugs can enter the eye through the cornea, conjunctiva and sclera. However, the corneal and conjunctival epitheliums restrict drug permeability, and typically less than 5% penetrates the eye (Del Amo and Urtti, 2008; Janoria et al., 2007; Hughes et al., 2005). Of this small percentage, minute quantities reach the posterior segment of the eye. Topical administration can cause blurred vision, and requires repeated applications for long-term action. Thus, topical administration would be inappropriate for long-term delivery of drugs targeting the retina. Systemic administration also poses the problem of poor bioavailability in the retina due to the presence of the blood-retina barrier, composed of the RPE and tight retinal capillary walls (Del Amo and Urtti, 2008). To obtain adequate drug levels in the retina, frequent administration of high doses would be required, which presents risks of systemic toxicity (Duvvuri et al., 2003).

Direct intraocular delivery bypasses the barriers presented by topical and systemic administration, and allows targeted delivery to the retina. Drugs can be delivered directly into the vitreous, for example for targeting diseases affecting the inner retinal layers, such as retinal ischemia, or into the subretinal space (between the neural retina and the RPE), for example after a retinal detachment, to target photoreceptor cells. However, drugs such as proteins delivered directly into the eye typically have short half-lives. They are usually

eliminated within a few days by protein turnover, or simply by diffusion away from the site of action (Marmor et al., 1985). Where long-term action is desired, repeated intravitreal or subretinal injections would be needed. In addition to reduced patient compliance, repeated injections present risks of retinal detachment, vitreal hemorrhages, and endophthalmitis, among others (Ausayakhun et al., 2005).

1.7.2 Sustained Delivery Systems

To address the need for long-duration drug delivery in the posterior segment of the eye, several approaches to sustained delivery have been or are presently being developed. This section addresses a few of the available systems. Viral vectors, liposomes, intravitreal implants and micro- and nanoparticles are discussed, as well as advantages and disadvantages associated with each system. Other approaches include periocular delivery, cellular encapsulation and iontophoresis.

Viral vectors constitute a useful delivery tool for retinal gene therapy. Commonly used is the adeno-associated virus (AAV), which offers the advantages of high efficiency, versatility, long-term gene expression and no known adverse effects *in vivo* (Surace and Auricchio, 2008; Alexander and Hauswirth, 2008). Depending on the choice of promoter, gene expression can be modulated to target specific cell types, or to fall under the control of different factors. One disadvantage of viral delivery is the slow initiation of gene expression, which can take weeks (Surace and Auricchio, 2008). Gene upregulation is dependent on virus transduction into cells, transport to the nucleus, decapsidation, and expression of the transgene (Rabinowitz and Samulski, 2000). Another disadvantage is that once AAV has

been delivered and has spread through the retina, it cannot be switched off or removed in the event of complications with the transgene.

Liposomes are membranous vesicles, containing one or more lipid bilayers, ranging in diameter in the nanometer to micrometer scale (Del Amo and Urtti, 2008). They can be used to deliver lipophilic or water-soluble drugs, as they present hydrophobic and hydrophilic compartments (either within the membrane or in the aqueous core). Advantages of liposomes include improved drug half-life in the eye (Le Bourlais et al., 1996) and biocompatibility (Del Amo and Urtti, 2008). Liposomes present the disadvantages of being difficult to sterilize, having a short shelf life, and causing clouding of the vitreous (Del Amo and Urtti, 2008; Janoria et al., 2007).

Intravitreal implants, as their name indicates, are implanted into the vitreal cavity or through the sclera (usually called scleral plugs) for long-term drug release. Biodegradable implants are usually made of biodegradable polymers, can be hydrophilic or hydrophobic, and can be used to deliver a variety of drugs (Janoria et al., 2007). Nonbiodegradable implants require surgical removal, but can deliver drugs for longer periods and are easier to control than biodegradable implants. Intravitreal implants avoid problems caused by repeated intraocular injections, and can deliver drugs up to six months (Del Amo and Urtti, 2008). A few biodegradable implants have reached clinical trial stages, including poly(lactic-co-glycolic) acid (PLGA) implants (Seah et al., 2005; Kuppermann et al., 2007). Disadvantages associated with this technology include increased risks of cataracts, retinal detachment, vitreal hemorrhage and increased intraocular pressure (Del Amo and Urtti, 2008; Lim et al., 1999). In addition, surgical implantation and removal is invasive and does not encourage patient compliance.

Micro- and nanoparticles range in size from 1-1000 μm and 1-1000 nm, respectively. Nanoparticles, more suited to subretinal applications due to their small size, can be synthesized as nanocapsules or nanospheres. Nanocapsules consist of a polymeric shell and inner core containing the drug, and nanospheres consist of a matrix structure containing compounds either embedded in the matrix or at the surface (Sahoo et al., 2008). *In vivo*, the encapsulated drug is normally released by diffusion, chemical reaction, polymer degradation or an ion-exchange mechanism (Mainardes et al., 2005). The choice of material used to produce nanoparticles depends on various factors such as release kinetics, biodegradable properties, transparency, toxicity and minimal inflammatory response induction. Depending on the material, nanoparticles have been associated with relatively few risks compared to other sustained release systems. They can release drugs for several weeks (avoiding the need for repeated injections), bypass ocular barriers, allow delivery directly to the target, and can be injected in the subretinal space for direct action on photoreceptors (Del Amo and Urtti, 2008).

1.7.3 Polymeric Nanoparticles

Polymers such as poly(lactic-co-glycolic) acid (PLGA) and poly(ethylene glycol)-poly(lactic) acid (PEG-PLA) are a popular choice of material for nanoparticle synthesis because of their high stability *in vitro* and *in vivo*, their release profile (exhibiting a burst of release in the initial stages followed by slow, sustained release over several weeks), and FDA approval (Del Amo and Urtti, 2008). As nanoparticle degradation and protein release rates are dependent on various factors including the type of drug being released and geometry of the nanoparticles (Klose et al., 2008), as well as the material, formulation and synthesis protocol (Blanco and Alonso, 1997), there is no universal formula for synthesizing

nanoparticles with particular release kinetics. Several factors such as molecular weight, polymer and protein concentration can be modified during synthesis to influence degradation and consequent protein release. For example, when producing PLGA nanoparticles, changing the poly-lactic acid (PLA) to poly-glycolic acid (PGA) ratio can modify polymer degradation rates. This was shown in a study where the release of ovalbumin encapsulated in PLGA nanoparticles was monitored over time: PLGA 50/50 showed a higher degradation rate than PLGA 85/15 (Cao and Schoichet, 1999). Coating nanoparticles with poly(ethylene glycol) (PEG) can increase the stability of hydrophobic polymers in an aqueous (or physiological) environment, as PEG has a high hydrophilicity, chain flexibility, and absence of functional groups (Gref et al., 1995). In one study, PLGA nanoparticles in a PBS solution were shown to release close to 50% of the loaded BSA protein within the first week (Li et al., 2001), while coating the nanoparticles with PEG increased drug release to 70% in 7 days. In the case of polymeric nanoparticles, degradation of the polymer results from the hydrolytic cleavage of ester bonds. Increased PEG content on nanoparticle surfaces has been associated with increased rates of polymer degradation, probably because of increased hydrophilicity (Avgoustakis et al., 2002).

The potential for polymeric nanoparticles to deliver proteins in the eye has been shown in a few studies. One study in primates demonstrated the ability of PLGA nanoparticles to deliver drugs into the vitreous cavity. Two drugs were injected into the eye, and both were still detectable after 11 days (Peyman et al., 1992). Another study used PLA and PLGA microspheres to deliver a fluorescent dye targeting the RPE. These nanoparticles were administered subretinally, and were observed in the RPE cells for four weeks following injection (Ogura and Kimura, 1995). Interestingly, intravitreal injections of PLA

nanoparticles encapsulating Rhodamine 6G and Nile red in rats have shown an initial localization at the inner limiting membrane (INL), followed by a transretinal movement of the nanoparticles, and presence in the RPE as long as four months after injection (Bourges et al., 2003). More recently, intravitreal injections of GDNF-loaded PLGA microspheres have shown a neuroprotective effect in an rd1/rd1 mouse model of retinitis pigmentosa (Andrieu-Soler et al., 2005) and in a rat model of glaucoma (Jiang et al., 2007). In the mouse model, a delay in photoreceptor degeneration was observed, as well as increased b-wave amplitude in ERGs, suggesting both structural and functional protection of photoreceptors after a single injection of nanoparticles encapsulating neurotrophic factors. Similarly, in the rat glaucoma model, PLGA nanoparticle-delivered GDNF increased survival of retinal ganglion cells (RGCs) and showed preservation of inner plexiform layer (IPL) thickness.

1.8 Project Rationale and Overview

While it has been demonstrated that a viral delivery of XIAP can prevent cell-death in animal models of acute retinal degeneration, in the clinic a viral delivery of XIAP would be impractical. Following retinal detachment, apoptosis of photoreceptors peaks within days, and would likely precede upregulation of the transgene in an AAV vector. Thus, a new system is required to deliver high levels of XIAP in a short time. A direct delivery of XIAP, combined with a transduction signal for cellular uptake seems a favorable solution. However, protein degradation and diffusion away from the target site would warrant repeated injections, which would decrease patient compliance and increase risks of complications.

The current project investigated the use of biodegradable polymeric nanoparticles for the encapsulation and sustained delivery of Tat-XIAP. The main objective was to develop a formulation that can release protein for up to two months. Experiments were conducted with Tat-EGFP, more readily available, and easier to detect using fluorescence and immunological techniques than Tat-XIAP. Various formulations were designed and *in vitro* release kinetics were established. The effect of sonication on nanoparticle size, dispersion and release as well as on protein function was assessed. Tat-EGFP release and cellular uptake were assessed *in vitro* in two different cell types. *In vivo* experiments were conducted to determine Tat-EGFP release and tropism, and to test for any signs of toxicity or effects on retinal function (determined by electroretinography).

2. Procedures

2.1 Nanoparticle Design and Synthesis

For the current project, one formulation of PLGA nanoparticles (NP1) and six formulations of PEG-PLA nanoparticles (NP2-NP7) were designed and synthesized by Dr. Mehrdad Rafat, Ph.D. (Post-Doctoral Fellow, University of Ottawa Eye Institute). The different formulations are summarized in Table I. All PLGA and PEG-PLA nanoparticles were prepared by a water/oil/water (W/O/W) double emulsion solvent evaporation method as established by McGinity and O'Donnell (1997).

PLGA nanoparticles (NP1) were prepared from PLGA (50/50) and loaded with 1 mL of a 1.5 mg/mL Tat-EGFP solution. Their preparation involved the dispersion of the (aqueous) protein solution in 5mL of a 2% polymer solution by sonication/homogenization. The resulting primary emulsion was poured into a 0.4% aqueous poly-vinyl alcohol (PVA) solution and homogenized to form a secondary emulsion. The secondary emulsion was then poured into another solution of 0.2% PVA and stirred for 1 h for stabilization, followed by a vacuum extraction to evaporate the organic solvent. The hardened micro/nanospheres were collected by centrifugation, washed 3 times with deionized water or PBS, freeze-dried, and stored at 4°C.

Six different formulations of PEG-PLA nanoparticles were developed (NP2-NP7). Tat-EGFP at 3mg/mL or 6mg/mL in PBS was dispersed in 6mL of a 2% or 4% w/v solution of PEG-PLA by sonication (see Table I for specific conditions of each formulation). The resulting primary emulsion was poured into 40 mls of 1% aqueous PVA solution,

Table I. Summarized composition of nanoparticle formulations.

	Material	PEG MW (kDa)	Protein Concentration (mg/mL)	Polymer Concentration (%)
NP1	PLGA	NA	1.5	3
NP2	PEG-PLA	1	1.5	2
NP3	PEG-PLA	5	1.5	2
NP4	PEG-PLA	1	3	2
NP5	PEG-PLA	1	3	4
NP6	PEG-PLA	1	6	2
NP7	PEG-PLA	1	6	4

homogenized to form a secondary emulsion, and stirred for 3 hours for stabilization of the particles and evaporation of the organic solvent. The solidified particles were centrifuged and washed three times with PBS, frozen at -20 °C overnight, lyophilized for 7 hours and stored in 4 °C until used.

2.2 Characterization of in vitro Tat-EGFP Release

To monitor Tat-EGFP release, freeze-dried nanoparticles were resuspended in DMEM high glucose media (HyClone), supplemented with 10% heat-inactivated fetal bovine serum (HyClone or Biowest), 10000 units/mL Penicillin and 10 mg/mL Streptomycin (Gibco), 2mM L-glutamine (Gibco) and 1mM sodium pyruvate (Sigma) (supplemented medium will hereafter be referred to as "culture medium"). Nanoparticles were resuspended at 10mg/mL by sonication using a Microson^{TM} XL sonicator (Misonix) at a power output of 3W for 45 seconds or 10W for 180 seconds. Samples, in 2mL microcentrifuge tubes, were incubated at 37°C with agitation to allow protein release over time.

Tubes were spun at 15k rpm in a microcentrifuge for 10 minutes, and the supernatant was read for EGFP fluorescence at 509 nm following excitation at 480 nm with a BioTek® Synergy HT plate reader. A 10% aliquot of NP1 samples was spun down, the supernatant removed and analyzed. The pelleted particles were resuspended in an equal volume of fresh medium and returned to the original tubes. For later formulations (NP2 and onwards), the entire sample was centrifuged, the full supernatant was removed for analysis and replaced with fresh medium. Negative controls consisted of tubes of medium devoid of nanoparticles (subject to the same incubations). Positive controls consisted of a 0.5 μg/mL solution of Tat-EGFP in medium. For nanoparticle formulations NP1 to NP3, samples were taken at

irregular intervals, every few hours for the first day, then every 2 to 3 days. For formulations NP4-NP7, sampling time points were fixed at 3 hrs, 6 hrs, 24 hrs, and every 3 days for up to 31 days. Tat-EGFP was quantified by referencing fluorescence readings to a linear standard curve generated from known Tat-EGFP concentrations.

To obtain more accurate data, samples from formulations NP5 and NP6 were also analyzed for Tat-EGFP content by an Enzyme-linked immunosorbent assay (ELISA). The Abcam® sandwich ELISA protocol was followed. A polyclonal goat anti-GFP antibody (Abcam) at a concentration of 1ug/mL in a carbonate/bicarbonate buffer (pH 7.4) was used as a capture antibody. The detection antibody used was a rabbit anti-GFP IgG fraction (Invitrogen) diluted 1/1000, and the secondary antibody was an alkaline phosphatase-conjugated goat anti-rabbit IgG (Jackson ImmunoResearch) at 1/5000. A 1% BSA solution was used as a blocking agent. Detection was performed by adding 100 μL substrate (pNPP, Calbiochem) dissolved in the appropriate buffer to each well, and incubating for 15-60min. The reaction was stopped by adding 100 μL 1N NaOH, and absorbance was read at 405 nm. Protein was quantified by referencing to standards of known concentrations.

2.3 Microscopy

2.3.1 Scanning Electron Microscopy (SEM)

Morphology of the freeze-dried PEG-PLA nanoparticles was investigated at Health Canada by Dr. Merhdad Rafat using a scanning electron microscope (SEM, Model S-2250N, HITACHI, Japan). The particles were mounted on metal holders using a conductive double-sided tape, and sputter coated with a gold layer for 60 seconds at 0.1 bar vacuum pressure.

2.3.2 Immunofluorescence and Phase Contrast Microscopy

In experiments testing the effect of sonication on particle size and morphology, nanoparticles were visualized by inverted fluorescence microscopy (excitation at 495nm, emission at 519nm) using a Nikon Eclipse TE2000-E microscope equipped with a DXM1200C Nikon digital camera (Nikon, Japan). Observations in early experiments assessing cellular uptake of released Tat-EGFP by human embryonic kidney cells (HEK293A) were conducted by phase contrast and inverted fluorescence microscopy.

In all experiments involving immunocytochemistry or immunohistochemistry (cellular uptake of Tat-EGFP and CTP-EGFP, and *in vivo* experiments), observations were made by brightfield fluorescence microscopy (excitation at 495nm, emission at 519nm) using a Zeiss Axioskop 2 microscope equipped with an AxioCam HRc digital camera (Carl Zeiss, Germany).

2.4 Effect of Sonication on Nanoparticles and Protein

Further experiments were conducted on nanoparticles of the NP6 formulation to determine the ideal sonication duration and intensity for optimal nanoparticle redispersion, as well as assess effects of sonication on *in vitro* protein release and function. This involved sonicating particles at different intensities (varying from 3W to 10W) and durations (from 45s to 180s), followed by assessing particle size and morphology, *in vitro* release profiles and Tat-EGFP fluorescence.

2.4.1 Effects on Particle Re-Dispersion

Nanoparticles were re-dispersed in PBS by sonication for 45 s at a power output of 3W, 100s at a power output of 10W or for 180s at a power output of 10W. Particles were visualized by inverted fluorescence microscopy.

2.4.2 Effects on in vitro Release

Two samples of freeze-dried nanoparticles of the NP6 formulation were resuspended by sonication for 25s at a power output of 3W or 180s at a power output of 10W. Release was assessed as previously described in section 2.2.

2.4.3 Effects on Protein Function

Tat-EGFP protein was diluted in PBS to a concentration of 2μg/mL and sonicated either 45s at a power setting of 3W, 100s at 10W or 180s at 10W. Protein fluorescence was read at 509 nm following excitation at 480 nm with a BioTek® Synergy HT plate reader. Fluorescence readings were referenced to a standard Tat-EGFP curve to estimate concentration.

2.5 Tat-EGFP Release in Cell Culture

In early experiments, 293A human embryonic kidney cells were plated in 6-well culture plates, and incubated at 37 °C in culture medium. The following day, medium was replaced with a suspension of Tat-EGFP loaded PEG-PLA nanoparticles (NP3 formulation) at 500 μg/mL or 100 μg/mL in culture medium. Controls were cells cultured in medium devoid of particles (negative), and Tat-EGFP at 100μg/ml Tat-EGFP (positive). Cellular

uptake of released Tat-EGFP was assessed by washing the cells in PBS, replacing with medium to maintain membrane integrity, and observing live cells by phase contrast and inverted fluorescence microscopy. Cells were observed after 3hrs, 6hrs, 24hrs and 48hrs of incubation with nanoparticles.

In subsequent experiments, 661W mouse cone-derived cells were cultured in 24-well plates on microscope cover glass, and incubated at 37°C in culture medium. The following day, medium was replaced with a suspension of PEG-PLA nanoparticles (NP6 formulation) at 500 μg/mL or 100 μg/mL in culture medium. Controls were cells cultured in medium devoid of nanoparticles (negative) and cells cultured in medium containing 50 μg/mL Tat-EGFP (positive). Cellular uptake of released Tat-EGFP protein was assessed by immunocytochemistry. After 1 hour, 1 day, 2 days and 4 days of incubation with nanoparticles, cells were washed with PBS and fixed in 4% PFA for 5 minutes (Paraformaldehyde, Acros) in PBS, followed by four 5 minute washes in PBS. Cells were incubated overnight at 4°C with primary antibody (1/1000 anti-GFP rabbit IgG fraction (Invitrogen) with 100 μg/mL BSA, 1% goat serum and 0.2% Triton X-100). Cells were then washed in PBS and incubated with secondary antibody (Alexa fluorophor 488 goat anti-rabbit IgG (Molecular Probes)) for one hour at room temperature, with agitation. Cells were washed four more times in PBS, and counterstained with 1/2000 DAPI during the second wash. Cover glasses were then mounted on slides with Antifade (50:50 PBS:Glycerol (Fisher Scientific) with 1% N-propyl Gallate (Sigma)). Images were taken by fluorescence and brightfield microscopy.

2.6 Cellular uptake of Tat-EGFP and CTP-EGFP protein

293A human embryonic kidney cells were plated in a 12-well culture plate with microscope cover glasses, and incubated at 37°C in cell culture medium. On the following day, medium was replaced with fresh medium containing Tat-EGFP protein or CTP-EGFP protein at concentrations of 12.5 μg/ml, 25μg/ml, 50 μg/ml and 100 μg/ml, to compare cellular localization of the two transduction domains. Fresh culture medium (without protein) was used as a negative control. After a 24-hour period, these cells were fixed and immunocytochemistry was performed as previously described in section 2.5. Cells were also incubated with protein concentrations of 50 μg/ml and 100 μg/ml for 48 hours. This experiment was performed both with plates coated with poly L-lysine and with uncoated plates. Images were taken by fluorescence microscopy.

2.7 Characterization of in vivo Tat-EGFP Release

2.7.1 Subretinal Injections

Tat-EGFP-loaded PEG-PLA nanoparticles (NP6 formulation, 6 mg/mL Tat-EGFP) were suspended in sterile PBS at a concentration of 10 mg/mL by sonication for 160s at 10W. Injections were carried out in the left eye of 18 female Long-Evans rats. Six animals were injected with PEG-PLA nanoparticles (NP6 formulation, 6mg/mL Tat-EGFP), six with empty nanoparticles (devoid of protein) of the same composition, and six with an AAV-CBA-GFP viral construct at 5.6×10^{13} particles/mL. The right eyes were uninjected controls. Animals were placed under isofluorane anesthesia for the injection procedures. An incision was made in the sclera with a 20 gauge V-lance ophthalmic knife, through which a Hamilton

Syringe was inserted, passed around the lens and through the retina to inject a 2μL suspension of nanoparticles or virus in the subretinal space. One week post-injections, observations were carried out by retina specialist Dr. Brian C. Leonard (University of Ottawa Eye Institute) to detect signs of retinal detachment, cataract development or any other abnormalities. 3 weeks and 9 weeks post-injection, fundus images were taken of a subset of injected eyes, using the Retcam II wide-field digital imaging system (Clarity Medical Systems) with the assistance of ophthalmologist Dr. Michael O'Connor (University of Ottawa Eye Institute).

2.7.2 Electroretinography (ERG)

Scotopic/photopic ERGs were generated using the ESPION system (Diagnosys LLC, Littleton, MA). Before performing ERGs, rats were dark-adapted overnight. Animals were placed under anesthesia by intraperitonial injection of 30 mg/kg ketamine hydrochloride (Bimeda-MTC, Cambridge, ON) and 0.5 mg/kg medetomidine hydrochloride (Domitor, Novartis, Finland). Metedomidine was reversed after one hour using 1 mg/kg of atipamezole hydrochloride (Antisedan, Novartis, Finland). One drop of each 1% tropicamide (Mydriacyl, Alcon Canada), 2.5% phenylephrine hydrochloride (Mydfrin, Alcon Canada) was administered to each eye 10-15 minutes before tests to dilate the pupils, and one drop 0.5% proparcaine hydrochloride (Alcaine, Alcon Canada) as a topical anesthetic. Silver wire loop electrodes were placed on the cornea of each eye, and a drop of 0.3% hypromellose (GenTeal, Novartis Pharmaceuticals) was added to maintain proper hydration. A gold minidisc reference electrode was placed on the tongue, and a ground needle electrode in the tail. Animals were subject to a single flash light stimulus of 4ms duration at 11 intensities increasing from 0.001 cd.s/m^2 to 25 cd.s/m^2, from a Ganzfeld dome placed above the head.

For each intensity step, five recordings were generated and averaged. Data analysis was performed using MS Excel software, and one-way analysis of variance (ANOVA) was performed to establish significance between treated and untreated eyes.

2.7.3 Sampling and Tissue Processing

Animals were sacrificed and the eyes sampled at 9 weeks post-injection. Rats were injected intraperitoneally with euthansol (pentobarbital sodium) and trans-cardially perfused with 4% PFA for tissue fixation. The eyes were scored with a white-hot 18-gauge needle before their removal to facilitate orientation during embedding. After enucleation, the cornea was punctured, and the eyes were placed in 4% PFA for one hour. Eyes were then washed three times in PBS. Incisions were made in the corneas to remove the lenses, and the eyes were placed in 30% sucrose and left at 4°C until saturated. The eyes were then placed in a 50:50 mixture of 30% sucrose-OCT compound and left to equilibrate for 1 to 2 hours at 4°C. The left and right eyes from each rat were placed in plastic molds filled with 50:50 sucrose:OCT, cornea side up, and aligned by their score mark. The mold was lowered onto a Petri dish floating on liquid nitrogen for freezing. Frozen molds were stored at -80°C until use. Cryosections (10 μm) were prepared using a Shandon Cryotome E cryostat (Thermo Scientific). Sections were air dried for 2 hours, and stored at -20° with desiccant.

2.7.4 Immunohistochemistry

Immunohistochemistry was performed on cryosections using rabbit anti-GFP IgG fraction (Invitrogen) as a primary antibody, and Alexa Fluor 488 goat anti-rabbit antibody (Molecular Probes) as a secondary. Slides were pre-fixed in 4% PFA for 3 minutes, and blocked in 1% BSA in TBS with 5% goat serum for 30 minutes. They were incubated in a

humidified chamber at 4°C overnight with the primary antibody (1/200 in block solution with 0.3% Triton X-100, (Sigma)), and for 60 min at room temperature with the secondary antibody (1/200). All washes were done in TBS. Slides were counterstained with DAPI in the final washes, and mounted with coverslips in Antifade. Stained sections were observed by fluorescence microscopy.

3. Results

3.1 In vitro Assessments

3.1.1 Release Profiles

Poly(Lactic-co-Glycolic) Acid (PLGA) nanoparticles (NP1 formulation) suspended in culture medium yielded a very slow Tat-EGFP release over 14 days (a total of 17 ng of protein released per mg of nanoparticles), and no initial burst effect was observed (Fig. 4). In order to determine whether these protein levels reflected an accurate release by the nanoparticles or were affected by rapid protein degradation in the culture medium, controls were run simultaneously that contained pure Tat-EGFP protein suspended in culture medium at a concentration of 1.5 μg/mL. These controls assessed protein stability over time. A gradual decrease in Tat-EGFP fluorescence was seen in the control, suggesting slow protein degradation in the culture medium.

Protein release from PEG-PLA nanoparticles was assessed using two formulations differing in polymer molecular weight. The first formulation (NP2) was made using a 1 kDa PEG molecular weight, and the second (NP3) using a 5 kDa PEG molecular weight. For both formulations, a 5 kDa PLA molecular weight was used. In both cases, nanoparticles released Tat-EGFP rapidly for the first 24 hours, followed by very slow, gradual release (fig. 5). The rate of release after the first 24 hours for the NP2 nanoparticle formulation was higher than that of the NP3 nanoparticles (21.2 ng per day per mg of NP2 nanoparticles vs. 12.8 ng per day per mg of NP3 nanoparticles). Overall, PEG-PLA nanoparticles released Tat-EGFP at considerably higher levels than PLGA nanoparticles, and showed an initial burst effect, thus appear better suited for the delivery of proteins at therapeutic levels in the eye.

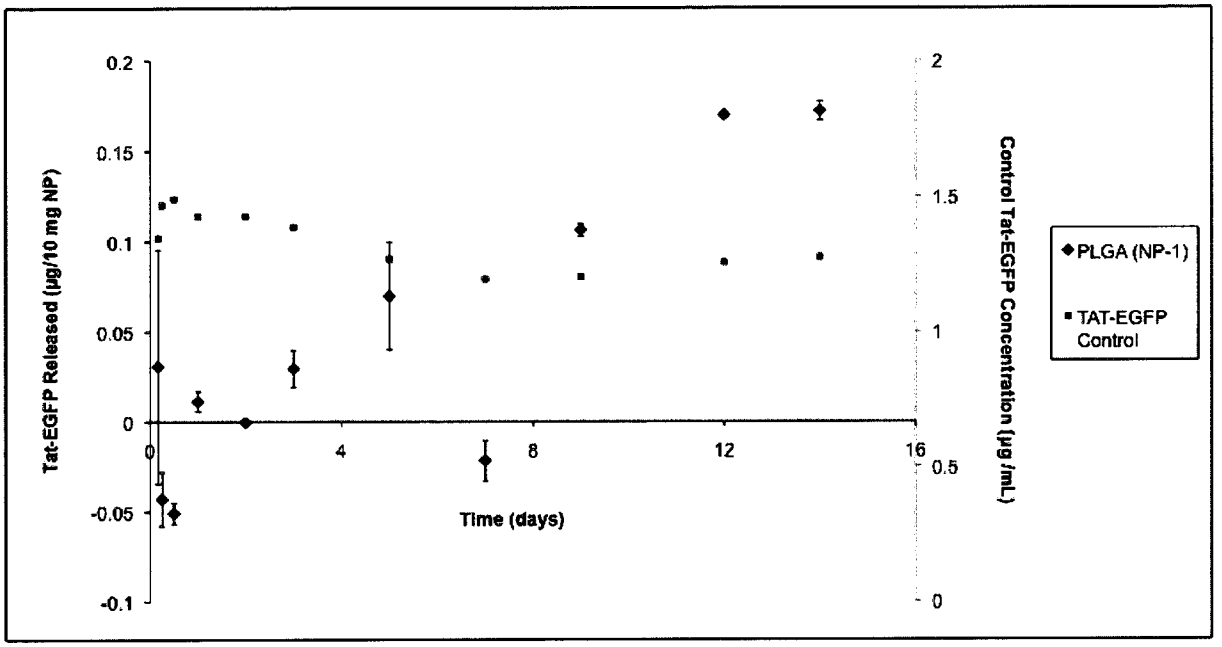

Figure 4. Cumulative *in vitro* release of Tat-EGFP from PLGA nanoparticles over a period of 14 days. EGFP release at each time point was assessed by measuring fluorescence at 509 nm following excitation at 480 nm, and referencing fluorescence readings to Tat-EGFP standards of known concentration. A solution of Tat-EGFP at 1.5 µg/mL in culture medium was used as a control to monitor protein degradation (shown on the secondary axis). Data shown is an average from two replicates along with standard error. By 14 days, only 58 ng per 10 mg of nanoparticles was released.

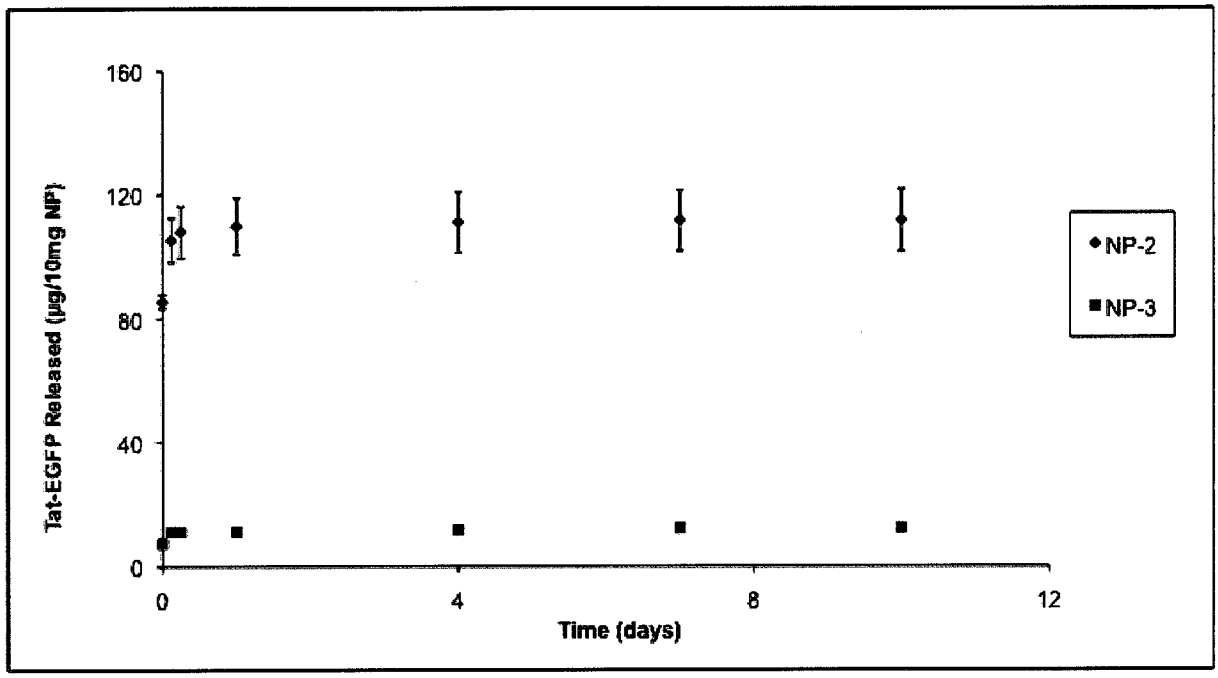

Figure 5. *In vitro* cumulative release of Tat-EGFP from NP-2 (1kDa PEG) and NP-3 (5kDa PEG) PEG-PLA nanoparticles. Tat-EGFP release in culture medium was assessed by measuring fluorescence as described. The mean from 3 replicates is shown at each time point along with standard error.

Between the two molecular weights assessed, NP2 nanoparticles had the higher total yield, a higher rate of release and had a lower tendency to aggregate in solution. Further experiments with PEG-PLA nanoparticles were therefore based on the NP2 formulation (with a 1 kDa PEG molecular weight).

Further modifications to PEG-PLA nanoparticle formulations were carried out to optimize the initial burst as well as the subsequent rate of protein release. Four new formulations were designed, modifying polymer and protein concentration, and subsequently assessed for *in vitro* protein release. These formulations are summarized in Table I. Release from all four nanoparticle formulations presented an initial burst, followed by sustained release for up to 31 days (fig. 6a). The NP6 formulation yielded the highest total amount of protein over 31 days, presented the highest initial burst, and the second highest rate of release after the first 24 hours. On the other hand, the NP5 formulation presented the highest rate of sustained release after the first 24 hours (0.029 μg per day, per 10mg of nanoparticles). Nanoparticles with a NP6 formulation also aggregated less in solution than other formulations. To obtain more precise data, protein content for samples of the NP6 and NP7 formulations was measured by enzyme-linked immunosorbent assay (ELISA). While protein levels deteted by ELISA were higher than by fluorescence, overall trends were the same (fig. 6b).

3.1.2 Scanning Electron Microscopy (SEM)

SEM images of nanoparticle formulations NP4 to NP7 are shown in figure 7. These show that increasing protein concentration from 3mg/mL to 6mg/mL resulted in smaller sized particles (when comparing formulations NP4/NP6 and NP5/NP7). Comparing

A

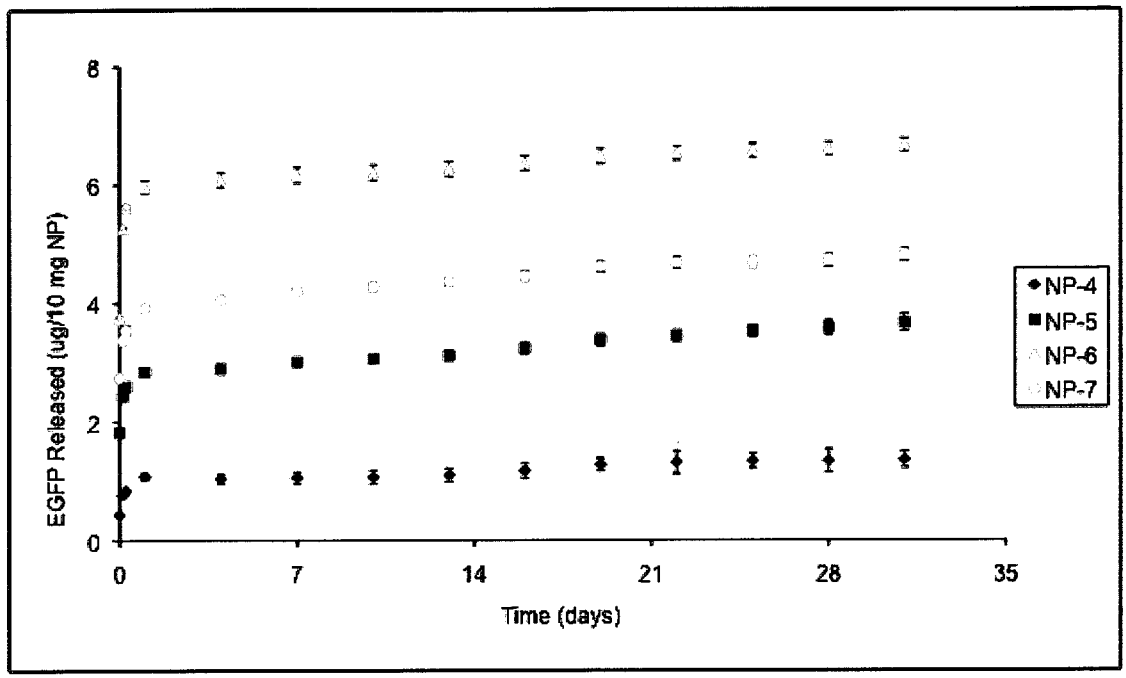

B

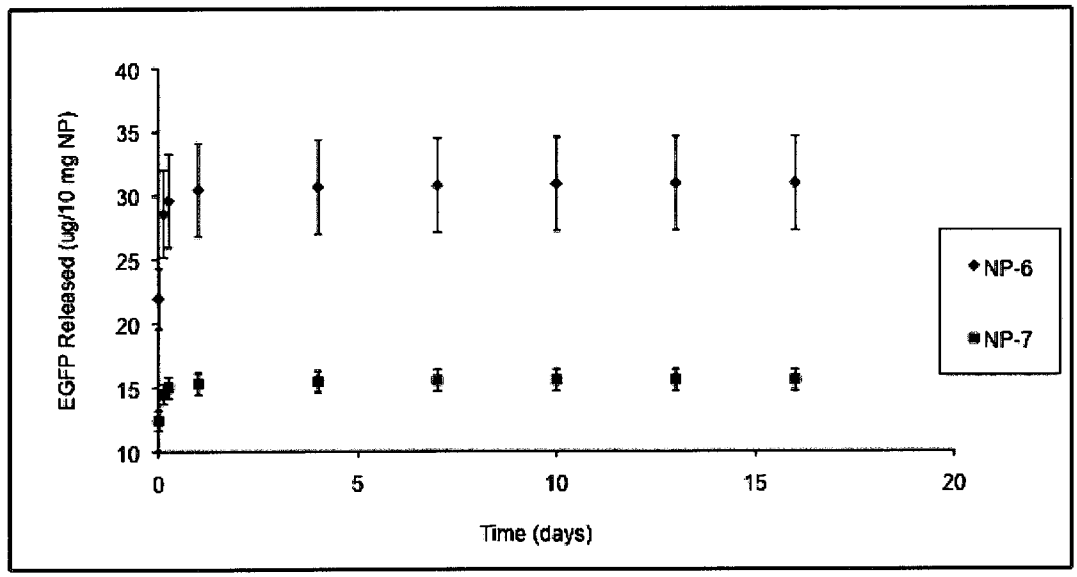

Figure 6. Cumulative *in vitro* release of Tat-EGFP from four formulations of PEG-PLA nanoparticles of varying protein and polymer concentrations. Tat-EGFP release of formulations NP4 (3 mg/mL Tat-EGFP, 2% PEG-PLA), NP5 (3 mg/mL Tat-EGFP, 4% PEG-PLA), NP6 (6 mL/mg Tat-EGFP, 2% PEG-PLA) and NP7 (6 mg/mL Tat-EGFP, 4% PEG-PLA) at each time point was assessed by measuring fluorescence (A) and by ELISA (B). The mean from 3 replicates is shown at each time point along with standard error. All release profiles show an initial burst, followed by sustained release for as long as 31 days (when the experiment was terminated).

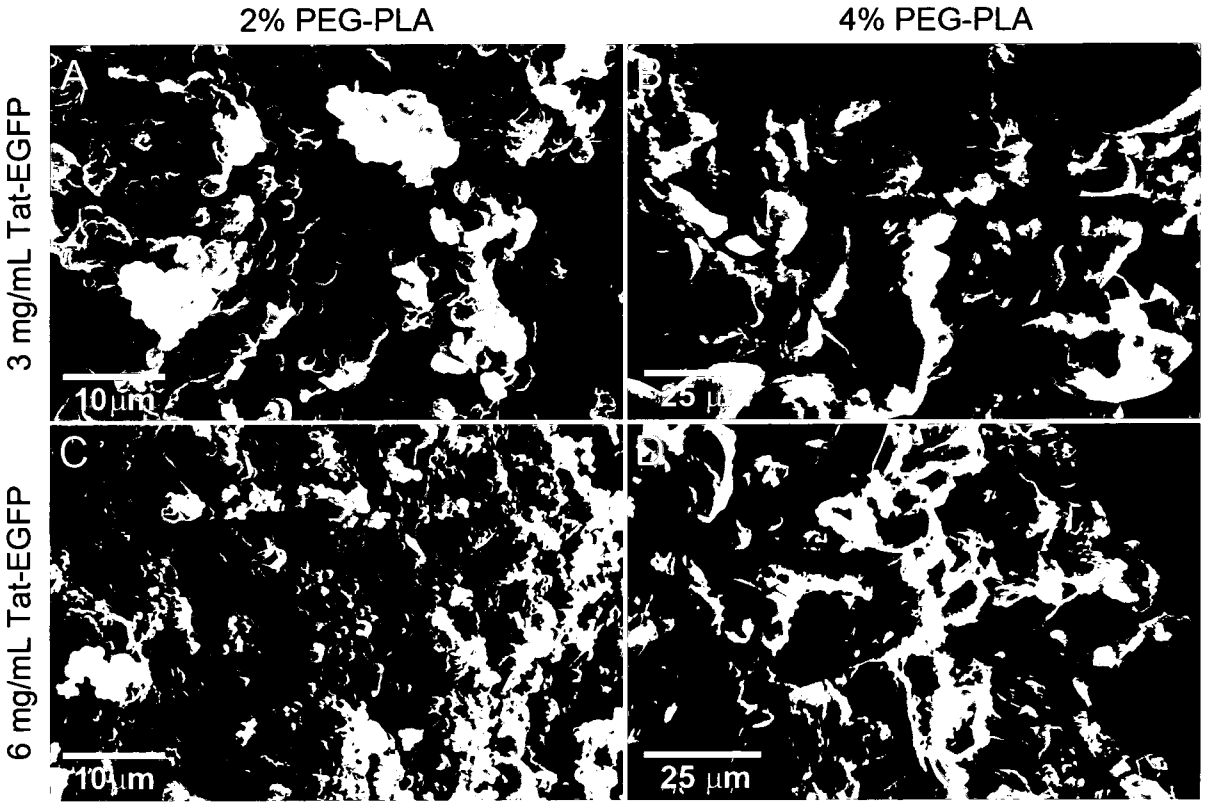

Figure 7. Scanning electron microcscopy imaging of select nanoparticle formulations. Particles of formulations NP4 (A), NP5 (B), NP6 (C) and NP7 (D) were mounted on metal holders, coated with a layer of gold and observed by SEM to determine size and morphology. SEM shows that the smallest nanoparticles (NP7) are formed by the higher protein concentration and lower polymer concentration. *Images taken by Dr. Mehrdad Rafat, Ph.D. (Post-Doctoral Fellow, University of Ottawa Eye Institute).*

formulations of a given protein concentration while varying polymer concentrations, however, reveals that increases in polymer concentration (from 2% to 4%) result in irregularly shaped, larger particles. Results altogether show that both protein and polymer concentrations have an impact on particle size and morphology. The NP6 formulation was chosen as an optimal formulation for subsequent tests as it yielded the highest total protein levels *in vitro* and presented the best particle size and morphology.

3.1.3 Effect of Sonication Duration and Intensity

The effect of sonication duration and intensity during resuspension on particle size and on release kinetics was also addressed. Fluorescence microscopy images of NP6 PEG-PLA nanoparticles sonicated at different power settings and for different durations show that higher sonication intensity and duration result in smaller, less aggregated nanoparticles (Fig. 8). To determine the effect of sonication duration and intensity on release kinetics, two sets of NP6 nanoparticles were suspended by sonication, one for 25 seconds at a power output setting of 3W and the other for 180 seconds at a power setting of 10W. Release from both sets was then assessed as previously. While longer, more intense sonication resulted in a higher initial burst (about 2-fold higher), there was little effect on long-term release of Tat-EGFP (Fig. 9). Particles sonicated at a power output of 3W for 25 seconds released protein at 13.2 nm per day per 10mg of nanoparticles, compared to 12.3 ng for particles sonicated at a setting of 10W for 180 seconds. For all further experiments, nanoparticles were resuspended by sonication at a power setting of 10 for 180 seconds.

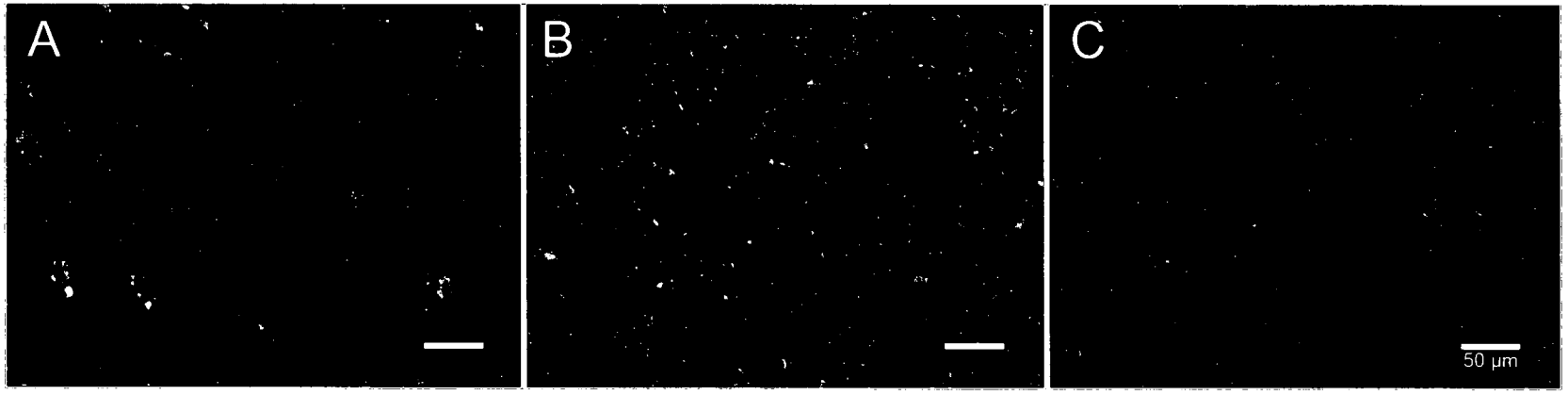

Figure 8. Effect of sonication time and power on aggregation and size of redispersed nanoparticles. Freeze-dried nanoparticles were resuspended at 6mg/mL in PBS by sonication. Different sonication times and powers were compared. (A) duration: 45 s, power: 2W. (B) duration: 100 s, power: 10. (C) duration: 180 s, power: 10. Resuspended spheres were visualized by fluorescence microscopy. Higher sonication times and power yielded smaller, less aggregated particles.

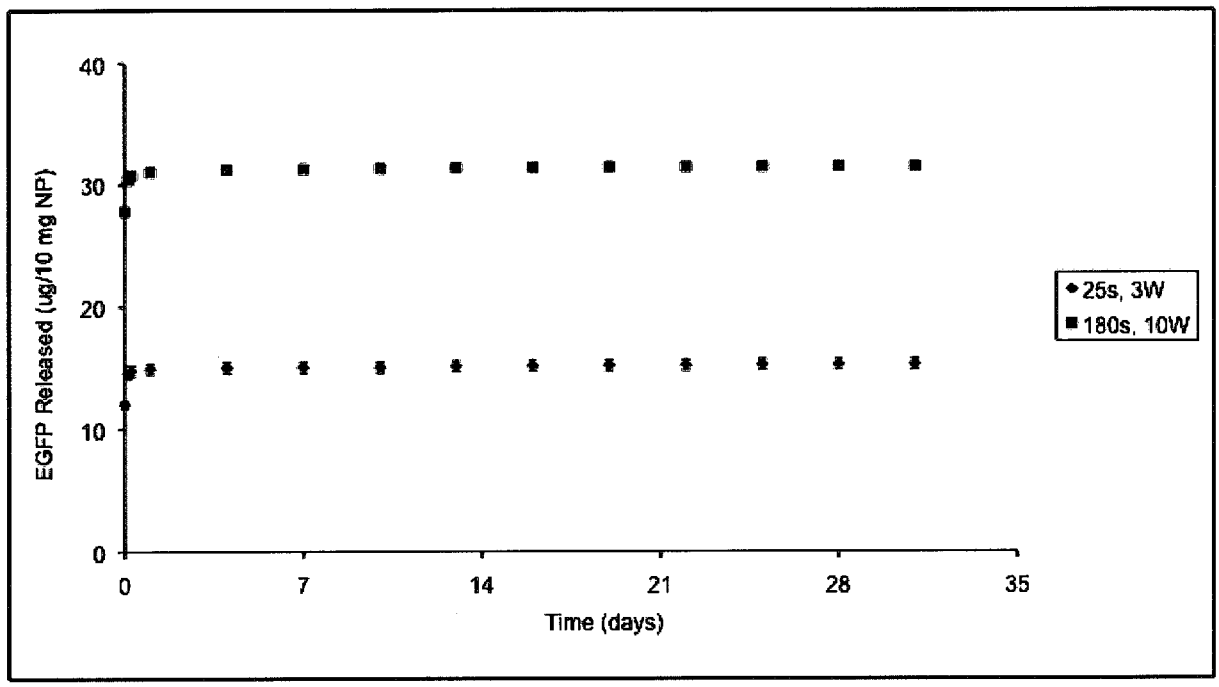

Figure 9. Effect of sonication time and power output on Tat-EGFP release from PEG-PLA nanoparticles. Tat-EGFP release at each time point was assessed by measuring fluorescence as described. The mean from 3 replicates is shown at each time point The cumulative Tat-EGFP release of 1K-6-2 nanoparticles with two different sonication times and power are shown. Both profiles show an initial burst, followed by sustained release for at least 31 days. Nanoparticles sonicated at a 10W power output for 180s show a higher release burst, but a comparable long-term rate of release to those sonicated at a 3W power output for 25s.

To establish whether sonication affects protein function, Tat-EGFP protein samples were sonicated for different time durations and at different intensities. EGFP fluorescence after sonication was used as a measure of protein function. Readings were referenced to a standard curve to quantify protein. Protein amounts detected are shown in Table II. Sonication significantly affected protein fluorescence. Barely any protein can be detected by fluorescence for both samples sonicated at a power output of 10W.

3.2 Cellular Uptake of Tat-EGFP in Culture

3.2.1 Human Embryonic Kidney (HEK293A) Cells

Early experiments assessed the cellular internalization and localization of EGFP constructs containing two different protein transduction domains, Tat and CTP, into cultured human embryonic kidney (HEK293A) cells. Cells were incubated 48 hours with a 50 μg/mL suspension of either Tat-EGFP or CTP-EGFP protein, then fixed and stained. Cells incubated with Tat-EGFP revealed a strong EGFP signal in the cytoplasm, while cells incubated with CTP-EGFP did not show any EGFP internalization (fig. 10). Accordingly, the Tat-EGFP construct was used for all further experiments requiring cellular internalization of Tat-EGFP. Human embryonic kidney (HEK293A) cells were incubated with Tat-EGFP loaded PEG-PLA nanoparticles of the NP6 formulation, to assess cellular uptake and interactions of cells with nanoparticles after different incubation times. At various time points, cells were directly observed by fluorescence microscopy. Fluorescence and brightfield images of these cells are shown in figure 11. As early as 6 hours after the introduction of nanoparticles into the culture medium, a GFP signal associated with the cells could be seen, suggesting that nanoparticles have an affinity to the cells or cell membranes, or are being internalized by cells. This signal

Table II. Effect of sonication time and intensity on Tat-EGFP fluorescence. Samples of Tat-EGFP were sonicated in triplicates under the specified conditions and EGFP fluorescence read as a measure of function. Fluorescence readings were referenced to a standard curve to estimate functional protein amounts.

Sonication conditions	Fluorescence reading	Functional protein amount (μg/mL)	Average amount detected (μg/mL)	Percentage relative to total protein (%)[a]	Standard deviation
45s 3W	2501	1.224	1.211	49.93	0.024
	2505	1.226			
	2418	1.183			
100s 10W	21	0.010	0.024	0.98	0.017
	89	0.043			
	36	0.018			
180s 10W	13	0.006	0.004	0.18	0.008
	23	0.011			
	-9	-0.004			
No sonication	4956	2.425	2.425	100.00	0.082

[a] Total amount is the amount of protein detected in the control non-sonicated sample

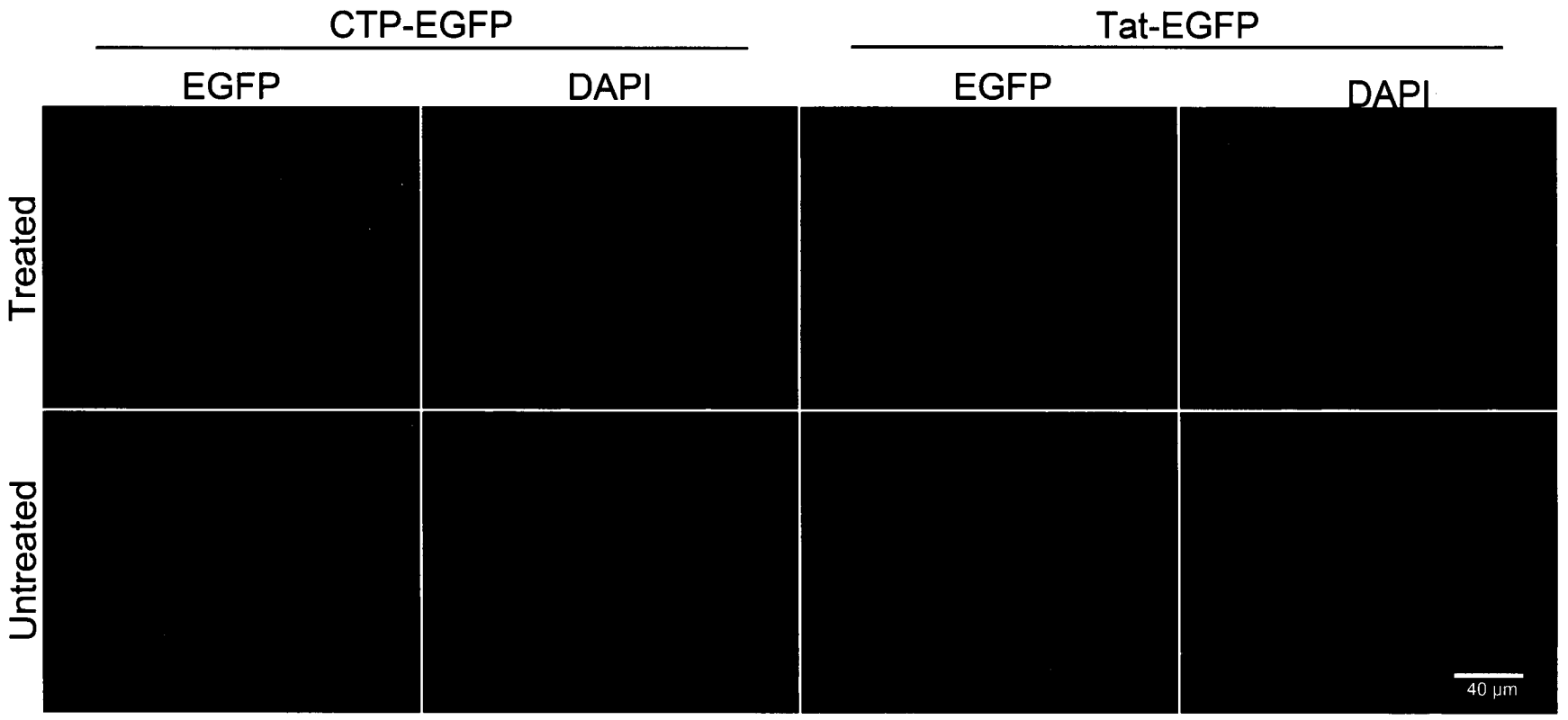

Figure 10. Cellular uptake of Tat-EGFP and CTP-EGFP in cone derived 661W cells. Cells were cultured in media containing 100µg/mL of protein and incubated at 37°C for 48hrs. Immunocytochemistry directed against EGFP was performed on fixed cells at 48h. Untreated cells were used as a negative control. A cytoplasmic Tat-EGFP signal can be seen in treated cells, however there was no apparent CTP-EGFP uptake.

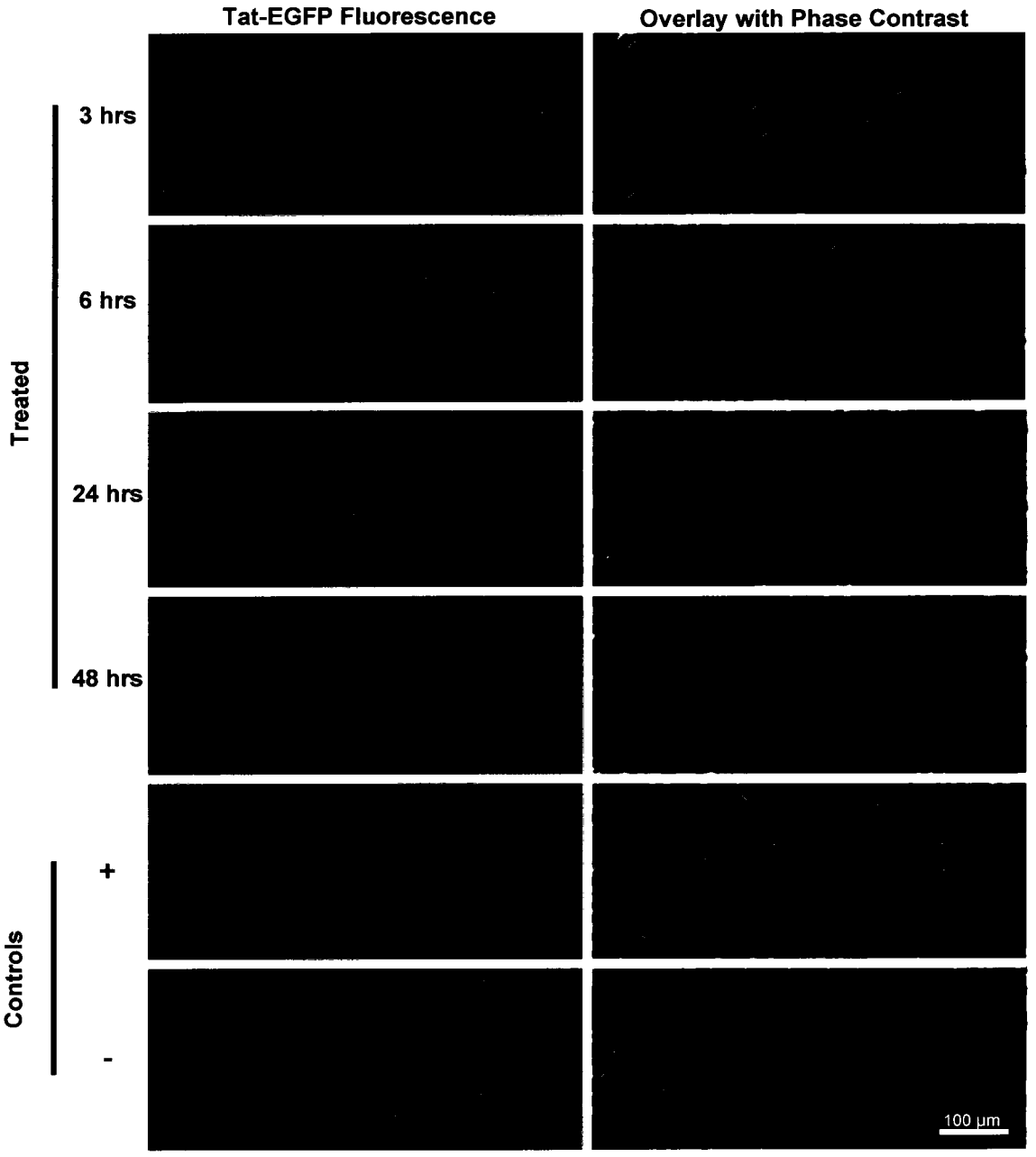

Figure 11. Tat-EGFP fluorescence in HEK293A cells treated with (NP2) PEG-PLA nanoparticles. Cells were incubated in culture medium containing 500 µg/mL of nanoparticles. Fluorescence and phase contrast microscopy images were taken after 3, 6, 24 and 48 hours. Cells cultured without nanoparticles were used as a negative control, and cells cultured in a 100 µg/ml suspension of a Tat-EGFP protein as a positive control.

was still present after 48 hours of incubation. Overlay of fluorescence images with the corresponding brightfield images reveals a co-localization of the Tat-EGFP signal with cells.

3.2.2 Mouse Photoreceptor-Derived (661W) Cells

The above experiment was repeated to acquire more detailed information regarding cellular uptake of Tat-EGFP released from PEG-PLA nanoparticles. For clearer images, cells were plated on microscope cover glasses, and immunostained with an anti-EGFP antibody. Cells were also sampled at an earlier time point, and after a longer period of time. Cells of the murine 661W cell line were used for this experiment, as they are cone-derived and may better represent the behaviour of photoreceptor cells than the previously used HEK293A line. Cells were incubated in the presence of Tat-EGFP encapsulated PEG-PLA nanoparticles (dispersed in the culture medium) and sampled after 1 hour, 24 hours, 48 hours and 96 hours of incubation.

Fluorescence microscopy and brightfield images are shown in figure 12. Cells cultured in the presence of nanoparticles appeared similar to untreated controls both in terms of growth rate and appearance, and showed no apparent signs of toxicity. In treated samples, nanoparticles containing Tat-EGFP were present at high levels at all time points. While at early time points they did not appear to specifically co-localize with cells, by 48 hours, a strong Tat-EGFP signal was observed at the level of the cytoplasm, suggesting internalization of some of the nanoparticles (at the 48 hour time point in figure 12, particles appear to surround the nucleus). A fainter, more diffuse signal was also observed in the cell cytoplasm after one hour of incubation, indicative of rapid Tat-EGFP

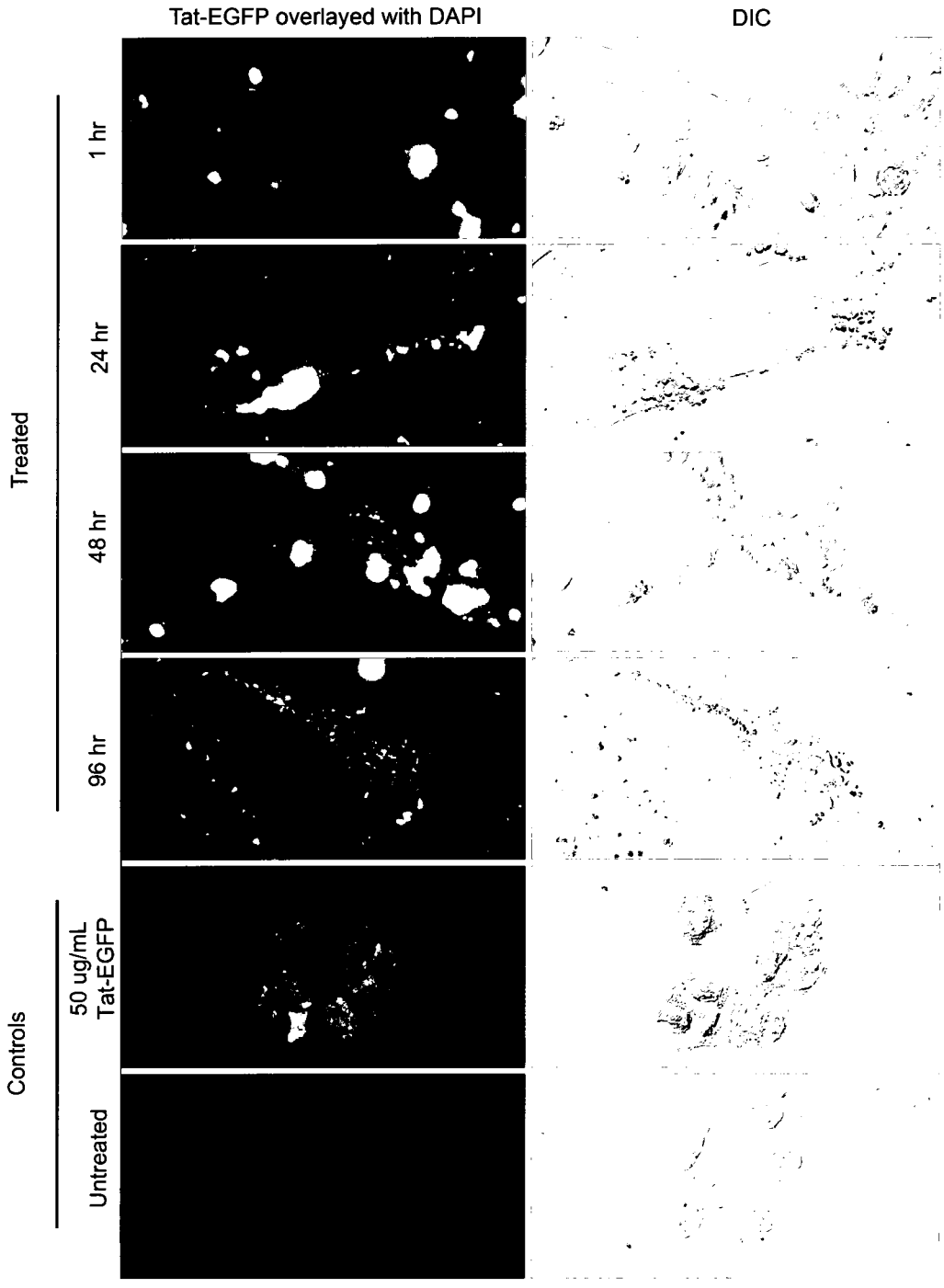

Figure 12. Cellular uptake of Tat-EGFP released from PEG-PLA nanoparticles in cone-derived 661W cells. Cells were incubated in culture medium containing 500μg/mL of nanoparticles. After 1, 24, 48 and 96 hours, cells were fixed and immunostained and fluorescence and differential interference contrast (DIC) microscopy images were taken. Cells cultured without nanoparticles were used as a negative control, and cells cultured in a 50 μg/ml suspension of a Tat-EGFP protein as a positive control (sampled at 1 hour).

uptake by 661W cells. Incubation of cells with 50 μg/mL Tat-EGFP protein in medium confirmed that cellular uptake of Tat peptides occurs within one hour.

3.3 Release of Tat-EGFP in vivo

3.3.1 Physiological Observations

To assess for potential toxicity of PEG-PLA nanoparticles, as well as determine *in vivo* localization of released protein, sub-retinal injections were carried out in Long-Evans rats. Six rats received injections of an AAV-CBA-GFP viral vector, six received injections of Tat-EGFP loaded PEG-PLA nanoparticles (NP6 formulation) and six received injections of empty PEG-PLA nanoparticles (NP6 formulation). In the case of nanoparticle injections, a trail of opaque matter (presumably nanoparticles) was commonly observed in the vitreous, rising from the puncture site (following the needle tract). Also common were minor retinal bleeds at the injection site. Observations of animals one week post-injections revealed the presence of membranes rising from the puncture site in the vitreous of most animals, consistent with notes taken at the time of surgery. Few eyes showed any significant retinal detachment, and the lenses all appeared clear.

At 3 and 9 weeks post-injections, digital fundus photos of a few select animals injected with PEG-PLA nanoparticles were taken with the assistance of Dr. Brian C. Leonard and Dr. Michael O'Connor (University of Ottawa Eye Institute). Obtained images are shown in figures 13 and 14. No lens opacity was observed at either time point, in any of the observed animals. Particulate matter (indicative of nanoparticles) could be seen in the

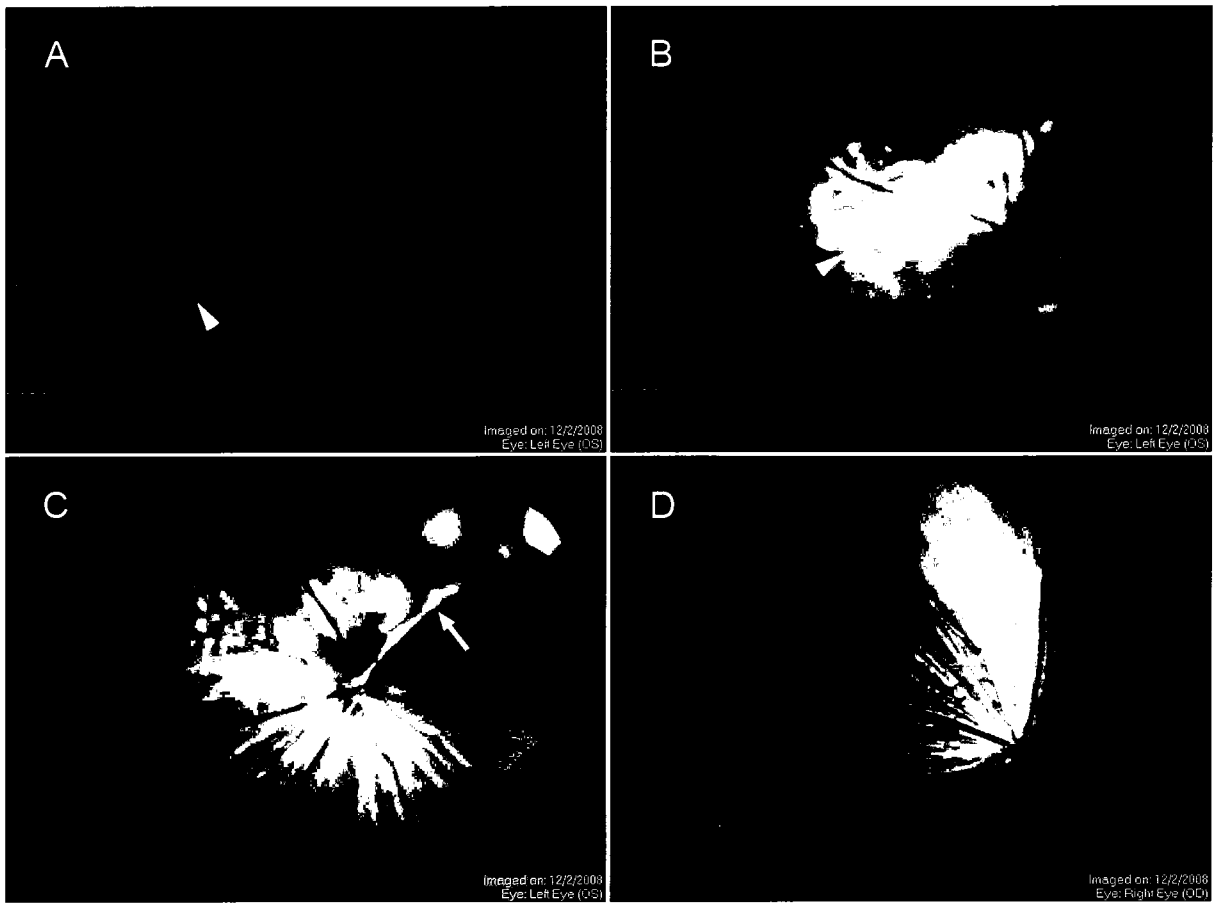

Figure 13. Digital fundus images of rat retinas 3 weeks after nanoparticle injections. Eyes were injected subretinally with PEG-PLA nanoparticles (NP6) (A-C). Arrowheads indicate particulate matter in the subretinal space. The animal in (B) shows a small retinal bleed from the site of injection. The membrane extending from the puncture site in (C) is marked with an arrow. An uninjected control is also shown (D).

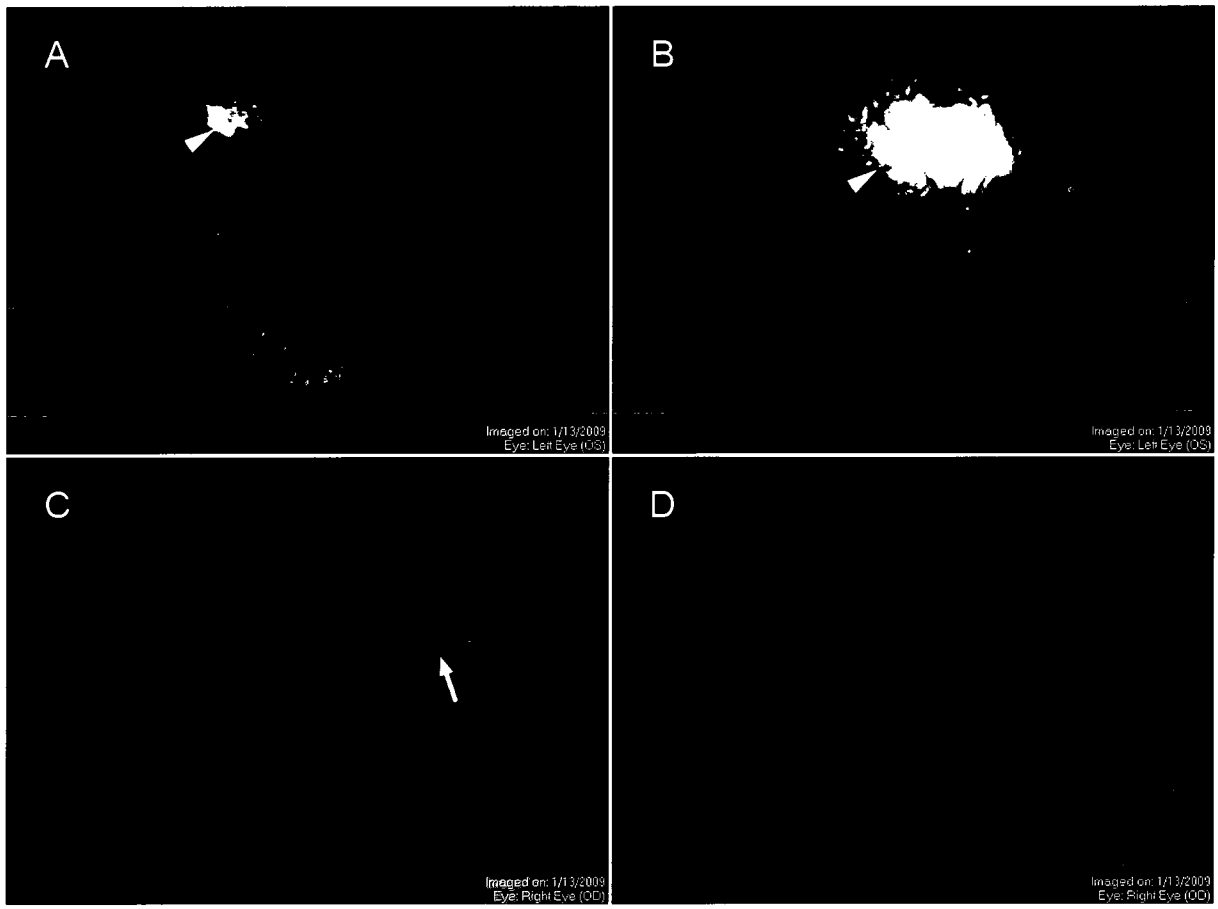

Figure 14. Digital fundus images of rat retinas 9 weeks after nanoparticle injections. Eyes were injected subretinally with PEG-PLA nanoparticles (NP6) (A-C). Arrowheads indicate particulate matter in the subretinal space. The membrane extending from the puncture site in (C) is marked with an arrow. An uninjected control is also shown (D).

subretinal space (fig. 13a,b and 14a,b), and particulate membranes rising from the puncture site were visible in most eyes (fig. 13c and 14c), although these appeared much smaller by 9 weeks. At 3 weeks post-injection, one animal displayed bleeding from the puncture site, which was resolved by 9 weeks (fig. 13b and 14b).

3.3.2 Electroretinography

Elecroretinography traces of animals injected with PEG-PLA nanoparticles, either loaded with Tat-EGFP or empty, were recorded at 9 weeks post-injection to assess for altered retinal function. Two of the injected animals were deceased prior to this time point (unrelated to the experimental procedure), and were therefore not included in this analysis. Average a-wave and b-wave amplitudes for all animals are shown in Figure 15, along with standard error. One-way ANOVA was performed to compare injected left eyes to uninjected right eyes, both for a-wave amplitude and b-wave amplitude. For all light intensity steps, differences in a-wave amplitude between treated and untreated eyes were not statistically significant (at $p>0.05$). b-wave amplitude was not significantly affected for 9 out of the 11 light intensities.

3.3.3 Immunohistochemistry

At 9 weeks post-injections, western analysis was conducted to determine levels of Tat-EGFP protein in the whole retina, and did not reveal any detectable Tat-EGFP in animals injected with Tat-EGFP loaded PEG-PLA nanoparticles (data not shown). Immunostaining of sections of retinas sampled at 9 weeks post-injection revealed the presence of Tat-EGFP protein in the outer nuclear layer (fig. 16), where photoreceptor cells are located. A similar localization was seen in eyes injected with an AAV-GFP viral construct. The clustered

appearance of Tat-EGFP protein observed within this layer suggests that most of the protein is still contained within nanoparticles, some of which appear to have infiltrated the retinal outer nuclear layer.

A

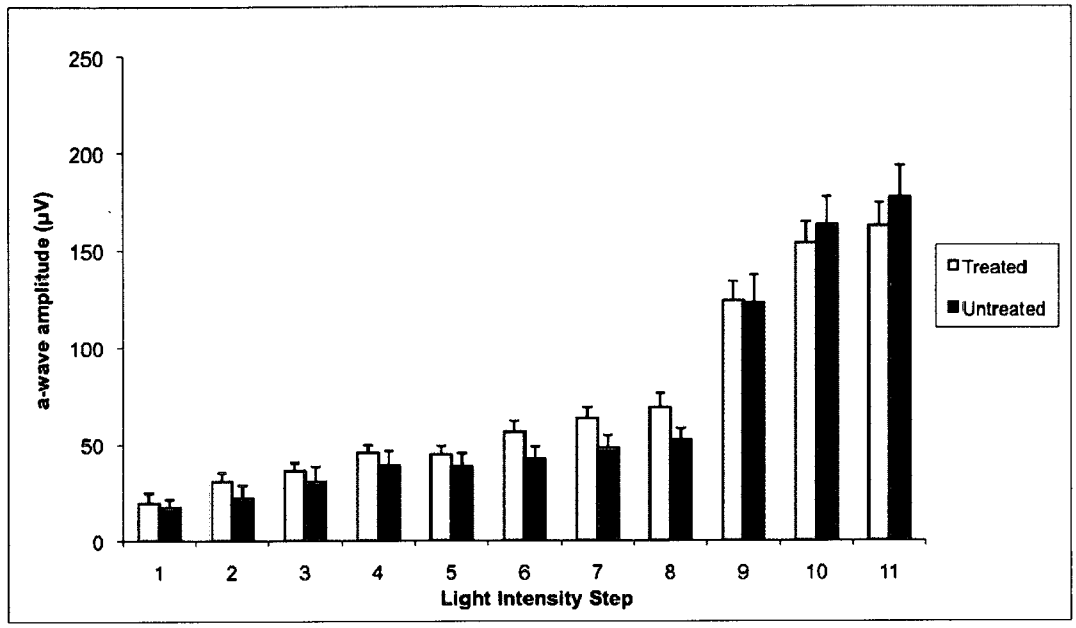

B

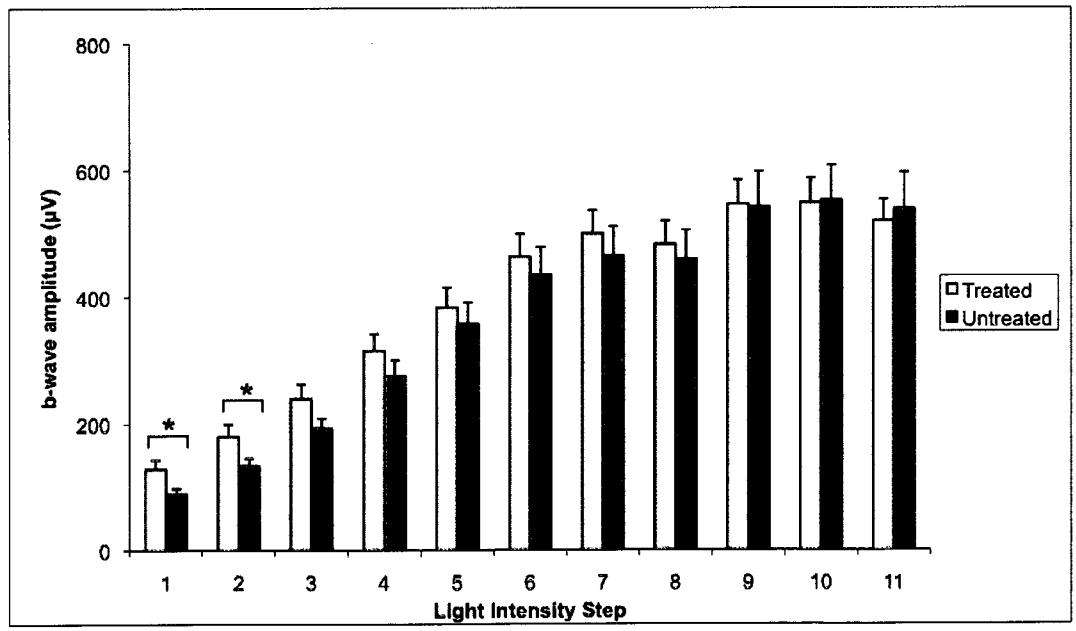

Figure 15. ERG a-wave and b-wave amplitudes of eyes injected with 10mg/mL NP-6 PEG-PLA nanoparticles. Mean a-wave amplitudes (A) and b-wave amplitudes (B) from 10 animals are shown at 11 different light intensity levels ranging from 0.001 cd.s/m^2 to 25 cd.s/m^2. The asterisks indicate significant differences in mean between treated and control eyes ($p<0.05$).

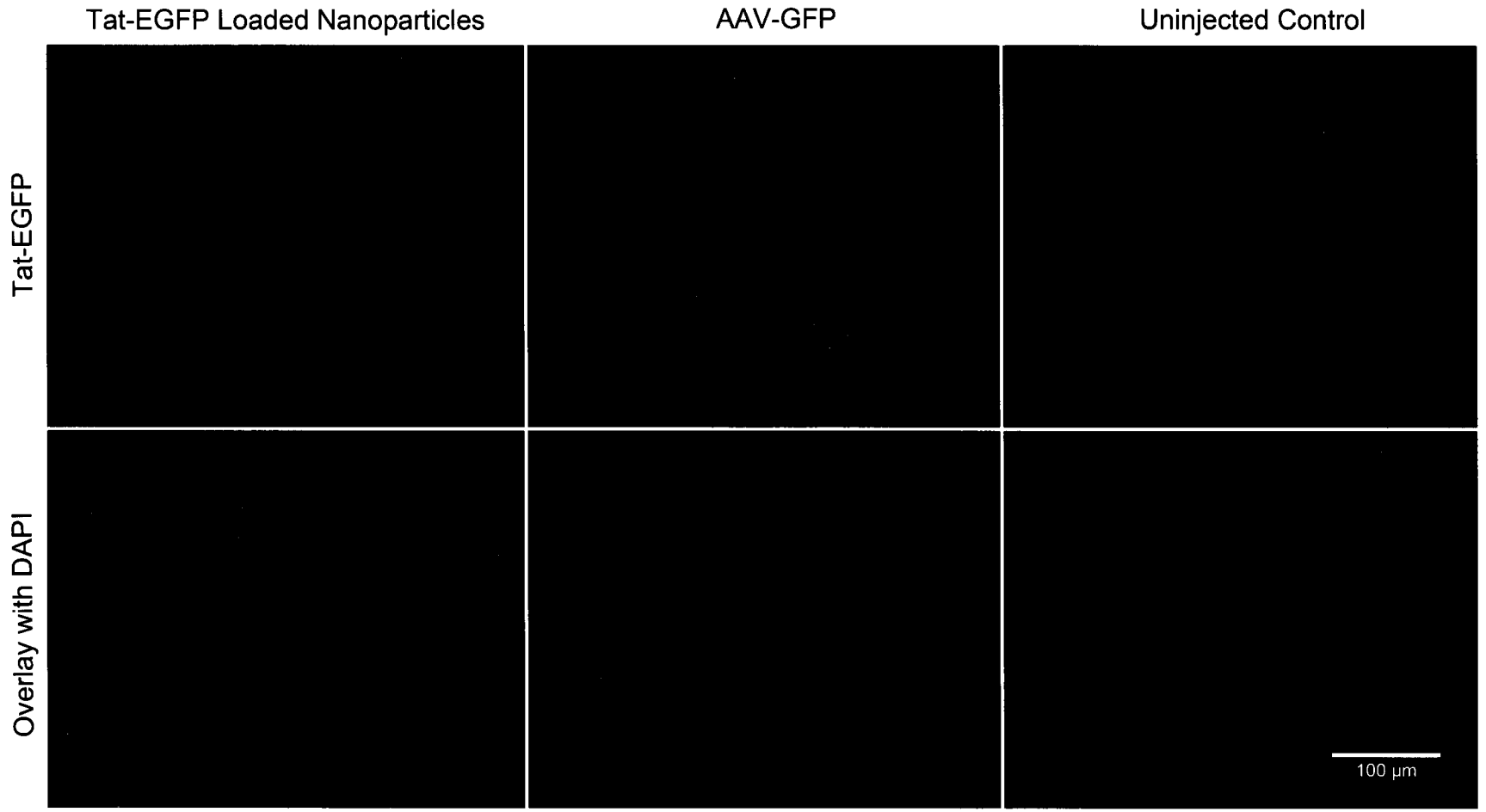

Figure 16. Immunohistochemistry of Tat-EGFP following nanoparticle injections in rat eyes. Eyes were subretinally injected with Tat-EGFP-loaded PEG-PLA (NP-6) nanoparticles, sampled at 9 weeks post-injection, and stained with antibodies against EGFP. An eye injected with a viral construct carrying EGFP is shown for comparison. The negative control is an uninjected right eye.

4. Discussion

The objective of the current project was to develop a biodegradable nanoparticle system for the delivery of therapeutic compounds specifically targeting the outer layers of the retina, and to evaluate the practicability of such a system in the prevention of vision loss following acute retinal insults. More specifically, the primary aim was to determine whether biodegradable nanoparticles could be used to deliver XIAP, an inhibitor of apoptosis, rapidly enough and at high enough levels to confer neuroprotection and prevent excessive photoreceptor cell death following acute events such as retinal detachment or retinal ischemia, both of which often result in rapid cell-death by apoptosis.

The present study investigated the use of a combination approach to deliver target proteins to the retina: the fusion of the target protein with a protein transduction domain (in this case Tat), and the encapsulation of the resulting fusion protein in biodegradable nanoparticles. The advantage of such an approach is that encapsulated protein released by nanoparticles in the subretinal space can then be internalized by surrounding cells, allowing for intracellular delivery of the protein even if the particles are localized in the extracellular space. Furthermore, the presence of the Tat peptide at the particle surface may increase cellular uptake of smaller-sized particles. It has been reported that nanoparticles ranging between 50nm and 250nm in size can be internalized by cells by endocytosis, however specific uptake mechanisms are still unclear. The mode of internalization is, however, known to be highly dependant on particle surface properties (Musyanovych et al., 2008; Mailander and Landfester, 2009). In this study, particles used for cell culture and *in vivo* experiments were not filtered, and ranged in size in the nanometer to micrometer scale. Whether smaller

particles were internalized in cultured cells or *in vivo* was not addressed within the scope of the current project.

4.1 In vitro Tat-EGFP Release

4.1.1 Protein Encapsulation Efficiency

Encapsulation efficiency was evaluated by determining Tat-EGFP concentration in nanoparticle synthesis wash supernatants. Trace amounts of protein were detected in these supernatants by ELISA, and suggest an encapsulation efficiency above 98%. Drug encapsulation in PEG-PLA nanoparticles is difficult to predict, and is dependant on many factors such as drug solubility in the polymer, drug-polymer interactions, molecular weight, preparation method, pH, etc. It was suggested by Olivier (2005) that loading of hydrophilic drugs into hydrophobic PLA nanoparticles might be limited by diffusion of the drug to aqueous phases during preparation. It is unlikely that the high drug-loading efficiency estimated reflects the true encapsulation. Instead, it is likely that significant amounts of protein were denatured or degraded during the synthesis process, and could not be detected in the wash supernatants.

Attempts were made to dissolve PEG-PLA nanoparticles to measure encapsulated protein, but have proven a challenge. To effectively measure nanoparticle encapsulation efficiency would require a method to break down nanoparticles without denaturing or degrading protein. Attempts to fully dissolve PEG-PLA nanoparticles in this project were unsuccessful. Low protein encapsulation could explain the low levels of protein release obtained in *in vitro* release studies. Methods to increase protein encapsulation could result in higher protein release from particles, and warrant future investigation.

4.1.2 Selection of Material

Poly(lactic-co-glycolic) acid (PLGA) and Poly(ethylene glycol)-Poly(Lactic) acid (PEG-PLA) were the chosen materials for nanoparticle synthesis for this project because of their high biocompatibility, and because release kinetics can easily be modulated by adjusting different factors in the nanoparticle formulation. Early experiments were geared towards selecting a nanoparticle formulation for optimal release *in vitro*. Preliminary release tests comparing the two materials revealed a significantly higher rate of release from PEG-PLA nanoparticles compared to PLGA. This can be explained by the high hydrophilicity of the PEG component, which may facilitate access of water molecules to cleave the ester bonds between polymer subunits by hydrolysis, thus favoring polymer degradation. Of the two PEG molecular weights tested in the PEG-PLA formulations, nanoparticles with a 1kDa PEG molecular weight yielded higher release than the 5kDa molecular weight, both in the initial burst stage and subsequent sustained release period. In addition, the lower molecular weight particles also displayed better dispersion in aqueous solution, and lower aggregation. It is possible that using a lower-molecular weight PEG increases the molar ratio of PEG to PLA, thus augmenting the hydrophilicity of the nanoparticles. By allowing for better dispersion of the nanoparticles in solution, and reducing aggregation, the 1kDa-based formula increases the surface area to volume ratio of the particles, which can explain the increased rate of protein release (a higher surface-volume ratio can impact both polymer degradation, and protein diffusion from the particle core). The two-phase release profile obtained from both formulations of PEG-PLA nanoparticles (the initial burst phase, followed by a sustained release phase) has often been reported in the literature (Peracchia et al., 1997; Quellec et al., 1999; Gref et al., 2001; Avgoustakis, 2004). The initial burst phase is associated with the

release of protein at the particle surface, while the sustained phase represents the slow diffusion of protein from the particle core.

4.1.3 Optimization of the Nanoparticle Formulation

Further nanoparticle formulations were designed to optimize *in vitro* release, by changing polymer concentration and protein concentration. Increases in protein concentration or in polymer concentration appear to have an increasing effect on the rate of sustained protein release after the first 24 hours. For a given polymer concentration, an increase in protein concentration (from 3 to 6 mg/mL) resulted in higher protein release. This was also observed at set protein concentrations, where increasing the polymer concentration from 2% to 4% also resulted in higher release.

Effects on initial burst release, however, were not as clear. For both polymer concentrations used, an increase in protein concentration resulted in higher amounts of protein released from the particles, indicating that protein release in the initial stage is relative to the initial amount encapsulated. For a given polymer concentration, a higher protein concentration may increase the population of oppositely charged molecules, and result in higher coagulation and particle formation rates during synthesis, resulting in smaller particles (ex. NP6 particles compared to NP4, and NP7 compared to NP5). These changes in particle size and morphology can impact the initial burst of release.

For a given protein concentration, the effect of modifying the polymer concentration was not consistent. At a protein concentration of 3mg/mL, increasing the polymer concentration from 2% to 4% resulted in an increase in protein release, while at a protein concentration of 6mg/mL, the same change in polymer concentration resulted in reduced

protein release. This suggests that factors other than polymer concentration or protein concentration have an impact on initial burst release, and that while at low protein concentrations polymer concentration has a direct effect, at higher protein concentrations other factors dominate. This phenomenon may be caused by the polar interactions and population imbalance between oppositely charged molecules. Protein release rates from nanoparticles can be affected by several factors in addition to chemical composition, such as particle size and dispersion, as well as encapsulation, and release is often the result of the interaction of various factors.

Formulation NP6 was chosen as the optimal formulation as it presented the best overall characteristics in terms of initial burst and subsequent sustained release. In addition, SEM showed that particles synthesized using a 2% polymer concentration are smaller and less clustered than those made from a 4% polymer concentration, preferable for ocular applications.

4.1.4 Effect of Sonication Time and Intensity

The effect of sonication time and power output during redispersion on the size, aggregation and release kinetics of nanoparticles was assessed before proceeding to *in vivo* experiments. For ocular applications, a small particle size and little to no aggregation are preferable. In addition to providing a barrier to reattachment of the retina following a subretinal injection, the introduction of large, or clustered nanoparticles into the subretinal space could cause more serious detachments, and would be detrimental to treatment in patients presenting acute retinal detachments. While sonication for longer durations and at higher intensities resulted in smaller, less aggregated particles, only the initial burst phase of

protein release appeared to be affected. No considerable effect was seen on sustained protein release following the first 24 hours.

Sonication of protein suspensions under different conditions showed that protein function is significantly affected at high power outputs. Protein function may be hindered by denaturation or by degradation of the protein. Studies have shown that sonication can affect protein stability as a result of localized high temperatures and the formation of free radicals (Suslick et al., 1986; Riesz and Kondo, 1992). Release profiles of particles sonicated at higher intensities indicate that only the initial burst phase is affected. This suggests that while sonication affects the function of free protein in solution, protein encapsulated within nanoparticles may be protected from this effect. Protein denaturation by sonication would also explain why quantities detected by ELISA were higher in the initial burst phase than by fluorescence, while quantities detected in the sustained release phase were similar for both measurement methods.

4.2 Release Behavior in Cell Culture

4.2.1 Tat and CTP: two Cell Penetrating Peptides

Aside from developing a nanoparticle formulation for optimal release, it was important to establish that encapsulated protein, once released from nanoparticles, can be internalized by surrounding cells. Cells incubated in the presence of Tat-EGFP were able to internalize protein in as little as one hour. This is consistent with early findings that Tat peptides can enter cells in as little as 10 minutes (Vives et al., 1997). A study by Caron et al. (2001) reported internalization of a Tat-EGFP fusion protein by cultured myoblasts reaching maximum intracellular levels within 30 minutes of incubation (Caron et al., 2001). Tat-EGFP

in the culture medium was able to enter cells in a photoreceptor-derived 661W cell line, suggesting that cellular uptake mediated by Tat is possible in photoreceptor cells. Tat-EGFP was detected at all time points observed from one hour to 96 hours. Later time points would be difficult to assess, as the passaging of cells once they reach confluency would remove nanoparticles from the culture medium. Surprisingly, cells incubated with a CTP-EGFP protein did not appear to internalize the protein. It is unlikely that HEK293A cells are unable to internalize CTP-fused peptides, as CTP has been shown to internalize proteins into various cell types (Kim et al., 2006). More likely, the absence of cellular uptake could result from an improper protein fusion. Further investigation into the construct sequence, and possible re-design would be required to obtain a functional CTP-EGFP fusion. However this is beyond the scope of the current project, and the Tat transduction domain revealed appropriate cytoplasmic localization (for at least 48 hours), and entered cells rapidly, making it adequate for the delivery of XIAP following acute retinal insults, where increased intracellular levels of XIAP are desired for immediate protection of photoreceptors.

4.2.2 Tat-EGFP Loaded Nanoparticles

Nanoparticles incubated with 661W cells displayed a high co-localization of Tat-EGFP signal with cells after 24 hours. The detected protein had a clustered, particulate appearance, suggesting that particles were being detected within or around the cell. Whether these particles are internalized or bound to the cell membrane cannot be determined from the fluorescence and brightfield microscopy images, however the fluorescent signal appears to exclude the nucleus in some instances (for example at 48 hours), suggesting internalization of at least some particles. As previously mentioned, it is possible that smaller particles have been internalized, while larger ones could be membrane-bound. Over the past decade, several

studies have investigated the use of cell penetrating peptides (CPPs) such as Tat, to promote cellular uptake of small nanoparticles, and found that conjugation of particles with these peptides significantly increases uptake in various cell types (Torchilin, 2008). A recent study (Peetla et al., 2009) has found that conjugation of Tat at the surface of PLA nanoparticles increases physiochemical interactions between particles and an artificial membrane in comparison to nanoparticles conjugated with a scrambled Tat peptide. Cellular uptake of encapsulated protein in human vascular endothelial cells was also significantly increased. This suggests that even in the case of particles too large to cross the cell membrane, the presence of Tat at the particle surface may be useful in promoting intracellular delivery of particle-encapsulated proteins.

4.3 Subretinal Injections of Tat-EGFP Loaded Nanoparticles

4.3.1 Physiological observations

Tat-EGFP loaded PEG-PLA nanoparticles were injected into adult rat eyes to assess localization of released protein, possible toxicity associated with the nanoparticle formulation, and to determine whether particles and released protein can persist at the site of injection for a time period adequate for long-term prevention of photoreceptor cell-death following retinal detachment or ischemia. At the time of injection, minor bleeds were commonly observed at the puncture site. These are a common occurrence, due to the high vascularization of the retina, and most resolved within the first week following injections. Also commonly observed following injections were elongated, particulate membranes rising from the puncture site, presumably the reflux of the viscous particle suspension into the vitreous as the needle was withdrawn. The appearance of these membranes appeared thinner

at 9 weeks post-injections when compared to fundus images at 3 weeks post-injections, suggesting that over time these membranes dissipate and will have no long-term adverse effects. These membranes have been seen following subretinal injections of different compounds in the clinic (Dr. Brian Leonard, personal communication). Particulate matter observed behind the retina could still be seen at 9 weeks post-injections, indicating that nanoparticles are able to persist in the subretinal space for at least 2 months. This is desirable in the treatment of acute retinal insults. While it is important to provide protection against photoreceptor degeneration immediately following such events, it would also be beneficial to extend this protection beyond the initial treatment, to prevent vision loss in patients in the event of complications over the following weeks.

4.3.2 Retinal Function

Statistical analysis using one-way ANOVA revealed that differences in a-wave and b-wave amplitudes were not significantly different between treated and untreated eyes, indicating that injections of PEG-PLA in the subretinal space do not significantly alter retinal function, or that any changes are resolved after 9 weeks. The slight differences in b-wave amplitude at the lowest intensities of light are probably due to the high variability that can be observed between animals, and between the two eyes of animals, and likely represents normal variability within individuals. In support of these results, Timmers et al. (2001) found that b-wave amplitudes in rats subretinally injected with fluorescent microspheres with an average diameter of 1μm were not significantly different from those of uninjected animals (Timmers et al., 2001).

4.3.3 Released Tat-EGFP in the Retina

Immunohistochemistry on sections of retinas having received subretinal injections of Tat-EGFP loaded PEG-PLA nanoparticles revealed the presence of Tat-EGFP protein and nanoparticles within the outer nuclear layer, where photoreceptor cells are located. In contrast to eyes injected with an AAV-GFP vector, eyes injected with nanoparticles display a deeper infiltration of the retinal layers by (presumably) nanoparticles. While it would be expected to also find particles located in the subretinal space by immunohistochemistry, this was not the case. Nanoparticles remaining in the subretinal space were likely washed away during the sampling and staining process. These results support the efficacy of PEG-PLA nanoparticles for the delivery of proteins targeting cells of the outer nuclear layer. On the other hand, Western analysis of protein extracted from whole retinas at 9 weeks post-injections failed to reveal any detectable Tat-EGFP in eyes that received subretinal injections of Tat-EGFP loaded PEG-PLA nanoparticles. This means that despite being detected by immunofluorescence, Tat-EGFP protein levels within the retina (either intracellular or membrane-bound) are below the detection limits of Western analysis. For XIAP applications in the eye, an overexpression of XIAP is desired to provide protection from photoreceptor cell death and vision loss following acute retinal insults. It is therefore possible that protein release from the current nanoparticle formulation could be too low for ocular XIAP applications.

4.4 Conclusions

Despite the low levels of protein release, PEG-PLA nanoparticles of the NP6 formulation revealed a two-phase release profile *in vitro*, effectively delivered Tat-EGFP to

cells in culture, and were localized in the photoreceptor cell layer *in vivo,* ideal for the delivery of drugs targeting the photoreceptor cell layer. They also presented the best morphology and size. *In vivo* experiments in rats also suggest that PEG-PLA nanoparticles used in this project are biocompatible, as both physiological and histological observations revealed no evidence of toxicity. By 3 weeks post-injections there were no signs of cataracts or other abnormalities out of the ordinary, and all minor detachments resulting from subretinal injections were almost fully resolved by 9 weeks post-injections. Electroretinography traces revealed that nanoparticles did not significantly impede retinal function. While the issue of low levels of release may make nanoparticles of the NP6 formulation inappropriate for the delivery of XIAP for the prevention of apoptotic cell death following a retinal insult, similar nanoparticles could still be employed for the delivery of other compounds to the retina (such as growth factors), where higher levels are not required.

4.5 Future Directions

To obtain protein levels adequate for XIAP applications, modifications to the nanoparticle formulation, or a new material altogether, will be required. Aside from synthetic polymers, polysaccharides such as chitosan (CS) are also commonly used for the synthesis of nanoparticles. CS is derived from chitin, a long-chain polysaccharide naturally found in marine crustaceans, and offers several advantages as a drug delivery vehicle (reviewed by Agnihotri et al. 2004). It is biocompatible, nontoxic, and possesses good adhesion and antimicrobial properties. CS degradation *in vivo* produces amino sugars, which are absorbed by the body. CS nanoparticle synthesis does not require the use of organic solvents, and drug release is easily controlled. Crosslinking is possible due to the presence of amine groups and positive charges, and can be chemical or electrostatic. Similarly to synthetic polymers, drug

release from the CS nanoparticles is dependent on several factors such as the degree of cross-linking and size of the particles, environmental factors such as pH or the presence of enzymes, and the properties of the drug itself. Release can occur from the surface, by erosion and/or by diffusion. Like PEG-PLA nanoparticles, release profiles typically display an initial burst effect, however this can be prevented or limited by increased crosslinking. Studies have demonstrated the potential for chitosan particles to deliver drugs to the ocular surface (de la Fuente et al., 2008; Enriquez de Salamanca et al., 2006); however there has been little investigation into the use of CS nanoparticle for drug delivery to the posterior segment of the eye. *In vitro* release tests from chitosan (CS) nanoparticles have been initiated in our laboratory (see appendix VI for release profiles). Selection of ideal materials, formulation and synthesis parameters are still in process.

Once appropriate levels of Tat-EGFP release are obtained, the release behavior of nanoparticles loaded with Tat-XIAP must also be assessed. Tat-XIAP only possesses a small amino acid sequence (Tat) in common with Tat-EGFP, and one major difference between the two proteins is the size. This may have an impact on protein release when encapsulated into nanoparticles, and an *in vitro* release profile for Tat-XIAP will need to be established with the chosen formulation. To estimate levels of XIAP required to significantly inhibit apoptosis, a cell-death assay will be conducted in which cells will be subject to hypoxic or chemical stress, with and without the presence of Tat-XIAP at various concentrations.

Aside from sustained delivery systems, an alternative approach for delivering high levels of XIAP to the retina would be modifications to the protein itself, to increase *in vivo* stability. Studies have shown that disulfide bonds, for example, stabilize proteins by increasing the free energy of proteins in their unfolded state (Pace, 1990). Amino acid

substitutions have also been shown to improve protein resistance to thermal and chemical denaturation, and improve protein shelf life (Filikov et al., 2002; Luo et al., 2002; Fu et al., 2009). For example, one study showed that proline residue substitutions in the β-turns of protein secondary structure render proteins more resistant to thermal and urea denaturation (Fu et al., 2009). It has been proposed that amino acid substitutions may stabilize proteins by improving van der Waals interactions, or stabilizing hydrophobic groups in the protein core (Filikov et al., 2002). The effects of other protein modifications, such as glycosylation, have been extensively studied, and reviewed by Sola et al. (Sola and Griebenow, 2009). Glycosylation has been shown to provide protection against proteolytic degradation (Vegarud and Christensen, 1975; Raju and Scallon, 2007), likely by a mechanism of steric interference against the protease active site, against oxidation (Uchida et al., 1997), chemical crosslinking and aggregation (Baudys et al., 1995), precipitation (Sola et al., 2007), pH denaturation (Masarova et al., 2001), and chemical and thermal denaturation (Sundaram and Venkatesh, 1998; Kwon and Yu, 1997). While certain protein modifications might increase stability, they may also affect protein function. For this reason, any protein modification would require careful consideration and functional assessments.

On a long-term basis, the goal of this research is to design a delivery system that can deliver XIAP to photoreceptors at adequate levels *in vivo*, for at least four weeks. Ideally, this system will show rescue of photoreceptors, structurally and functionally, in animal models of acute apoptotic stress. The present study represents an important step towards achieving this goal. Although XIAP applications will require further optimization of the nanoparticle formulation, or perhaps a protein modification approach, the current project has shown that

PEG-PLA nanoparticles can be used for the delivery of drugs targeting the retina in a rat model, without causing toxicity or impeding vision.

5. References

Adrain, C., and S.J. Martin. 2001. The mitochondrial apoptosome: a killer unleashed by the cytochrome seas. *Trends Biochem.Sci.* 26:390-397.

Agnihotri, S.A., N.N. Mallikarjuna, and T.M. Aminabhavi. 2004. Recent advances on chitosan-based micro- and nanoparticles in drug delivery. *J.Control.Release.* 100:5-28.

Alberts, B., A. Johnson, J. Lewis, M. Raff, K. Roberts, and P. Walter. 2002. Programmed Cell Death (Apoptosis). Garland Science, New York.

Alexander, J.J., and W.W. Hauswirth. 2008. Adeno-associated viral vectors and the retina. *Adv.Exp.Med.Biol.* 613:121-128.

Andrieu-Soler, C., A. Aubert-Pouessel, M. Doat, S. Picaud, M. Halhal, M. Simonutti, M.C. Venier-Julienne, J.P. Benoit, and F. Behar-Cohen. 2005. Intravitreous injection of PLGA microspheres encapsulating GDNF promotes the survival of photoreceptors in the rd1/rd1 mouse. *Mol.Vis.* 11:1002-1011.

Arroyo, J.G., L. Yang, D. Bula, and D.F. Chen. 2005. Photoreceptor apoptosis in human retinal detachment. *Am.J.Ophthalmol.* 139:605-610.

Ausayakhun, S., P. Yuvaves, S. Ngamtiphakom, and J. Prasitsilp. 2005. Treatment of cytomegalovirus retinitis in AIDS patients with intravitreal ganciclovir. *J.Med.Assoc.Thai.* 88 Suppl 9:S15-20.

Avgoustakis, K. 2004. Pegylated poly(lactide) and poly(lactide-co-glycolide) nanoparticles: preparation, properties and possible applications in drug delivery. *Curr.Drug Deliv.* 1:321-333.

Avgoustakis, K., A. Beletsi, Z. Panagi, P. Klepetsanis, A.G. Karydas, and D.S. Ithakissios. 2002. PLGA–mPEG nanoparticles of cisplatin: in vitro nanoparticle degradation, in vitro drug release and in vivo drug residence in blood properties. *Journal of Controlled Release.* 79:123-135.

Baudys, M., T. Uchio, D. Mix, D. Wilson, and S.W. Kim. 1995. Physical stabilization of insulin by glycosylation. *J.Pharm.Sci.* 84:28-33.

Bear, M.F., B.W. Connors, and M.A. Paradiso. 2007. The Eye. *In* Neuroscience: Exploring the Brain. Lippincott Williams & Wilkins, Baltimore, MD. 277.

Blanco, M.D., and M.J. Alonso. 1997. Development and characterization of protein-loaded poly(lactide-co-glycolide) nanospheres. *European Journal of Pharmaceutics and Biopharmaceutics.* 43:287-294.

Bourges, J.L., S.E. Gautier, F. Delie, R.A. Bejjani, J.C. Jeanny, R. Gurny, D. BenEzra, and F.F. Behar-Cohen. 2003. Ocular drug delivery targeting the retina and retinal

pigment epithelium using polylactide nanoparticles. *Invest.Ophthalmol.Vis.Sci.* 44:3562-3569.

Bratton, S.B., G. Walker, S.M. Srinivasula, X.M. Sun, M. Butterworth, E.S. Alnemri, and G.M. Cohen. 2001. Recruitment, activation and retention of caspases-9 and -3 by Apaf-1 apoptosome and associated XIAP complexes. *EMBO J.* 20:998-1009.

Brown, K.T. 1968. The eclectroretinogram: its components and their origins. *Vision Res.* 8:633-677.

Budihardjo, I., H. Oliver, M. Lutter, X. Luo, and X. Wang. 1999. Biochemical pathways of caspase activation during apoptosis. *Annu.Rev.Cell Dev.Biol.* 15:269-290.

Cao, X., and M.S. Schoichet. 1999. Delivering neuroactive molecules from biodegradable microspheres for application in central nervous system disorders. *Biomaterials.* 20:329-339.

Caron, N.J., Y. Torrente, G. Camirand, M. Bujold, P. Chapdelaine, K. Leriche, N. Bresolin, and J.P. Tremblay. 2001. Intracellular delivery of a Tat-eGFP fusion protein into muscle cells. *Mol.Ther.* 3:310-318.

Chahory, S., and A. Torriglia. 2006. Apoptosis in the Eye. *In* New Developments in Eye Research. O.R. Ioseliani, editor. Nova Science Publishers, Inc., New York. 47.

Chao, D.T., and S.J. Korsmeyer. 1998. BCL-2 family: regulators of cell death. *Annu.Rev.Immunol.* 16:395-419.

Chiu, K., T.T. Lam, W.W. Ying Li, J. Caprioli, and J.M. Kwong Kwong. 2005. Calpain and N-methyl-d-aspartate (NMDA)-induced excitotoxicity in rat retinas. *Brain Res.* 1046:207-215.

Cook, B., G.P. Lewis, S.K. Fisher, and R. Adler. 1995. Apoptotic photoreceptor degeneration in experimental retinal detachment. *Invest.Ophthalmol.Vis.Sci.* 36:990-996.

Cregan, S.P., V.L. Dawson, and R.S. Slack. 2004. Role of AIF in caspase-dependent and caspase-independent cell death. *Oncogene.* 23:2785-2796.

Crocker, S.J., P. Liston, H. Anisman, C.J. Lee, P.D. Smith, N. Earl, C.S. Thompson, D.S. Park, R.G. Korneluk, and G.S. Robertson. 2003. Attenuation of MPTP-induced neurotoxicity and behavioural impairment in NSE-XIAP transgenic mice. *Neurobiol.Dis.* 12:150-161.

Daiger, S.P. Retinal Information Network (RetNet). 2009. The University of Texas Health Science Center. 28 Aug. 2009. <http://www.sph.uth.tmc.edu/retnet/>.

Dan, H.C., M. Sun, S. Kaneko, R.I. Feldman, S.V. Nicosia, H.G. Wang, B.K. Tsang, and J.Q. Cheng. 2004. Akt phosphorylation and stabilization of X-linked inhibitor of apoptosis protein (XIAP). *J.Biol.Chem.* 279:5405-5412.

de la Fuente, M., B. Seijo, and M.J. Alonso. 2008. Novel hyaluronic acid-chitosan nanoparticles for ocular gene therapy. *Invest.Ophthalmol.Vis.Sci.* 49:2016-2024.

Del Amo, E.M., and A. Urtti. 2008. Current and future ophthalmic drug delivery systems. A shift to the posterior segment. *Drug Discov.Today.* 13:135-143.

Derossi, D., A.H. Joliot, G. Chassaing, and A. Prochiantz. 1994. The third helix of the Antennapedia homeodomain translocates through biological membranes. *J.Biol.Chem.* 269:10444-10450.

Dewson, G., and R.M. Kluck. 2009. Mechanisms by which Bak and Bax permeabilise mitochondria during apoptosis. *J.Cell.Sci.* 122:2801-2808.

Kuwana, T., and D.D. Newmeyer. 2003. Bcl-2-family proteins and the role of mitochondria in apoptosis. *Curr.Opin.Cell Biol.* 15:691-699.

Dong, C.J., and W.A. Hare. 2000. Contribution to the kinetics and amplitude of the electroretinogram b-wave by third-order retinal neurons in the rabbit retina. *Vision Res.* 40:579-589.

Doonan, F., and T.G. Cotter. 2004. Apoptosis: a potential therapeutic target for retinal degenerations. *Curr.Neurovasc Res.* 1:41-53.

Duvvuri, S., S. Majumdar, and A.K. Mitra. 2003. Drug delivery to the retina: challenges and opportunities. *Expert Opin.Biol.Ther.* 3:45-56.

Earnshaw, W.C., L.M. Martins, and S.H. Kaufmann. 1999. Mammalian caspases: structure, activation, substrates, and functions during apoptosis. *Annu.Rev.Biochem.* 68:383-424.

Eberhardt, O., R.V. Coelln, S. Kugler, J. Lindenau, S. Rathke-Hartlieb, E. Gerhardt, S. Haid, S. Isenmann, C. Gravel, A. Srinivasan, M. Bahr, M. Weller, J. Dichgans, and J.B. Schulz. 2000. Protection by synergistic effects of adenovirus-mediated X-chromosome-linked inhibitor of apoptosis and glial cell line-derived neurotrophic factor gene transfer in the 1-methyl-4-phenyl-1,2,3,6-tetrahydropyridine model of Parkinson's disease. *J.Neurosci.* 20:9126-9134.

Emerson, M.V., and A.K. Lauer. 2008. Current and emerging therapies for the treatment of age-related macular degeneration. *Clin.Ophthalmol.* 2:377-388.

Enriquez de Salamanca, A., Y. Diebold, M. Calonge, C. Garcia-Vazquez, S. Callejo, A. Vila, and M.J. Alonso. 2006. Chitosan nanoparticles as a potential drug delivery system for the ocular surface: toxicity, uptake mechanism and in vivo tolerance. *Invest.Ophthalmol.Vis.Sci.* 47:1416-1425.

Fain, G.L. 2006. Why photoreceptors die (and why they don't). *Bioessays.* 28:344-354.

Fawell, S., J. Seery, Y. Daikh, C. Moore, L.L. Chen, B. Pepinsky, and J. Barsoum. 1994. Tat-mediated delivery of heterologous proteins into cells. *Proc.Natl.Acad.Sci.U.S.A.* 91:664-668.

Filikov, A.V., R.J. Hayes, P. Luo, D.M. Stark, C. Chan, A. Kundu, and B.I. Dahiyat. 2002. Computational stabilization of human growth hormone. *Protein Sci.* 11:1452-1461.

Foerg, C., and H.P. Merkle. 2008. On the biomedical promise of cell penetrating peptides: limits versus prospects. *J.Pharm.Sci.* 97:144-162.

Fontaine, V., S. Mohand-Said, N. Hanoteau, C. Fuchs, K. Pfizenmaier, and U. Eisel. 2002. Neurodegenerative and neuroprotective effects of tumor Necrosis factor (TNF) in retinal ischemia: opposite roles of TNF receptor 1 and TNF receptor 2. *J.Neurosci.* 22:RC216.

The Foundation Fighting Blindness. 2009. Toronto. 25 Aug. 2009. < http://www.ffb.ca/index.html>.

Fu, H., G.R. Grimsley, A. Razvi, J.M. Scholtz, and C.N. Pace. 2009. Increasing protein stability by improving Beta-turns. *Proteins.*

Garcia-Valenzuela, E., S. Shareef, J. Walsh, and S.C. Sharma. 1995. Programmed cell death of retinal ganglion cells during experimental glaucoma. *Exp.Eye Res.* 61:33-44.

Gotch, F. 1903. The time relations of the photo-electric changes in the eyeball of the frog. *J.Physiol.* 29:388-410.

Green, D.G., and N.V. Kapousta-Bruneau. 1999. A dissection of the electroretinogram from the isolated rat retina with microelectrodes and drugs. *Vis.Neurosci.* 16:727-741.

Greenstein, B., and A. Greenstein. 2000. Color atlas of neuroscience : neuroanatomy and neurophysiology.

Gref, R., A. Domb, P. Quellec, T. Blunk, R.H. Müller, J.M. Verbavatz, and R. Langer. 1995. The controlled intravenous delivery of drugs using PEG-coated sterically stabilized nanospheres. *Advanced Drug Delivery Reviews.* 16:215-233.

Gref, R., P. Quellec, A. Sanchez, P. Calvo, E. Dellacherie, and M.J. Alonso. 2001. Development and characterization of CyA-loaded poly(lactic acid)-poly(ethylene glycol)PEG micro- and nanoparticles. Comparison with conventional PLA particulate carriers. *Eur.J.Pharm.Biopharm.* 51:111-118.

Harada, H., M. Hiraoka, and S. Kizaka-Kondoh. 2002. Antitumor effect of TAT-oxygen-dependent degradation-caspase-3 fusion protein specifically stabilized and activated in hypoxic tumor cells. *Cancer Res.* 62:2013-2018.

Hébert, M., and P. Lachapelle. 2003. Evaluation of Retinal Function: Electroretinography. *In* Ocular Neuroprotection. L.A. Levin and A. Di Polo, editors. Marcel Dekker, Inc., New York. 249-249-272.

Hecht, S., S. Shlaer, and M.H. Pirenne. 1942. Energy, Quanta and Vision. *J. Gen. Physiol.* 25:819.

Heibein, J.A., I.S. Goping, M. Barry, M.J. Pinkoski, G.C. Shore, D.R. Green, and R.C. Bleackley. 2000. Granzyme B-mediated cytochrome c release is regulated by the Bcl-2 family members bid and Bax. *J.Exp.Med.* 192:1391-1402.

Ho, A.C., G.C. Brown, J.A. McNamara, F.M. Recchia, C.D. Regillo, and J.F. Vander. 2003. Retina: Color Atlas & Synopsis of Clinical Ophthalmology. McGraw-Hill Companies, Inc., New York.

Huang, Y., Y.C. Park, R.L. Rich, D. Segal, D.G. Myszka, and H. Wu. 2001. Structural basis of caspase inhibition by XIAP: differential roles of the linker versus the BIR domain. *Cell.* 104:781-790.

Hughes, P.M., O. Olejnik, J.E. Chang-Lin, and C.G. Wilson. 2005. Topical and systemic drug delivery to the posterior segments. *Adv.Drug Deliv.Rev.* 57:2010-2032.

Hunter, A.M., E.C. LaCasse, and R.G. Korneluk. 2007. The inhibitors of apoptosis (IAPs) as cancer targets. *Apoptosis.* 12:1543-1568.

Ignatovich, I.A., E.B. Dizhe, A.V. Pavlotskaya, B.N. Akifiev, S.V. Burov, S.V. Orlov, and A.P. Perevozchikov. 2003. Complexes of plasmid DNA with basic domain 47-57 of the HIV-1 Tat protein are transferred to mammalian cells by endocytosis-mediated pathways. *J.Biol.Chem.* 278:42625-42636.

Janoria, K.G., S. Gunda, S.H. Boddu, and A.K. Mitra. 2007. Novel approaches to retinal drug delivery. *Expert Opin.Drug Deliv.* 4:371-388.

Jiang, C., M.J. Moore, X. Zhang, H. Klassen, R. Langer, and M. Young. 2007. Intravitreal injections of GDNF-loaded biodegradable microspheres are neuroprotective in a rat model of glaucoma. *Mol.Vis.* 13:1783-1792.

Kang, H.K., and A.J. Luff. 2008. Management of retinal detachment: a guide for non-ophthalmologists. *BMJ.* 336:1235-1240.

Kaplan, I.M., J.S. Wadia, and S.F. Dowdy. 2005. Cationic TAT peptide transduction domain enters cells by macropinocytosis. *J.Control.Release.* 102:247-253.

Karwoski, C.J., and X. Xu. 1999. Current source-density analysis of light-evoked field potentials in rabbit retina. *Vis.Neurosci.* 16:369-377.

Katai, N., and N. Yoshimura. 1999. Apoptotic retinal neuronal death by ischemia-reperfusion is executed by two distinct caspase family proteases. *Invest.Ophthalmol.Vis.Sci.* 40:2697-2705.

Kaufmann, S.H., and M.O. Hengartner. 2001. Programmed cell death: alive and well in the new millennium. *Trends Cell Biol.* 11:526-534.

Kerr, J.F., A.H. Wyllie, and A.R. Currie. 1972. Apoptosis: a basic biological phenomenon with wide-ranging implications in tissue kinetics. *Br.J.Cancer.* 26:239-257.

Kerrigan, L.A., D.J. Zack, H.A. Quigley, S.D. Smith, and M.E. Pease. 1997. TUNEL-positive ganglion cells in human primary open-angle glaucoma. *Arch.Ophthalmol.* 115:1031-1035.

Kim, D., C. Jeon, J. Kim, M. Kim, C. Yoon, I. Choi, S. Kim, and Y. Bae. 2006. Cytoplasmic transduction peptide (CTP): New approach for the delivery of biomolecules into cytoplasm in vitro and in vivo. *Experimental Cell Research.* 312:1277-1288.

Klose, D., F. Siepmann, K. Elkharraz, and J. Siepmann. 2008. PLGA-based drug delivery systems: importance of the type of drug and device geometry. *Int.J.Pharm.* 354:95-103. doi: 10.1016/j.ijpharm.2007.10.030.

Koch, A.M., F. Reynolds, M.F. Kircher, H.P. Merkle, R. Weissleder, and L. Josephson. 2003. Uptake and metabolism of a dual fluorochrome Tat-nanoparticle in HeLa cells. *Bioconjug.Chem.* 14:1115-1121.

Kolb, H., E. Fernandez, and R. Nelson. 2009. Webvision: The Organization of the Retina and Visual System.

Kugler, S., G. Straten, F. Kreppel, S. Isenmann, P. Liston, and M. Bahr. 2000. The X-linked inhibitor of apoptosis (XIAP) prevents cell death in axotomized CNS neurons in vivo. *Cell Death Differ.* 7:815-824.

Kuppermann, B.D., M.S. Blumenkranz, J.A. Haller, G.A. Williams, D.V. Weinberg, C. Chou, S.M. Whitcup, and Dexamethasone DDS Phase II Study Group. 2007. Randomized controlled study of an intravitreous dexamethasone drug delivery system in patients with persistent macular edema. *Arch.Ophthalmol.* 125:309-317.

Kuroiwa, S., N. Katai, H. Shibuki, T. Kurokawa, J. Umihira, T. Nikaido, K. Kametani, and N. Yoshimura. 1998. Expression of cell cycle-related genes in dying cells in retinal ischemic injury. *Invest.Ophthalmol.Vis.Sci.* 39:610-617.

Kwon, K.S., and M.H. Yu. 1997. Effect of glycosylation on the stability of alpha1-antitrypsin toward urea denaturation and thermal deactivation. *Biochim.Biophys.Acta.* 1335:265-272.

Lafuente, M.P., M.P. Villegas-Perez, I. Selles-Navarro, S. Mayor-Torroglosa, J. Miralles de Imperial, and M. Vidal-Sanz. 2002. Retinal ganglion cell death after acute retinal

ischemia is an ongoing process whose severity and duration depends on the duration of the insult. *Neuroscience.* 109:157-168.

Le Bourlais, C., F. Chevanne, P. Ropert, G. Bretagne, L. Acar, H. Zia, P.A. Sado, T. Needham, and R. Leverge. 1996. Release kinetics of liposome-encapsulated ganciclovir after intravitreal injection in rabbits. *J.Microencapsul.* 13:473-480.

Leber, B., J. Lin, and D.W. Andrews. 2007. Embedded together: the life and death consequences of interaction of the Bcl-2 family with membranes. *Apoptosis.* 12:897-911.

Leonard, K.C., D. Petrin, S.G. Coupland, A.N. Baker, B.C. Leonard, E.C. LaCasse, W.W. Hauswirth, R.G. Korneluk, and C. Tsilfidis. 2007. XIAP protection of photoreceptors in animal models of retinitis pigmentosa. *PLoS ONE.* 2:e314. doi: 10.1371/journal.pone.0000314.

Lewin, M., N. Carlesso, C.H. Tung, X.W. Tang, D. Cory, D.T. Scadden, and R. Weissleder. 2000. Tat peptide-derivatized magnetic nanoparticles allow in vivo tracking and recovery of progenitor cells. *Nat.Biotechnol.* 18:410-414.

Letai, A., M.C. Bassik, L.D. Walensky, M.D. Sorcinelli, S. Weiler, and S.J. Korsmeyer. 2002. Distinct BH3 domains either sensitize or activate mitochondrial apoptosis, serving as prototype cancer therapeutics. *Cancer.Cell.* 2:183-192.

Lewis, G.P., D.G. Charteris, C.S. Sethi, W.P. Leitner, K.A. Linberg, and S.K. Fisher. 2002. The ability of rapid retinal reattachment to stop or reverse the cellular and molecular events initiated by detachment. *Invest.Ophthalmol.Vis.Sci.* 43:2412-2420.

Li, H., and J. Yuan. 1999. Deciphering the pathways of life and death. *Curr.Opin.Cell Biol.* 11:261-266.

Li, H., H. Zhu, C.J. Xu, and J. Yuan. 1998. Cleavage of BID by caspase 8 mediates the mitochondrial damage in the Fas pathway of apoptosis. *Cell.* 94:491-501.

Li, P., D. Nijhawan, I. Budihardjo, S.M. Srinivasula, M. Ahmad, E.S. Alnemri, and X. Wang. 1997. Cytochrome c and dATP-dependent formation of Apaf-1/caspase-9 complex initiates an apoptotic protease cascade. *Cell.* 91:479-489.

Li, Y., Y. Pei, X. Zhang, Z. Gu, Z. Zhou, W. Yuan, J. Zhou, J. Zhu, and X. Gao. 2001. PEGylated PLGA nanoparticles as protein carriers: synthesis, preparation and biodistribution in rats. *J.Control.Release.* 71:203-211.

Lim, J.I., R.A. Wolitz, A.H. Dowling, H.R. Bloom, A.R. Irvine, and D.M. Schwartz. 1999. Visual and anatomic outcomes associated with posterior segment complications after ganciclovir implant procedures in patients with AIDS and cytomegalovirus retinitis. *Am.J.Ophthalmol.* 127:288-293.

Liston, P., W.G. Fong, and R.G. Korneluk. 2003. The inhibitors of apoptosis: there is more to life than Bcl2. *Oncogene.* 22:8568-8580.

Luo, P., R.J. Hayes, C. Chan, D.M. Stark, M.Y. Hwang, J.M. Jacinto, P. Juvvadi, H.S. Chung, A. Kundu, M.L. Ary, and B.I. Dahiyat. 2002. Development of a cytokine analog with enhanced stability using computational ultrahigh throughput screening. *Protein Sci.* 11:1218-1226.

MacFarlane, M., and A.C. Williams. 2004. Apoptosis and disease: a life or death decision. *EMBO Rep.* 5:674-678. doi: 10.1038/sj.embor.7400191.

Mailander, V., and K. Landfester. 2009. Interaction of Nanoparticles with Cells. *Biomacromolecules.*

Mainardes, R.M., M.C. Urban, P.O. Cinto, N.M. Khalil, M.V. Chaud, R.C. Evangelista, and M.P. Gremiao. 2005. Colloidal carriers for ophthalmic drug delivery. *Curr.Drug Targets.* 6:363-371.

Marmor, M.F., A. Negi, and D.M. Maurice. 1985. Kinetics of macromolecules injected into the subretinal space. *Exp.Eye Res.* 40:687-696.

Marigo, V. 2007. Programmed cell death in retinal degeneration: targeting apoptosis in photoreceptors as potential therapy for retinal degeneration. *Cell.Cycle.* 6:652-655.

Masarova, J., D. Mislovicova, P. Gemeiner, and E. Michalkova. 2001. Stability enhancement of Escherichia coli penicillin G acylase by glycosylation with yeast mannan. *Biotechnol.Appl.Biochem.* 34:127-133.

Massey, S.C. 1990. Cell types using glutamate as a neurotransmitter in the vertebrate retina. *Prog Retinal Res.* 9:399.

Masu, M., H. Iwakabe, Y. Tagawa, T. Miyoshi, M. Yamashita, Y. Fukuda, H. Sasaki, K. Hiroi, Y. Nakamura, and R. Shigemoto. 1995. Specific deficit of the ON response in visual transmission by targeted disruption of the mGluR6 gene. *Cell.* 80:757-765.

McGinity, J.W., and P.B. O'Donnell. 1997. Preparation of microspheres by the solvent evaporation technique. *Adv.Drug Deliv.Rev.* 28:25-42.

McKinnon, S.J., D.M. Lehman, N.G. Tahzib, N.L. Ransom, H.A. Reitsamer, P. Liston, E. LaCasse, Q. Li, R.G. Korneluk, and W.W. Hauswirth. 2002. Baculoviral IAP repeat-containing-4 protects optic nerve axons in a rat glaucoma model. *Mol.Ther.* 5:780-787.

Miller, R.F. 1973. Role of K + in generation of b-wave of electroretinogram. *J.Neurophysiol.* 36:28-38.

Morishima, N., K. Nakanishi, H. Takenouchi, T. Shibata, and Y. Yasuhiko. 2002. An endoplasmic reticulum stress-specific caspase cascade in apoptosis. Cytochrome c-independent activation of caspase-9 by caspase-12. *J.Biol.Chem.* 277:34287-34294.

Musyanovych, A., J. Schmitz-Wienke, V. Mailander, P. Walther, and K. Landfester. 2008. Preparation of biodegradable polymer nanoparticles by miniemulsion technique and their cell interactions. *Macromol.Biosci.* 8:127-139.

Nagata, S. 2000. Apoptotic DNA fragmentation. *Exp.Cell Res.* 256:12-18.

Nicholls, J.G. 2001. From neuron to brain.

Nickells, R.W., and D.J. Zack. 1996. Apoptosis in ocular disease: a molecular overview. *Ophthalmic Genet.* 17:145-165.

Ogura, Y., and H. Kimura. 1995. Biodegradable polymer microspheres for targeted drug delivery to the retinal pigment epithelium. *Surv.Ophthalmol.* 39 Suppl 1:S17-24.
Olivier, J.C. 2005. Drug transport to brain with targeted nanoparticles. *NeuroRx.* 2:108-119.

Pace, C.N. 1990. Conformational stability of globular proteins. *Trends Biochem.Sci.* 15:14-17.

Peetla, C., K.S. Rao, and V. Labhasetwar. 2009. Relevance of Biophysical Interactions of Nanoparticles with a Model Membrane in Predicting Cellular Uptake: Study with TAT Peptide-Conjugated Nanoparticles. *Mol.Pharm.*

Penn, R.D., and W.A. Hagins. 1969. Signal transmission along retinal rods and the origin of the electroretinographic a-wave. *Nature.* 223:201-204.

Peracchia, M.T., R. Gref, Y. Minamitake, A. Domb, N. Lotan, and R. Langer. 1997. PEG-coated nanospheres from amphiphilic diblock and multiblock copolymers: Investigation of their drug encapsulation and release characteristics. *J.Controlled Release.* 46:223-231.

Petrin, D., A. Baker, S.G. Coupland, P. Liston, M. Narang, K. Damji, B. Leonard, V.A. Chiodo, A. Timmers, W. Hauswirth, R.G. Korneluk, and C. Tsilfidis. 2003. Structural and functional protection of photoreceptors from MNU-induced retinal degeneration by the X-linked inhibitor of apoptosis. *Invest.Ophthalmol.Vis.Sci.* 44:2757-2763.

Peyman, G.A., M. Conway, B. Khoobehi, and K. Soike. 1992. Clearance of microsphere-entrapped 5-fluorouracil and cytosine arabinoside from the vitreous of primates. *Int.Ophthalmol.* 16:109-113.

Purves, D., G.J. Augustine, D. Fitzpatrick, W.C. Hall, A. LaMantia, J.O. McNamara, and L.E. White. 2008. Vision: The Eye. *In* Neuroscience. Sinauer Associates, Inc., Sunderland, Massachusetts. 253.

Quellec, P., R. Gref, E. Dellacherie, F. Sommer, M.D. Tran, and M.J. Alonso. 1999. Protein encapsulation within poly(ethylene glycol)-coated nanospheres. II. Controlled release properties. *J.Biomed.Mater.Res.* 47:388-395.

Quigley, H.A., and W.R. Green. 1979. The histology of human glaucoma cupping and optic nerve damage: clinicopathologic correlation in 21 eyes. *Ophthalmology.* 86:1803-1830.

Rabinowitz, J.E., and R.J. Samulski. 2000. Building a better vector: the manipulation of AAV virions. *Virology.* 278:301-308.

Raju, T.S., and B. Scallon. 2007. Fc glycans terminated with N-acetylglucosamine residues increase antibody resistance to papain. *Biotechnol.Prog.* 23:964-971.

Ren, H., and G. Wilson. 1996. Apoptosis in the corneal epithelium. *Invest.Ophthalmol.Vis.Sci.* 37:1017-1025.

Renwick, J., M.A. Narang, S.G. Coupland, J.Y. Xuan, A.N. Baker, J. Brousseau, D. Petrin, R. Munger, B.C. Leonard, W.W. Hauswirth, R.G. Korneluk, and C. Tsilfidis. 2006. XIAP-mediated neuroprotection in retinal ischemia. *Gene Ther.* 13:339-347.

Richard, J.P., K. Melikov, H. Brooks, P. Prevot, B. Lebleu, and L.V. Chernomordik. 2005. Cellular uptake of unconjugated TAT peptide involves clathrin-dependent endocytosis and heparan sulfate receptors. *J.Biol.Chem.* 280:15300-15306.

Richard, J.P., K. Melikov, E. Vives, C. Ramos, B. Verbeure, M.J. Gait, L.V. Chernomordik, and B. Lebleu. 2003. Cell-penetrating peptides. A reevaluation of the mechanism of cellular uptake. *J.Biol.Chem.* 278:585-590.

Riesz, P., and T. Kondo. 1992. Free radical formation induced by ultrasound and its biological implications. *Free Radic.Biol.Med.* 13:247-270.

Rivas, M.A., and E. Vecino. 2009. Animal models and different therapies for treatment of retinitis pigmentosa. *Histol.Histopathol.* 24:1295-1322.

Rosenbaum, D.M., P.S. Rosenbaum, A. Gupta, M.D. Michaelson, D.H. Hall, and J.A. Kessler. 1997a. Retinal ischemia leads to apoptosis which is ameliorated by aurintricarboxylic acid. *Vision Res.* 37:3445-3451.

Rosenbaum, P.S., H. Gupta, S.I. Savitz, and D.M. Rosenbaum. 1997b. Apoptosis in the retina. *Clin.Neurosci.* 4:224-232.

Rudolph, C., C. Plank, J. Lausier, U. Schillinger, R.H. Muller, and J. Rosenecker. 2003. Oligomers of the arginine-rich motif of the HIV-1 TAT protein are capable of transferring plasmid DNA into cells. *J.Biol.Chem.* 278:11411-11418.

Rumelt, S., Y. Dorenboim, and U. Rehany. 1999. Aggressive systematic treatment for central retinal artery occlusion. *Am.J.Ophthalmol.* 128:733-738.

Sahoo, S.K., F. Dilnawaz, and S. Krishnakumar. 2008. Nanotechnology in ocular drug delivery. *Drug Discov.Today.* 13:144-151.

Sanders, E.J., E. Parker, and S. Harvey. 2006. Retinal ganglion cell survival in development: mechanisms of retinal growth hormone action. *Exp.Eye Res.* 83:1205-1214.

Sanges, D., A. Comitato, R. Tammaro, and V. Marigo. 2006. Apoptosis in retinal degeneration involves cross-talk between apoptosis-inducing factor (AIF) and caspase-12 and is blocked by calpain inhibitors. *Proc.Natl.Acad.Sci.U.S.A.* 103:17366-17371.

Sanvicens, N., V. Gomez-Vicente, I. Masip, A. Messeguer, and T.G. Cotter. 2004. Oxidative stress-induced apoptosis in retinal photoreceptor cells is mediated by calpains and caspases and blocked by the oxygen radical scavenger CR-6. *J.Biol.Chem.* 279:39268-39278.

Schlegel, R.A., and P. Williamson. 2001. Phosphatidylserine, a death knell. *Cell Death Differ.* 8:551-563.

Schwarze, S.R., A. Ho, A. Vocero-Akbani, and S.F. Dowdy. 1999. In vivo protein transduction: delivery of a biologically active protein into the mouse. *Science.* 285:1569-1572.

Scorrano, L., S.A. Oakes, J.T. Opferman, E.H. Cheng, M.D. Sorcinelli, T. Pozzan, and S.J. Korsmeyer. 2003. BAX and BAK regulation of endoplasmic reticulum Ca2+: a control point for apoptosis. *Science.* 300:135-139.

Seah, S.K., R. Husain, G. Gazzard, M.C. Lim, S.T. Hoh, F.T. Oen, and T. Aung. 2005. Use of surodex in phacotrabeculectomy surgery. *Am.J.Ophthalmol.* 139:927-928.

Seigel, G.M., L. Chiu, and A. Paxhia. 2000. Inhibition of neuroretinal cell death by insulin-like growth factor-1 and its analogs. *Mol.Vis.* 6:157-163.

Shiozaki, E.N., J. Chai, D.J. Rigotti, S.J. Riedl, P. Li, S.M. Srinivasula, E.S. Alnemri, R. Fairman, and Y. Shi. 2003. Mechanism of XIAP-mediated inhibition of caspase-9. *Mol.Cell.* 11:519-527.

Simeoni, F., M.C. Morris, F. Heitz, and G. Divita. 2005. Peptide-based strategy for siRNA delivery into mammalian cells. *Methods Mol.Biol.* 309:251-260.

Singh, M., S.I. Savitz, R. Hoque, G. Gupta, S. Roth, P.S. Rosenbaum, and D.M. Rosenbaum. 2001. Cell-specific caspase expression by different neuronal phenotypes in transient retinal ischemia. *J.Neurochem.* 77:466-475.

Sola, R.J., and K. Griebenow. 2009. Effects of glycosylation on the stability of protein pharmaceuticals. *J.Pharm.Sci.* 98:1223-1245.

Sola, R.J., J.A. Rodriguez-Martinez, and K. Griebenow. 2007. Modulation of protein biophysical properties by chemical glycosylation: biochemical insights and biomedical implications. *Cell Mol.Life Sci.* 64:2133-2152.

Steinberg, R.H. 1987. Monitoring communications between photoreceptors and pigment epithelial cells: effects of "mild" systemic hypoxia. Friedenwald lecture. *Invest.Ophthalmol.Vis.Sci.* 28:1888-1904.

Stoka, V., B. Turk, S.L. Schendel, T.H. Kim, T. Cirman, S.J. Snipas, L.M. Ellerby, D. Bredesen, H. Freeze, M. Abrahamson, D. Bromme, S. Krajewski, J.C. Reed, X.M. Yin, V. Turk, and G.S. Salvesen. 2001. Lysosomal protease pathways to apoptosis. Cleavage of bid, not pro-caspases, is the most likely route. *J.Biol.Chem.* 276:3149-3157.

Strasser, A., L. O'Connor, and V.M. Dixit. 2000. Apoptosis signaling. *Annu.Rev.Biochem.* 69:217-245.

Sugita, T., T. Yoshikawa, Y. Mukai, N. Yamanada, S. Imai, K. Nagano, Y. Yoshida, H. Shibata, Y. Yoshioka, S. Nakagawa, H. Kamada, S.I. Tsunoda, and Y. Tsutsumi. 2008. Comparative study on transduction and toxicity of protein transduction domains. *Br.J.Pharmacol.* 153:1143-1152.

Sun, C., M. Cai, A.H. Gunasekera, R.P. Meadows, H. Wang, J. Chen, H. Zhang, W. Wu, N. Xu, S.C. Ng, and S.W. Fesik. 1999. NMR structure and mutagenesis of the inhibitor-of-apoptosis protein XIAP. *Nature.* 401:818-822.

Sundaram, P.V., and R. Venkatesh. 1998. Retardation of thermal and urea induced inactivation of alpha-chymotrypsin by modification with carbohydrate polymers. *Protein Eng.* 11:699-705.

Surace, E.M., and A. Auricchio. 2008. Versatility of AAV vectors for retinal gene transfer. *Vision Res.* 48:353-359.

Suslick, K.S., D.A. Hammerton, and R.E. Cline. 1986. Sonochemical hot spot. *J.Am.Chem.Soc.* 108:5641-5642.

Suzuki, Y., Y. Nakabayashi, K. Nakata, J.C. Reed, and R. Takahashi. 2001a. X-linked inhibitor of apoptosis protein (XIAP) inhibits caspase-3 and -7 in distinct modes. *J.Biol.Chem.* 276:27058-27063. doi: 10.1074/jbc.M102415200.

Suzuki, Y., Y. Nakabayashi, and R. Takahashi. 2001b. Ubiquitin-protein ligase activity of X-linked inhibitor of apoptosis protein promotes proteasomal degradation of caspase-3 and enhances its anti-apoptotic effect in Fas-induced cell death. *Proc.Natl.Acad.Sci.U.S.A.* 98:8662-8667.

Timmers, A.M., H. Zhang, A. Squitieri, and C. Gonzalez-Pola. 2001. Subretinal injections in rodent eyes: effects on electrophysiology and histology of rat retina. *Mol.Vis.* 7:131-137.

Torchilin, V.P. 2008. Tat peptide-mediated intracellular delivery of pharmaceutical nanocarriers. *Adv.Drug Deliv.Rev.* 60:548-558.

Travis, G.H. 1998. Mechanisms of cell death in the inherited retinal degenerations. *Am.J.Hum.Genet.* 62:503-508.

Trehin, R., H.M. Nielsen, H.G. Jahnke, U. Krauss, A.G. Beck-Sickinger, and H.P. Merkle. 2004. Metabolic cleavage of cell-penetrating peptides in contact with epithelial models: human calcitonin (hCT)-derived peptides, Tat(47-57) and penetratin(43-58). *Biochem.J.* 382:945-956.

Uchida, E., K. Morimoto, N. Kawasaki, Y. Izaki, A. Abdu Said, and T. Hayakawa. 1997. Effect of active oxygen radicals on protein and carbohydrate moieties of recombinant human erythropoietin. *Free Radic.Res.* 27:311-323.

Vallee, J.N., M. Paques, A. Aymard, P. Massin, P.Y. Santiago, P. Adeleine, A. Gaudric, and J.J. Merland. 2002. Combined central retinal arterial and venous obstruction: emergency ophthalmic arterial fibrinolysis. *Radiology.* 223:351-359.

Vecino, E., M. Hernandez, and M. Garcia. 2004. Cell death in the developing vertebrate retina. *Int.J.Dev.Biol.* 48:965-974.

Vegarud, G., and T.B. Christensen. 1975. The resistance of glycoproteins to proteolytic inactivation. *Acta Chem.Scand.B.* 29:887-888.

Violini, S., V. Sharma, J.L. Prior, M. Dyszlewski, and D. Piwnica-Worms. 2002. Evidence for a plasma membrane-mediated permeability barrier to Tat basic domain in well-differentiated epithelial cells: lack of correlation with heparan sulfate. *Biochemistry.* 41:12652-12661.

Vives, E., P. Brodin, and B. Lebleu. 1997. A Truncated HIV-1 Tat Protein Basic Domain Rapidly Translocates through the Plasma Membrane and Accumulates in the Cell Nucleus. *J.Biol.Chem.* 272:16010-16017.

Wadia, J.S., and S.F. Dowdy. 2002. Protein transduction technology. *Curr.Opin.Biotechnol.* 13:52-56.

Wadia, J.S., R.V. Stan, and S.F. Dowdy. 2004. Transducible TAT-HA fusogenic peptide enhances escape of TAT-fusion proteins after lipid raft macropinocytosis. *Nat.Med.* 10:310-315.

Wilson, S.E., S.S. Chaurasia, and F.W. Medeiros. 2007. Apoptosis in the initiation, modulation and termination of the corneal wound healing response. *Exp.Eye Res.* 85:305-311.

Xu, D., Y. Bureau, D.C. McIntyre, D.W. Nicholson, P. Liston, Y. Zhu, W.G. Fong, S.J. Crocker, R.G. Korneluk, and G.S. Robertson. 1999. Attenuation of ischemia-induced cellular and behavioral deficits by X chromosome-linked inhibitor of apoptosis protein overexpression in the rat hippocampus. *J.Neurosci.* 19:5026-5033.

Xu, G.Z., W.W. Li, and M.O. Tso. 1996. Apoptosis in human retinal degenerations. *Trans.Am.Ophthalmol.Soc.* 94:411-30; discussion 430-1.

Yang, Y., S. Fang, J.P. Jensen, A.M. Weissman, and J.D. Ashwell. 2000. Ubiquitin protein ligase activity of IAPs and their degradation in proteasomes in response to apoptotic stimuli. *Science.* 288:874-877.

Zacks, D.N., V. Hanninen, M. Pantcheva, E. Ezra, C. Grosskreutz, and J.W. Miller. 2003. Caspase activation in an experimental model of retinal detachment. *Invest.Ophthalmol.Vis.Sci.* 44:1262-1267.

Zadro-Lamoureux, L.A., D.N. Zacks, A.N. Baker, Q.D. Zheng, W.W. Hauswirth, and C. Tsilfidis. 2009. XIAP effects on retinal detachment-induced photoreceptor apoptosis [corrected]. *Invest.Ophthalmol.Vis.Sci.* 50:1448-1453.

Zou, H., Y. Li, X. Liu, and X. Wang. 1999. An APAF-1.cytochrome c multimeric complex is a functional apoptosome that activates procaspase-9. *J.Biol.Chem.* 274:11549-11556.

APPENDIX I

Protein Constructs

PROTEIN CONSTRUCTS

Protein constructs were designed and purified by Dr. Wai Gin Fong, Ph.D. (University of Ottawa Eye Institute).

Tat-EGFP

CTP-EGFP

Purification protocol for Tat-EGFP:

The pET28a Tat-EGFP vector was constructed by PCR amplification using a 5' primer containing a BamHI restriction site, the 11aa Tat protein transduction domain (PTD) and the first 15 nucleotides of the EGFP cDNA. The vector adds a His tag in frame to the 5'end of Tat-EGFP. BL21 E.coli containing the pET28a Tat-EGFP was grown overnight in 1L of Terrific broth at 22°C and induced with 0.5mM IPTG for 12h. The bacterial pellet was lysed in 50ml of solubilization buffer (50mM Tris-Cl (pH8.0), 150mM NaCl, 8M urea and 25mM imidazole) (Sigma) and sonicated (4 x 20s at 25W) to reduce the viscosity of the solution. After centrifugation, the supernatant was applied to a column containing a 10ml bed volume of NiNTA agarose (Qiagen) and washed 3x with 5 bed volumes of solubilization buffer. Tat-EGFP was eluted in solubilization buffer supplemented with 150mM imidazole and dialyzed three times in 4L PBS. Protein was concentrated on Vivaspin20 (10,000 mwco) (Sigma) and quantified using Bradford reagent (Bio-rad).

(The same protocol was followed for CTP-EGFP)

APPENDIX II

Buffer Recipes

BUFFER RECIPES

Phosphate buffered saline (PBS)

Dissolve in 800mL of dH_2O:

- 4.26g $Na_2HPO_4.7H_2O$
- 1.44g KH_2PO_4
- 90g NaCl

Adjust pH to 7.4 with NaOH or HCl

Adjust to final 1000mL volume with dH_2O

Tris buffered saline (TBS)

Dissolve in 800mL of dH_2O:

- 6.05g Tris (50mM)
- 8.76g NaCl

Adjust pH to 7.5 with HCl

Adust to final 1000mL volume with dH_2O

4% Paraformaldehyde (PFA)

Heat 400mL PBS to 65°C

Add 20g PFA

Dissolve PFA by adding NaOH pellets one at a time (approx. 2-3)

Filter

Adjust pH to 7.5 with HCl

Adjust to 500mL with dH_2O

APPENDIX III

Raw Data: Tat-EGFP Release

RAW PROTEIN RELEASE DATA

NP-1 Formulation:

	Fluorescence Readings			Tat-EGFP Release (μg/mL)[c]			Corrected Release (μg/mL)[d]			
Time[a]	Control[b]	Sample 1	Sample 2	Control	Sample 1	Sample 2	Sample 1	Sample 2	Mean	SE[e]
0.167	6189	837	-323	0.185	0.185	-0.067	0.095	-0.034	0.031	0.065
0.25	6744	-535	-268	-0.113	-0.113	-0.055	-0.058	-0.028	-0.043	0.015
0.5	6854	-525	-419	-0.110	-0.110	-0.087	-0.057	-0.045	-0.051	0.006
1	6551	34	132	0.011	0.011	0.032	0.006	0.017	0.011	0.005
2	6552	-12	-30	0.001	0.001	-0.003	0.000	-0.002	-0.001	0.001
3	6364	154	337	0.037	0.037	0.077	0.019	0.040	0.029	0.010
5	5825	872	339	0.193	0.193	0.077	0.099	0.040	0.070	0.030
7	5484	-310	-110	-0.064	-0.064	-0.020	-0.033	-0.011	-0.022	0.011
9	5524	964	903	0.213	0.213	0.200	0.110	0.103	0.106	0.003
12	5762	1515	1487	0.332	0.332	0.326	0.171	0.168	0.170	0.002
14	5854	1566	1476	0.343	0.343	0.324	0.177	0.167	0.172	0.005

[a]Time: in days

[b]Control: Tat-EGFP protein in culture medium (without nanoparticles)

[c]Amount released per 19.4 mg of nanoparticles, calculated using standard curve equation y = 4606.4x - 16.146, where y = fluorescence, x = protein concentration

[d]Corrected release: amount released per 10mg of nanoparticles

[e]Standard error calculated using the formula $SE = \frac{STDEV}{\sqrt{n}}$ (standard deviation was determined using MS Excel)

NP-2 Formulation:

	Fluorescence Readings			Tat-EGFP Release (μg/mL)[b]			Cummulative Release (μg/mL)[c]			Corrected Release (μg/mL)[d]				
Time[a]	1	2	3	1	2	3	1	2	3	1	2	3	Mean	SE[e]
0	129960	136450	141760	21.406	22.479	23.357	21.406	22.479	23.357	81.547	85.634	88.978	85.386	2.149
0.125	23004	24498	48484	3.727	3.974	7.938	25.133	26.452	31.295	95.744	100.771	119.219	105.245	7.136
0.25	3311	2439	8891	0.471	0.327	1.394	25.604	26.780	32.689	97.539	102.018	124.528	108.029	8.351
1	2033	1883	5872	0.260	0.235	0.895	25.864	27.015	33.583	98.530	102.914	127.937	109.794	9.159
4	1526	1796	4153	0.176	0.221	0.611	26.041	27.236	34.194	99.202	103.756	130.263	111.074	9.684
7	324	1647	2037	-0.022	0.196	0.261	26.018	27.432	34.455	99.117	104.504	131.256	111.626	9.938
10	198	637	1054	-0.043	0.029	0.098	25.975	27.462	34.553	98.952	104.616	131.631	111.733	10.082

[a]Time: in days

[b]Amount released per 2.63 mg of nanoparticles, calculated using standard curve equation y = 6049.7x + 459.34, where y = fluorescence, x = protein concentration

[c]Each time point represents a sum of the release to date

[d]Corrected release: amount released per 10mg of nanoparticles

[e]Standard error calculated using the formula $SE = \frac{STDEV}{\sqrt{n}}$, based on cumulative release values (standard deviation was determined using MS Excel)

NP-3 Formulation:

	Fluorescence Readings			Tat-EGFP Release (μg/mL)[b]			Cummulative Release (μg/mL)[c]			Corrected Release (μg/mL)[d]				
Time[a]	1	2	3	1	2	3	1	2	3	1	2	3	Mean	SE[e]
0	12390	12670	11580	1.972	2.018	1.838	1.972	2.018	1.838	7.513	7.689	7.003	7.402	0.206
0.125	6433	6203	6264	0.987	0.949	0.959	2.960	2.968	2.798	11.274	11.306	10.658	11.079	0.211
0.25	795	836	809	0.055	0.062	0.058	3.015	3.030	2.856	11.486	11.543	10.878	11.302	0.213
1	488	516	551	0.005	0.009	0.015	3.020	3.039	2.871	11.504	11.579	10.936	11.339	0.203
4	1369	1488	424	0.150	0.170	-0.006	3.170	3.209	2.865	12.077	12.227	10.914	11.739	0.415
7	454	1647	2037	-0.001	0.196	0.261	3.169	3.406	3.126	12.073	12.974	11.907	12.318	0.332
10	209	637	1054	-0.041	0.029	0.098	3.128	3.435	3.224	11.916	13.086	12.282	12.428	0.346

[a]Time: in days

[b]Amount released per 2.75 mg of nanoparticles, calculated using standard curve equation y = 6049.7x + 459.34, where y = fluorescence, x = protein concentration

[c]Each time point represents a sum of the release to date

[d]Corrected release: amount released per 10mg of nanoparticles

[e]Standard error calculated using the formula $SE = \frac{STDEV}{\sqrt{n}}$, based on cumulative release values (standard deviation was determined using MS Excel)

NP-4 Formulation:

	Fluorescence Readings			Tat-EGFP Release (μg/mL)[b]			Cummulative Release (μg/mL)[c]				
Time[a]	1	2	3	1	2	3	1	2	3	Mean	SE[d]
0	1513	1518	1713	0.417	0.418	0.472	0.417	0.418	0.472	0.435	0.018
0.125	1200	1320	1118	0.330	0.363	0.308	0.747	0.781	0.779	0.769	0.011
0.25	183	263	355	0.050	0.072	0.098	0.797	0.854	0.877	0.843	0.024
1	1786	463	339	0.492	0.127	0.093	1.289	0.981	0.970	1.080	0.104
4	-16	-201	-185	-0.004	-0.055	-0.051	1.284	0.926	0.919	1.043	0.121
7	119	69	21	0.033	0.019	0.006	1.317	0.945	0.925	1.062	0.128
10	63	-2	31	0.017	-0.001	0.009	1.335	0.944	0.934	1.071	0.132
13	117	122	125	0.032	0.034	0.034	1.367	0.978	0.968	1.104	0.131
16	255	293	286	0.070	0.081	0.079	1.437	1.058	1.047	1.181	0.128
19	346	351	373	0.095	0.097	0.103	1.532	1.155	1.150	1.279	0.127
22	73	144	216	0.020	0.040	0.059	1.552	1.195	1.209	1.319	0.117
25	67	92	107	0.018	0.025	0.029	1.571	1.220	1.239	1.343	0.114
28	-29	18	7	-0.008	0.005	0.002	1.563	1.225	1.240	1.343	0.110
31	71	89	73	0.020	0.025	0.020	1.582	1.250	1.261	1.364	0.109

[a]Time: in days

[b]Amount released per 10 mg of nanoparticles, calculated using standard curve equation y = 3632.6x, where y = fluorescence, x = protein concentration

[c]Each time point represents a sum of the release to date

[d]Standard error calculated using the formula $SE = \frac{STDEV}{\sqrt{n}}$, based on cumulative release values (standard deviation was determined using MS Excel)

NP-5 Formulation:

	Fluorescence Readings			Tat-EGFP Release (μg/mL)[b]			Cummulative Release (μg/mL)[c]				
Time[a]	1	2	3	1	2	3	1	2	3	Mean	SE[d]
0	6667	6676	6576	1.835	1.838	1.810	1.835	1.838	1.810	1.828	0.009
0.125	2612	2218	1887	0.719	0.611	0.519	2.554	2.448	2.330	2.444	0.065
0.25	703	581	505	0.194	0.160	0.139	2.748	2.608	2.469	2.608	0.081
1	674	762	1216	0.186	0.210	0.335	2.933	2.818	2.804	2.852	0.041
4	103	259	184	0.028	0.071	0.051	2.962	2.889	2.854	2.902	0.032
7	329	746	208	0.091	0.205	0.057	3.052	3.095	2.911	3.020	0.055
10	103	307	186	0.028	0.085	0.051	3.081	3.179	2.963	3.074	0.063
13	140	249	211	0.039	0.069	0.058	3.119	3.248	3.021	3.129	0.066
16	290	548	416	0.080	0.151	0.115	3.199	3.399	3.135	3.244	0.079
19	496	581	474	0.137	0.160	0.130	3.336	3.559	3.266	3.387	0.088
22	124	315	268	0.034	0.087	0.074	3.370	3.645	3.339	3.452	0.097
25	194	233	474	0.053	0.064	0.130	3.423	3.709	3.470	3.534	0.089
28	106	318	261	0.029	0.088	0.072	3.452	3.797	3.542	3.597	0.103
31	190	228	402	0.052	0.063	0.111	3.505	3.860	3.652	3.672	0.103

[a]Time: in days

[b]Amount released per 10 mg of nanoparticles, calculated using standard curve equation y = 3632.6x, where y = fluorescence, x = protein concentration

[c]Each time point represents a sum of the release to date

[d]Standard error calculated using the formula $SE = \frac{STDEV}{\sqrt{n}}$, based on cumulative release values (standard deviation was determined using MS Excel)

NP-6 Formulation:

	Fluorescence Readings			Tat-EGFP Release (μg/mL)[b]			Cummulative Release (μg/mL)[c]				
Time[a]	1	2	3	1	2	3	1	2	3	Mean	SE[d]
0	13541	13714	13642	3.728	3.775	3.755	3.728	3.775	3.755	3.753	0.014
0.125	5878	5544	5112	1.618	1.526	1.407	5.346	5.301	5.163	5.270	0.055
0.25	1198	1421	1256	0.330	0.391	0.346	5.676	5.693	5.508	5.626	0.059
1	1213	1150	1409	0.334	0.317	0.388	6.009	6.009	5.896	5.972	0.038
4	378	546	299	0.104	0.150	0.082	6.114	6.160	5.979	6.084	0.054
7	274	363	218	0.075	0.100	0.060	6.189	6.259	6.039	6.162	0.065
10	141	290	111	0.039	0.080	0.031	6.228	6.339	6.069	6.212	0.078
13	213	225	180	0.059	0.062	0.050	6.286	6.401	6.119	6.269	0.082
16	355	446	266	0.098	0.123	0.073	6.384	6.524	6.192	6.367	0.096
19	448	387	405	0.123	0.107	0.111	6.507	6.631	6.303	6.480	0.095
22	148	175	244	0.041	0.048	0.067	6.548	6.679	6.371	6.533	0.089
25	160	236	175	0.044	0.065	0.048	6.592	6.744	6.419	6.585	0.094
28	24	275	40	0.007	0.076	0.011	6.599	6.819	6.430	6.616	0.113
31	98	463	122	0.027	0.127	0.034	6.626	6.947	6.463	6.679	0.142

[a]Time: in days

[b]Amount released per 10 mg of nanoparticles, calculated using standard curve equation y = 3632.6x, where y = fluorescence, x = protein concentration

[c]Each time point represents a sum of the release to date

[d]Standard error calculated using the formula $SE = \frac{STDEV}{\sqrt{n}}$, based on cumulative release values (standard deviation was determined using MS Excel)

NP-7 Formulation:

	Fluorescence Readings			Tat-EGFP Release (μg/mL)[b]			Cummulative Release (μg/mL)[c]				
Time[a]	1	2	3	1	2	3	1	2	3	Mean	SE[d]
0	9991	9972	9957	2.750	2.745	2.741	2.750	2.745	2.741	2.746	0.003
0.125	2285	2422	2156	0.629	0.667	0.594	3.379	3.412	3.335	3.375	0.022
0.25	596	596	639	0.164	0.164	0.176	3.543	3.576	3.510	3.543	0.019
1	1674	900	1527	0.461	0.248	0.420	4.004	3.824	3.931	3.920	0.052
4	765	467	312	0.211	0.129	0.086	4.215	3.952	4.017	4.061	0.079
7	652	474	463	0.179	0.130	0.127	4.394	4.083	4.144	4.207	0.095
10	442	177	222	0.122	0.049	0.061	4.516	4.131	4.205	4.284	0.118
13	291	296	286	0.080	0.081	0.079	4.596	4.213	4.284	4.364	0.118
16	356	407	308	0.098	0.112	0.085	4.694	4.325	4.369	4.463	0.116
19	417	416	757	0.115	0.115	0.208	4.809	4.440	4.577	4.609	0.108
22	211	175		0.058	0.048	0.000	4.867	4.488		4.677	0.190
25	169	76	311	0.047	0.021	0.086	4.914	4.509	4.663	4.695	0.118
28	34	52		0.009	0.014	0.000	4.923	4.523		4.723	0.200
31	454	227	556	0.125	0.062	0.153	5.048	4.585	4.816	4.816	0.134

[a]Time: in days

[b]Amount released per 10 mg of nanoparticles, calculated using standard curve equation y = 3632.6x, where y = fluorescence, x = protein concentration

[c]Each time point represents a sum of the release to date

[d]Standard error calculated using the formula $SE = \frac{STDEV}{\sqrt{n}}$, based on cumulative release values (standard deviation was determined using MS Excel)

ELISA Data

NP-6 Formulation:

	Absorbance Readings			Tat-EGFP Release (μg/mL)[d]			Cummulative Release (μg/mL)[e]				
Time[a]	1	2	3	1	2	3	1	2	3	Mean	SE[f]
0	0.972[b]	0.933[b]	0.924[b]	26.800	20.510	19.282	26.800	20.510	19.282	22.198	2.328
0.125	0.803[b]	0.803[c]	0.7[b]	8.409	8.409	4.149	35.209	28.919	23.431	29.187	3.403
0.25	0.884[c]	0.859[c]	0.754[c]	1.466	1.235	0.601	36.675	30.154	24.032	30.287	3.650
1	0.787[c]	0.856[c]	0.778[c]	0.753	1.210	0.708	37.428	31.363	24.741	31.177	3.664
4	1.291	1.267	1.275	0.239	0.203	0.214	37.667	31.566	24.955	31.396	3.671
7	1.228	1.196	1.13	0.155	0.125	0.079	37.822	31.691	25.034	31.516	3.693
10	1.103	1.232	1.142	0.066	0.159	0.086	37.888	31.850	25.120	31.619	3.688
13	0.928	1.085	1.025	0.020	0.058	0.039	37.908	31.908	25.159	31.658	3.683
16	0.985	1.029	1.029	0.029	0.040	0.040	37.937	31.948	25.198	31.694	3.680

[a]Time: in days

[b]Dilution factor: 1/1000

[c]Dilution factor: 1/100

[d]Amount released per 10 mg of nanoparticles, calculated using standard curve equation $y = 0.1458\ln(x) + 1.4997$, where y = fluorescence, x = protein concentration.

[e]Each time point represents a sum of the release to date

[f]Standard error calculated using the formula $SE = \frac{STDEV}{\sqrt{n}}$, based on cumulative release values (standard deviation was determined using MS Excel)

NP-7 Formulation:

	Absorbance Readings			Tat-EGFP Release (μg/mL)[d]			Cummulative Release (μg/mL)[e]				
Time[a]	1	2	3	1	2	3	1	2	3	Mean	SE[f]
0	0.878[b]	0.85[b]	0.853[b]	14.065	11.607	11.849	14.065	11.607	11.849	12.507	0.782
0.125	0.93[c]	0.941[c]	0.924[c]	2.009	2.167	1.928	16.074	13.774	13.777	14.542	0.766
0.25	0.781[c]	0.69[c]	0.756[c]	0.723	0.387	0.609	16.797	14.162	14.386	15.115	0.844
1	0.663[c]	0.669[c]	0.628[c]	0.322	0.335	0.253	17.119	14.497	14.639	15.419	0.851
4	1.194	1.267	1.218	0.123	0.203	0.145	17.242	14.700	14.784	15.575	0.834
7	1.206	1.097	1.152	0.133	0.063	0.092	17.376	14.763	14.876	15.672	0.853
10	0.896	0.872	0.874	0.016	0.013	0.014	17.392	14.776	14.890	15.686	0.853
13	0.704	0.815	0.703	0.004	0.009	0.004	17.396	14.786	14.894	15.692	0.853
16	0.906	1.228	0.407	0.017	0.155	0.001	17.413	14.941	14.895	15.749	0.832

[a]Time: in days

[b]Dilution factor: 1/1000

[c]Dilution factor: 1/100

[d]Amount released per 10 mg of nanoparticles, calculated using standard curve equation $y = 0.1458\ln(x) + 1.4997$, where y = fluorescence, x = protein concentration.

[e]Each time point represents a sum of the release to date

[f]Standard error calculated using the formula $SE = \frac{STDEV}{\sqrt{n}}$, based on cumulative release values (standard deviation was determined using MS Excel)

Effect of sonication on protein release

25s, 3W power output

	Fluorescence Readings			Tat-EGFP Release (μg/mL)[b]			Cummulative Release (μg/mL)[c]				
Time[a]	1	2	3	1	2	3	1	2	3	Mean	SE[d]
0	62277	62587	62287	12.015	12.075	12.017	12.015	12.075	12.017	12.036	0.020
0.125	12656	13881	12265	2.442	2.678	2.366	14.457	14.753	14.384	14.531	0.113
0.25	1197	1315	1205	0.231	0.254	0.232	14.688	15.007	14.616	14.770	0.120
1	1152	938	826	0.222	0.181	0.159	14.910	15.188	14.776	14.958	0.121
4	468	513	459	0.090	0.099	0.089	15.001	15.287	14.864	15.051	0.125
7	141	165	162	0.027	0.032	0.031	15.028	15.319	14.895	15.081	0.125
10	79	95	130	0.015	0.018	0.025	15.043	15.337	14.920	15.100	0.124
13	174	245	240	0.034	0.047	0.046	15.077	15.384	14.967	15.143	0.125
16	236	181	130	0.046	0.035	0.025	15.122	15.419	14.992	15.178	0.127
19	649	188	119	0.125	0.036	0.023	15.247	15.456	15.015	15.239	0.127
22	123	125	106	0.024	0.024	0.020	15.271	15.480	15.035	15.262	0.128
25	250	185	132	0.048	0.036	0.025	15.319	15.515	15.061	15.299	0.132
28	162	149	141	0.031	0.029	0.027	15.351	15.544	15.088	15.328	0.132
31	75	53	18	0.014	0.010	0.003	15.365	15.554	15.091	15.337	0.134

[a]Time: in days

[b]Amount released per 10 mg of nanoparticles, calculated using standard curve equation y = 5183.1x, where y = fluorescence, x = protein concentration

[c]Each time point represents a sum of the release to date

[d]Standard error calculated using the formula $SE = \frac{STDEV}{\sqrt{n}}$, based on cumulative release values (standard deviation was determined using MS Excel)

180s, 10W power output

Time[a]	Fluorescence Readings 1	2	3	Tat-EGFP Release (μg/mL)[b] 1	2	3	Cummulative Release (μg/mL)[c] 1	2	3	Mean	SE[d]
0	143270	142330	146850	27.642	27.460	28.332	27.642	27.460	28.332	27.812	0.266
0.125	14456	11507	14201	2.789	2.220	2.740	30.431	29.681	31.072	30.395	0.402
0.25	1931	1524	1911	0.373	0.294	0.369	30.803	29.975	31.441	30.740	0.425
1	1672	1433	1594	0.323	0.276	0.308	31.126	30.251	31.749	31.042	0.434
4	1018	945	885	0.196	0.182	0.171	31.322	30.433	31.919	31.225	0.432
7	346	346	300	0.067	0.067	0.058	31.389	30.500	31.977	31.289	0.429
10	364	135	144	0.070	0.026	0.028	31.459	30.526	32.005	31.330	0.432
13	288	211	185	0.056	0.041	0.036	31.515	30.567	32.041	31.374	0.431
16	204	154	127	0.039	0.030	0.025	31.554	30.597	32.065	31.405	0.430
19	180	67	54	0.035	0.013	0.010	31.589	30.609	32.076	31.425	0.431
22	171	96	98	0.033	0.019	0.019	31.622	30.628	32.094	31.448	0.432
25	187	152	105	0.036	0.029	0.020	31.658	30.657	32.115	31.477	0.430
28	198	168	135	0.038	0.032	0.026	31.696	30.690	32.141	31.509	0.429
31	91	13	3	0.018	0.003	0.001	31.714	30.692	32.141	31.516	0.430

[a]Time: in days

[b]Amount released per 10 mg of nanoparticles, calculated using standard curve equation y = 5183.1x, where y = fluorescence, x = protein concentration

[c]Each time point represents a sum of the release to date

[d]Standard error calculated using the formula $SE = \frac{STDEV}{\sqrt{n}}$, based on cumulative release values (standard deviation was determined using MS Excel)

APPENDIX IV

Raw Data: Electroretinography

RAW ELECTRORETINOGRAPHY DATA

Mean a-wave amplitude for treated left eye (OD) and untreated right eye (OS) of each test animal. Each reported amplitude represents the mean of the 5 acquired ERG traces

Intensity Step		a-wave amplitude (μV)									
		#1	#2	#3	#4	#5	#6	#7	#8	#9	#10
1	OD	0.965	18.91	20.1	44.44	10.04	22.76	9.88	4.854	17.9	26
	OS	5.334	18.96	26.2	58.54	13.84	24.97	13.57	13.81	6.014	16.04
2	OD	11.48	14.38	17.12	57	8.084	23.34	11.46	0.983	52.6	29.65
	OS	21.87	32.46	32.76	63.66	28.19	34.95	29.46	18	33.25	14.76
3	OD	6.319	32.45	13.61	80.71	7.869	39.26	18.05	9.62	46.7	53.95
	OS	14.94	41.01	32.46	55.29	48.12	50.3	31.5	24.46	23.29	41.69
4	OD	17.54	26.74	24.44	90.13	15	33.67	27.39	34.83	67.13	51.26
	OS	33.27	34.54	43.66	59.28	67.09	55.68	49.43	29.86	37.89	44.56
5	OD	12.04	29.77	30.55	91	25.73	32.66	31.14	39.91	45.65	44.97
	OS	35.32	36.26	39.84	70.88	58.77	63.68	40.33	30.95	33.64	37.56
6	OD	5.812	60.34	36.71	78.74	21.08	53.38	24	50.58	43.92	44.52
	OS	53.56	67.42	51.09	80.09	46.87	90.01	37.15	52.46	36.23	49.4
7	OD	9.271	76.23	37.31	73.64	40.87	52.97	35.44	41.12	73.75	41.13
	OS	73.53	76.48	54.4	75.52	66.39	96.27	43.33	49.53	62.79	36.8
8	OD	35.03	53.8	31.57	84.18	57	36.98	39.36	55.85	82.75	44.29
	OS	114.8	77.39	63.6	73.11	78.08	81.92	56.18	61.4	49.49	36.08
9	OD	68	92.98	88.68	185.7	98.7	117.2	73.83	151.2	181.7	167.9
	OS	155.4	100.1	114.6	127.2	138.6	189.5	105.7	86.65	88.82	132.5
10	OD	111.7	125.9	131.7	225.5	133	140.4	132.9	223.9	219.1	187.2
	OS	190	128	160.1	147.1	193.5	208	136.9	108.5	106.8	156.7
11	OD	150.1	133.8	156.5	226.9	125	161.5	149.2	276	242.6	149.5
	OS	209.4	135.3	169.6	168.3	206.9	214.1	140.2	142.3	122.5	115.4

Mean b-wave amplitude for treated left eye (OD) and untreated right eye (OS) of each test animal. Each reported amplitude represents the mean of the 5 acquired ERG traces

Intensity Step		b-wave amplitude (μV)									
		#1	#2	#3	#4	#5	#6	#7	#8	#9	#10
1	OD	48.75	87.52	63.74	103.2	105.6	112.6	90.67	71.11	113.6	107.1
	OS	145.2	124.2	141.7	185.7	98.09	213.5	105.4	106.8	94.19	70.41
2	OD	70.15	149.8	66.41	151.5	128.7	158.7	130.4	130.5	178	168.6
	OS	246.1	198.7	178.2	231	137	284.8	141.8	151	112	123.6
3	OD	95.83	226.1	117.2	208.8	180.3	245.7	168.2	202.9	246.2	233
	OS	334.6	270.8	251.5	256	207.4	371	183.7	191.3	142.3	187.3
4	OD	175.8	302.2	159.5	290.9	196.6	318.9	247	377.3	343.5	345.1
	OS	442.2	333.7	282.6	336.1	288.1	464.8	260.7	267.2	184.2	291.1
5	OD	241.5	366.8	226.6	408.5	234.9	389.8	309.5	569.7	410.7	419.9
	OS	523.2	397.8	329.1	423.9	343.7	557.5	328.9	330.1	221.5	375
6	OD	353	470.6	301.2	487.9	253.6	452.5	372.9	768	449.8	434.7
	OS	643.9	505.5	396.1	507.8	400.5	622.9	383	466.9	265.8	440.1
7	OD	420.1	522	327.6	540.6	249.3	415.2	400	799.2	495.4	472.9
	OS	702.6	570.2	396.8	557.3	429.9	613.8	410.3	509.4	324	484.8
8	OD	422.8	487.3	303.2	553.3	282.8	400.6	418	795.4	486.9	447.6
	OS	705.6	541.8	347.1	545.6	447.9	557.9	429.5	507.6	293.4	451.8
9	OD	480	543.1	348.5	699.1	318.7	464	454.7	918.1	595.2	598.2
	OS	758.2	596.7	411.6	599.2	527.1	639.1	465.4	573.1	327.1	560
10	OD	520.5	517	384.4	712	336.1	471.2	470.2	943.6	604.9	558.3
	OS	785.7	569.1	446.1	560.1	536.2	661.3	456.7	559.6	345.2	562.7
11	OD	537.9	495.3	407.1	698.8	290.3	452.3	461.1	955.5	591.2	498.1
	OS	729.5	514.5	438.4	560.9	527.2	596.2	425.8	553.5	340.6	509.9

STATISTICAL ANALYSIS

Means from all animals: a-wave

Intensity Step	Mean amplitude (μV)		Standard Deviation		Standard Error	
	Treated	Untreated	Treated	Untreated	Treated	Untreated
1	19.73	17.58	15.25	12.39	4.82	3.92
2	30.94	22.61	13.41	18.73	4.24	5.92
3	36.31	30.85	13.13	24.46	4.15	7.74
4	45.53	38.81	12.25	23.89	3.88	7.55
5	44.72	38.34	14.17	20.93	4.48	6.62
6	56.43	41.91	17.58	21.08	5.56	6.67
7	63.50	48.17	17.93	21.24	5.67	6.72
8	69.21	52.08	21.47	18.78	6.79	5.94
9	123.91	122.59	31.97	45.13	10.11	14.27
10	153.56	163.13	35.16	45.52	11.12	14.40
11	162.40	177.11	37.09	51.72	11.73	16.36

Means from all animals: b-wave

Intensity Step	Mean amplitude (μV)		Standard Deviation		Standard Error	
	Treated	Untreated	Treated	Untreated	Treated	Untreated
1	128.52	90.39	44.03	22.44	13.92	7.10
2	180.42	133.28	57.98	37.99	18.34	12.02
3	239.59	192.42	71.78	52.29	22.70	16.54
4	315.07	275.68	84.39	76.81	26.69	24.29
5	383.07	357.79	99.06	107.19	31.33	33.90
6	463.25	434.42	113.68	140.18	35.95	44.33
7	499.91	464.23	114.07	147.48	36.07	46.64
8	482.82	459.79	116.73	143.56	36.91	45.40
9	545.75	541.96	121.50	175.43	38.42	55.48
10	548.27	551.82	120.31	173.82	38.04	54.97
11	519.65	538.76	105.62	182.01	33.40	57.56

ANOVA

a-wave

Intensity Step	P Value (%)
1	73.42
2	26.8
3	52.24
4	43.94
5	43.51
6	11.16
7	9.82
8	7.38
9	94.08
10	60.52
11	47.43

b-wave

Intensity Step	P Value (%)
1	2.53
2	4.53
3	11.03
4	28.94
5	59.06
6	61.96
7	55.26
8	69.85
9	95.58
10	95.82
11	77.73

APPENDIX V

Chitosan-Based Nanoparticles: Preliminary Data

Preliminary release data from chitosan-based nanoparticles

CNP1: 8kDa MW chitosan
Formulation: 10ml chitosan @ 0.2% w/v + 4ml TPP @ 0.1% w/v + 2ml tat-EGFP @ 0.7 mg/ml

Time (days)	Protein amount (μg)	Cummulative Released (μg)
0	1.734	1.734
0.125	2.600	4.334
0.25	0.868	5.202
1	0.945	6.148
4	0.912	7.060
7	0.472	7.532
10	0.259	7.791
15	0.066	7.858